Atlas of high-resolution emission and shell lines in Be stars. Line profiles and short-term variability[*]

R.W. Hanuschik[1,2], W. Hummel[3], E. Sutorius[1], O. Dietle[1] and G. Thimm[4]

[1] Astronomisches Institut, Ruhr-Universität Bochum, D-44780 Bochum, Germany
[2] Astronomisches Institut, Universität Tübingen, Waldhäuser Str. 64, D-72076 Tübingen, Germany
[3] Astrofysisch Instituut, Vrije Universiteit Brussel, Pleinlaan 2, B-1050 Brussel, Belgium
[4] European Southern Observatory, Karl-Schwarzschild-Straße 2, D-85748 Garching, Germany

Abstract. — We present an atlas of high-S/N, high-resolution ($\Delta v \leq 6$ km s^{-1}) data of Be star emission and shell profiles. We have collected profiles of Hα and of Fe II, mostly of the $\lambda 5317$ transition. These lines have been selected to provide measures for the overall emission strength and for the velocity field in these disks. We have collected data for 77 southern and equatorial programme stars, covering the period 1982-1993. This is the most comprehensive overview of profile shapes in Be disks. We propose a three-dimensional scheme in which most observed profiles can be classified. The parameters are i) inclination, ii) optical depth, and iii) the pattern of the velocity field. A search for short-term variability (timescales between five days and a few minutes) in six stars ended with negative result. Shortest observed timescale for variability is a few days for well-developed disks in binary systems (HR 1910, HR 2142).

Key words: atlas — stars: Be — lines: profiles

1. Introduction

Be stars are early-type non-supergiant stars surrounded by a cooler, disk-like circumstellar envelope. The envelope becomes apparent at optical wavelengths by hydrogen and metallic emission lines, and in the IR range by continuous bound-free and free-free thermal emission. The origin and structure of the circumstellar disk has been the aim of many studies since Struve (1931).

Since the disk is optically thin to continuous radiation in the visible range, most information about its structure can be gained from spectroscopy of its Doppler broadened emission lines. Among the most interesting physical parameters which can be investigated by emission line spectroscopy are:

- the envelope geometry (disk-like vs. ellipsoidal shell),
- its extension (radius, mass and emissivity distribution),
- its kinematics (Keplerian rotation vs. outflow),
- its density structure (hydrostatic equilibrium vs. wind-compressed disk, density waves).

While the importance of studying emission lines has been recognized since long, the observational capabilities

were quite limited as long as photographic plates were the standard detectors. Since the achievement of fast linear photoelectric devices in the past two decades, high-resolution, high-S/N spectroscopy has become possible, the only technique adequate for obtaining fully resolved line profiles free from instrumental effects.

Among the first steps towards such high-quality data were the atlases of Andrillat & Fehrenbach (1982) and Andrillat (1983) who presented data for a large sample of northern and equatorial Be stars suffering only from insufficient S/N, and of Dachs et al. (1981, 1986) with a similarly large sample of southern and equatorial objects, measured at, however, insufficient resolution. Furthermore there exist three atlases in the infrared region (Andrillat et al. 1988, 1990, 1994), the first two at low, the last at medium resolution.

While these atlases represented a large step forward for Be star diagnostics, they still kept some important fine-structure properties of emission line profiles hidden. This became apparent in the first high-S/N *and* high-resolution atlases by Hanuschik (1986, 1987), Hanuschik et al. (1988, = HKK88), Doazan et al. (1991), Slettebak et al. (1992, = Sl92) and Dachs et al. (1992). Good examples for such detection of important fine-structure are:

- the winebottle-type structure typical of emission line profiles in many low-to-intermediate inclination Be

stars, formerly hidden in the flanks of low-S/N data (Hanuschik 1986, HKK88);

– the detection of narrow emission peaks (of width ≤ 20 km s^{-1}) in Fe II emission line profiles ("steeple"-type; Hanuschik 1987; Hanuschik et al. 1995a);

– the detection of an extremely narrow component in Fe II shell (absorption) lines (width ≤ 6 km s^{-1}; Sect. 3.2, this paper).

Apart from the quest for high spectral resolution, another goal of Be star spectroscopy has always been a good time coverage of the variability behaviour. The papers of Dachs et al. (1981, 1986) were the first to present a long-term overview of the emission behaviour in a larger sample of Be stars. In the meanwhile they represent important cornerstones for long-term variability studies. Other such studies, like the atlases mentioned above, form snapshots only.

We feel that a synoptic time-resolved study of high-resolution, high-S/N emission line profiles of Be stars is both desirable and still missing. To present such study is the purpose of the present paper. We provide a collection of data for 77 southern and equatorial Be stars, most of which have not yet been published. Our data cover more than a full decade for many objects. We are convinced that this number is sufficient to cover all important phenomena connected with Be stars and visible in optical emission lines.

In a forthcoming paper we will analyze these data, with emphasize on the long-term variability behaviour of Be star disks.

In Sect. 2 we present a short overview of the selected lines and stars, and of the measurements and reduction procedure. The atlas with the full set of profiles is presented in Sect. 3. A three-dimensional classification scheme for Be star profiles is devised in Sect. 4. Finally we present a search for short-term variability in Sect. 5.

2. Data

2.1. Selection of lines

A combined study of *high-opacity Balmer lines* and *low-opacity Fe II lines* is very efficient in distinguishing the different shaping and broadening effects in emission line profiles due to kinematics and radiative transfer.

Hα measurements are mainly valuable as indicators for overall emission strength and its variability, and for asymmetry of the density distribution.

Fe II lines are optically thin and unperturbed by photospheric features. They reflect the pure kinematical broadening function in the emitting part of the Be disk (if thermal and turbulent motions are negligible) and offer highly valuable insight into processes within the disk.

We have selected profiles of

– Hα $\lambda6562.8$, and

– Fe II $\lambda5316.6$.

During the 1985 Feb./March and the 1989 March runs, occasionally the Fe II $\lambda5169$ line was measured instead.

During some of the runs, Hβ, Hγ and He I lines were measured in addition. These profiles have not been included in this study to avoid overcrowding. They can be found in Hanuschik (1987, together with some more Fe II lines), HKK88, Sl92 and Dachs et al. (1992).

2.2. Measurements and reduction

Most data have been measured at ESO's 1.4m Coudé Auxiliary Telescope, using the Coudé Echelle Spectrograph and a reticon (until 1987) or a CCD (as of 1988), resp., as detector. The spectrograph operated at high resolution, $R = \lambda/\Delta\lambda \geq 50\,000$, corresponding to $\Delta\lambda \leq 0.13$ Å at Hα and $\Delta v \leq 6$ km s^{-1}. This is sufficient to fully resolve all intrinsic structure of the Hα profiles (thermal velocity about 20 km s^{-1} at 10^4 K), and also practically all intrinsic structure of the Fe II profiles. The signal-to-noise ratio (S/N) is usually in the range $100-1000$ (the higher value being representative for the brightest Hα profiles). An overview of the measuring campaigns and the observers involved is contained in Table 1.

The reduction of the data has been standard. The steps were bias subtraction, division by the normalized flat field, extraction in case of CCD data (integration perpendicular to the dispersion of all pixels in which $S \geq N$), normalization to the stellar continuum, calibration to heliocentric radial velocity scale, and correction for telluric absorption lines (except for the 1982 CAT data and those of Sl92, see below). This latter step was performed using a mask provided by an almost featureless comparison spectrum (mostly of the O5Ia star ζ Pup). More details can be found in Hanuschik (1986) and Dachs et al. (1992).

Where appropriate, we have included for comparison Hα and some Hβ data from the atlas of Sl92. These data are usually not fully resolved, $R = 15\,000$, but have been included here in order to fill the time record.

2.3. Programme stars

Our programme stars are collected in Table 2. They have been selected by apparent brightness and overlap with older data bases like the atlases of Dachs et al. (1981, 1986). Furthermore an attempt has been made to include at least one measurement of as many southern and equatorial stars from the list of Slettebak (1982) as possible, motivated by the consideration that a study of Be disk behaviour containing as much information as possible should include a *cross-section* (many stars measured once) as well as a *longitudinal section* (few stars measured frequently).

Table 3 contains the approximate dates of measurements. The periods are coded following Table 1. The exact dates can be found as labels in the profile figures (see below).

Table 1. Observing campaigns at ESO 1.4 m CAT

No.	Date (UT)	Observer	Detector	Source of publication
#1	1982 Aug 15–Sep 15 (13 nights)	J.R. Kozok	Reticon	Hanuschik et al. 1988
#2a	1985 Jan 01–04	R.W. Hanuschik	Reticon	Hanuschik (1986, 1987)
#2b	1985 Feb 27–Mar 03	R.W. Hanuschik	Reticon	Hanuschik (1986, 1987)
#3	1987 Feb 07–13	J. Dachs	Reticon	Dachs et al. (1992)
#4a	1988 Dec 03–04	G. Thimm	CCD	unpublished
#4b	1989 Mar 02–05	G. Thimm	CCD	unpublished
#5	1989 Sep 26–Oct 01	R.W. Hanuschik	CCD	unpublished
#6a	1992 Jan 11–13	W. Hummel, R.W. Hanuschik	CCD	unpublished
#6b	1992 Mar 24–25	W. Hummel	CCD	unpublished
#7a	1993 Apr 18	R.W. Hanuschik	CCD	unpublished
#7b	1993 Sep 08–09	R.W. Hanuschik	CCD	unpublished
some profiles are added from the following campaigns:				
S1	1989 Jan 06–09	A. Slettebak	[a]	Sl92
S2	1989 Oct 06–09	A. Slettebak	[a]	Sl92

[a] KPNO Coudé Feed Telescope, CCD

3. The atlas

3.1. The profiles

In Figs. 5–82, we show the full set of our profiles for 77 southern and equatorial Be and shell stars from 1982–1993.

For each star with multiple measurements, we show three panels which essentially contain the same information but emphasize different aspects of variability. In panel a, all profiles are plotted on top of each other which pronounces variations in radial velocity and line profile shape. Panel b provides an overview of the overall emission strength behaviour, e.g. variations of central intensity. In panel c, both aspects (profile shape and emission strength) are combined. This latter plot is intended as demonstration of the degree of constancy (of the whole profile or parts thereof). In case of strongly variable profiles, or many measurements, this panel may become a bit overcrowded and is only thought as visualization of variability (or constancy).

In panels a and b, profiles of Hα and Fe II λ5317 (or Fe II λ5169, if noted) are plotted together. These measurements are quasi-simultaneous, i.e. separated by at most 2–3 days (usually one day).

Since the Fe II lines are comparably faint (peak flux $\leq$ 1.2 F_c), their profiles have been blown up according to

$$F'(\lambda)/F_c = (F(\lambda)/F_c - 1) \cdot k + 1 , \qquad (1)$$

where $F(\lambda)$ denotes the measured, and $F'(\lambda)$ the displayed flux, resp. The expansion factor k is in the range $5-20$ and displayed in the figures.

If the Fe II region has been measured, but no emission has been found, the pure stellar continuum is plotted since this negative result about Fe II emission is as valuable as a positive one, e.g. for further investigations of the ionization conditions in the disk.

3.2. Individual stars

We will emphasize here new results about the most interesting objects. Overviews about the history of objects already observed earlier may be found, e.g., in Slettebak (1982) or the atlases cited in the Introduction.

HR 1180 = 28 Tau = Pleione. This star is famous for its phase transitions between Be and Be-shell spectrum. It is the only example in our atlas showing such behaviour. We have caught the star in its most recent transition where it lost its shell characteristics at some time between 1989 (when the Hα profile still shows a deep central depression) and 1993 when the Fe II profile clearly exhibits pure emission characteristics (see Fig. 9). The whole transition, however, has been quite a smooth process lasting for about a decade. The depth of the Hα depression has continuously decreased since 1982, while the Hα equivalent width has increased. Furthermore, in 1993 the profile has become asymmetric and presumably shows onset of cyclic V/R variability.

HR 1423 = 28 Eri. This star has lost its disk almost entirely between 1989 and 1992 (Fig. 10). The 920111 profile of Hα looks quite bizarre since it shows, apart from its double peak, secondary ondulations in the wings (Fig. 10d) which are unlike anything visible in Figs. 1 or 2. These are likely to be indicators of a strongly distorted velocity field. The distortion may either be linked to the decay mechanism or to a highly inhomogeneous density

Table 2. Programme stars

HR	Name	MK type[a]	$v \sin i^a$/ km s^{-1}	Profile code[c]
472	α Eri	B4 V(e)	225	(L)1
1142	17 Tau	B6 IIIe	180	(L)1
1156	23 Tau	B6 IV(e)	280	L–H1
1165	η Tau	B7 IIIe	140	L:1
1180	28 Tau	B8 Ve-sh	320	E1→H2
1423	28 Eri	B1 Ve	230	L–H1
1508	56 Eri	B2 Ve	180	L1
1660	105 Tau	B3 Ve	200	L2
1679	λ Eri	B2 IIIe	220	(L)1
1772		B5 IVe[b]	...	E1
1789	25 Ori	B1 Ve	320	L–H1
1858	120 Tau	B1.5 IVe	210	L–H1
1910	ζ Tau	B1 IVe-sh	220	E1→2
1934	ω Ori	B2 IIIe	160	L1
1956	α Col	B7 IVe	180	L1
1961		B2.5Ve[b]	...	L2
2142		B2 IVe	350	...
2170		B5 Ve	220	L1
2284		B1.5 IVe	200	L2:
2343	ν Gem	B6 IVe	170	E2
2356	β^1 Mon	B4 Ve-sh	300	H2
2492	10 CMa	B2 IIIe	200	L1
2538	κ CMa	B2 IVe	220	L2
2545		B6IVe + A	220	...
2690		B2 IVe	200	L:1
2745	27 CMa	B3 III(e)-sh	150:	abs
2749	ω CMa	B2.5 Ve	80	L1
2787		B2 Ve	220	L1
2825		B3 Ve	$\leq$ 40	P1[d]
2845	β CMi	B8Ve	245	L–H1
2855		B0.5 IVe	280	...
2911		B3 Ve	245	H1
2921		B3 IV	230	L:1
3034	o Pup	B1 IVe	320	L–H2
3135		B2.5 Ve	140	L1
3186		B2.5 Vn[b]	292[b]	H:1
3237		B1.5 IVe	115	P–L2

[a] taken from Slettebak (1982), if not otherwise noted
[b] Bright Star Catalogue
[c] see text (Sect. 4.3) for codes
[d] 850104: peak splitting due to NSB

Table 2. continued

HR	Name	MK type[a]	$v \sin i^a$/ km s^{-1}	Profile code
3498		B2.5 V(e)	240	(L)1
3858		B5 Ve	260	L1 (2?)
3946		B4 Ve[b]	220[b]	L1 (2?)
4009		B2 IVe	220	L2
4037	ω Car	B8 IIIe-sh	220	H–E1
4123		B9 IVe	250	L–H1
4140	p Car	B4 Ve	250	L2
4621	δ Cen	B2 IVe	220	L2
4823		B6 IVe	250	H1
4830		B1 IIIe	300	L–H1
4899	μ^2 Cru	B5 IVe	220	L–H1
4930		B2 IIIe	300	L–H2
5193	μ Cen	B2 IV-Ve	155	L1
5223		B2 IIIep	70	P1 (2?)
5316		B4 Ve	300	H1
5440	η Cen	B2 IV(e)	350	H–E1
5551	θ Cir	B3 V(e)	100	(L2?)
5661		B0 V	130	abs
5730	κ^1 Aps	B3 IVe	250–350	H–E1
5941	48 Lib	B3 IV e-sh	400	E2
6118	χ Oph	B1.5 Ve	140	P2[e]
6304		B2 IVne[b]	201[b]	L–H2?
6397		O7.5 IIIe	115	...
6451	ι Ara	B2.5 IVe	320	H2
6510	α Ara	B3 Ve	250	L–H1
6712	66 Oph	B2 IV-Ve	240	L2
6819		B3 III(e)	50	(L)1
6929		B2 IVpe[b]	...	...
7249		B2 V(e)	120	L1 (2?)
7415		B6 e-sh	300	E2
7789	25 Vul	B6 IVe	200	L1
8260	ϵ Cap	B3 IIIe	250	E1
8402	o Aqr	B7 IIIe-sh	300	E1
8438	25 Peg	B6 Ve	150	L1
8520	31 Peg	B1.5 Ve	100	L1
8539	π Aqr	B1 III-IVe	300	(H2?)
8628	ϵ PsA	B7 IVe	180	(L2?)
8773	β Psc	B5 Ve	100	P1
9076	ϵ Tuc	B8V	280	(H)1
9098	2 Cet	B9.5Vn[b]	186[b]	(L)1

[e] 3 peaks due to extreme development of winebottles

distribution with a high-density part producing electron scattering wings, and a low-density region without Thomson scattering. Since the ondulations are quite sharply limited, these regions may even be separated in space. Whatever the true origin for the unique profile shape is, it must be a transient phenomenon since neither before nor after 1992 such shape has been observed.

HR 1508 = 56 Eri. This star shows conspicuous line profile variations which appear as a change in typical line width (cf. the profiles in 1988 and 1982: Figs. 11c, d), with the whole profile remaining highly symmetric throughout the observed period. The 1982 Hα profile shows textbook examples of very pronounced winebottle inflections.

HR 1660. The profile asymmetry slowly changes on a timescale of about 10 years, accompanied by typical steeple-shape in the Fe II profile (Fig. 12).

HR 1679 = λ Eri. This star is a prototype example for flickering emission. λ Eri has shown this behaviour in 1980-1983 (Barker 1986; Dachs et al. 1986) as well as in the more recent past. It appears to be a twin of μ Cen (Hanuschik et al. 1993) and is known to exhibit a complex emission behaviour in the He I lines (Smith 1989). Its last outburst was reported in August 1994 (Štefl 1994).

HR 1910 = ζ Tau. The behaviour of the Hα line is quite complex: starting from a minimum emission strength and symmetric shape in 1982, the profile gets brighter till 1993 and starts cyclic V/R activity in about 1989. The estimated cycle duration is about $6-7$ years, with a $V = R$ transition between 1992 February and November (Guo 1994). The profiles look smooth, except for the 1982 set, see Fig. 17d. Since ζ Tau is a well-known binary ($P_{\rm orb} = 132.91^{\rm d}$, Pols et al. 1991), the 1982 finestructure may indicate interaction or disk distortion.

Alternatively, the finestructure could indicate an unstable state of the disk, e.g. a density wave with increasing amplitude getting non-linear.

HR 2142. Its binary nature with $P_{\rm orb} = 80.860$ days has been determined by Peters (1983). We clearly see the rare case of an interacting binary Be star of the same kind of behaviour as ϕ Per (Gies et al. 1993). We show in Fig. 23 the whole set of Hα profiles collected at the CAT over 11 years, phase binned with the above period. Although some secular variability in strength exists, the basic shape of the Hα profile is repeated, even after 50 orbital periods.

HR 2343 = ν Gem. From all stars in our sample showing cyclical V/R variability, this star has the faintest emission (Fig. 25). We estimate its cycle duration to about 5 years, but it might also be that we observe orbital modulation with a much shorter period since ν Gem is a binary Be star ($P_{\rm orb} = 40.198^{\rm d}$, Jarad et al. 1989). Note also the very narrow and untypical Fe II absorption and emission in 1992 (Fig. 25).

HR 2538 = κ CMa. Since 1982, this star has been observed to show an asymmetric Hα profile and steeple-type Fe II profile (Fig. 28). Contrary to all other such stars

in our survey, it has not shown any considerable variation of this asymmetry, thus making it the star with the longest cycle duration in our sample ($P \gg 20$ yr).

HR 2749 = ω CMa. This star has shown development of broad Thomson wings in 1987 and 1993 (cf. Fig. 32d).

HR 2825. Like ω CMa, this star shows Thomson wing variability, with broad wings in 1992/93 and a narrow profile in 1987-1989 (Fig. 34). These variations indicate a considerable change in electron density. Note also the extreme anticorrelation between the width and strength of the Fe II emission and the strength of Hα emission (Fig. 34d) which is also observed in HR 5223 (Fig. 56d).

HR 3034 = o Pup. The line profiles show cyclical V/R variability, with $P \approx 8$ years, as well as some short-term variability in 1992 January–March (Fig. 39).

HR 3237. This star is a typical V/R variable star with steeple-type Fe II profiles at certain epochs of its cycle (present duration: 9 years, Hanuschik et al. 1995a; Fig. 42). Emission of this pole-on star is among the strongest in our sample.

HR 4009. A quite pronounced V/R activity has started between 1989 and 1992, with a very narrow steeple-shaped Fe II profile in 1992 (Fig. 46).

HR 4140 = p Car. This star exhibits cyclical V/R variability, with the 890304 Fe II profile being considerably asymmetric (Fig. 49). The cycle duration is not yet known.

HR 4621 = δ Cen. We observe prototype V/R variability, with $P \approx 10$yr (Hanuschik et al. 1995a), connected with typical steeple-shaped Fe II profiles in 1985 and 1989 (Fig. 50).

HR 4930. This star shows variability with an approximate cycle duration of about 10 years, with extreme asymmetry in 1987 ($V < R$) and 1992 ($V > R$), and approximate symmetry in 1993.

HR 5193 = μ Cen. This star is one of the few well studied southern Be stars and has become famous for its loss of disk emission in 1972-1976 (Peters 1979), and its flickering emission activity since then (Baade et al. 1988, Hanuschik et al. 1993). Since 1993, this star is building up a new permanent disk (Fig. 55).

HR 5223. This pole-on star shows weak V/R variability and variability of strength of the Thomson scattering wings in Hα and the Fe II width (Fig. 56).

HR 5551 = θ Cir. This star behaves atypical of Be stars in the way it shows irregular line profiles with short-term variability (Fig. 59). Its Fe II profiles are variable as well, with a very broad profile in 1993 as compared to the 1989 and 1992 profiles (Fig. 59).

HR 5941 = 48 Lib. Known as V/R variable star since long, its present cycle duration is 9yr (Hanuschik et al. 1995a and references therein). Its Hα and Fe II shell troughs are the deepest ones in our sample [$F/F_{\rm c}({\rm H}\alpha) = 0.11$ in 1985, $F/F_{\rm c}({\rm Fe~II}) = 0.095$ in 1993, Fig. 63).

Table 3. Dates of measurements (Hα and/or Fe II)

HR	#1	2a	2b	3	4a	S1	4b	5	S2	6a	6b	7a	7b	Further references to high-resolution profiles[a]
	1982	1985		1987	1988/89					1992		1993		
472	x			x				x		x				PS88, Do91
1142	x							x	x					AF82, Do91
1156	x							x	x				x	AF82, Do91
1165	x					x		x	x					AF82, Do91
1180	x					x		x	x				x	AF82, Ba87, Do91
1423	x			x	x			x		x			x	AF82, Do91
1508	x				x	x		x		x			x	AF82, Do91
1660	x				x	x		x		x			x	Do91
1679										x			x	Do91, Smith 1989
1772								x					x	
1789									x	x				AF82, Do91
1858										x				AF82
1910	x			x		x			x	x			x	AF82, Ba87, Do91, Guo 1994
1934	x	x		x					x	x				AF82, Do91
1956	x	x		x						x				Do91
1961													x	Do91
2142	x	x		x				x		x			x	AF82
2170													x	Do91
2284		x		x						x				AF82
2343						x			x	x			x	AF82, Do91
2356		x		x					x	x				AF82
2492				x						x				
2538	x	x	x	x				x	x	x	x	x	x	Do91
2545				x										
2690											x			Do91
2745										x				Do91
2749	x			x		x			x	x	x	x		
2787		x		x		x				x	x			
2825		x		x		x				x	x	x		AF82
2845						x				x				AF81, Do91
2855				x						x	x	x		Do91
2911			x							x	x			
2921											x			AF82
3034			x	x		x				x	x	x		
3135				x						x				AF82
3186											x			Do91
3237		x	x	x			x			x	x	x	x	Do91
3498							x				x		x	Do91
3858		x		x			x			x		x		

[a] An83 – Andrillat 1983
Ba87 – Ballereau et al. 1987
Do91 – Doazan et al. 1991
PS88 – Porri & Stalio 1988

Table 3. continued

HR	#1 1982	2a	2b	3 1987	4a	S1	4b	5	S2	6a	6b	7a	7b	Further references to high-resolution profiles[a]
		1985					1988/89			1992		1993		
3946		x		x			x			x	x	x		
4009		x		x			x			x	x	x		Do91
4037												x		Do91
4123											x	x		AF82, Do91
4140		x	x	x			x			x	x	x		PS88, Do91
4621		x	x	x			x			x	x	x		Baade 1987, Do91
4823				x			x			x	x	x		Do91
4830		x		x			x			x				Do91
4899				x										
4930				x						x	x	x	x	
5193			xx[b]	x			x			x	x	x	x	Peters 1986, Baade et al. 1988, Do91, Ghosh et al. 1991
5223		x		x			x			x	x	x	x	Do91
5316			x	x			x				x			Do91
5440	x			x			x			x		x		Do91
5551	x			x			x			x	x	x	x	
5661											x			
5730											x			Do91
5941		x		x							x	x	x	AF82
6118		x		x			x	x			x	x	x	AF82
6304								x			x	x	x	Do91
6397	x							x			x[c]	x[c]		
6451		x		x				x			x	x	x	Do91
6510	x	x		x				x			x		x	
6712								x	x		x	x	x	AF82, Peters 1988, Do91
6819								x						Do91
6929								x		x	x			
7249	x							x		x	x	x		Do91
7415												x	x	Ba87, Do91
7789									x				x	An83, Do91
8260	x							x				x	x	An83, PS88, Do91
8402	x				x			x				x	x	An83, Do91
8438	x							x					x	AF82, Do91
8520	x				x			x				x	x	AF82
8539	x				x			x				x	x	AF82, Do91
8628	x							x				x		Do91
8773	x				x			x					x	AF82, Do91
9076	x							x						
9098					x									

[b] two Hα profiles from 850424/25 (see Hanuschik 1986)

[c] Hα from 930418, Fe II from 920325

HR 6118 = χ Oph. Its profiles show a rare three peak appearance due to strongly developed winebottle-type shoulders (Fig. 62). We also observe a weakly developed V/R variability with a still undetermined period of certainly more than $15-20$ yr.

HR 6397. The rather odd profile of this O7.5e star in 1989 (Fig. 65) may indicate that in Oe-type stars kinematics in optical emission disks are different from those in ordinary Be stars.

HR 6712 = 66 Oph. This star has been observed to suddenly start V/R variability in the course of 1988, associated with the occurrence of prototype steeple-shaped Fe II line profiles (Hanuschik et al. 1995a, b; Fig. 68). Its present cycle duration is 5 years.

HR 6929. This star, with moderately strong emission in 1982, has lost its disk until 1989 (Fig. 70). It presently shows flickering emission, very similar to μ Cen or λ Eri.

HR 8402 = o Aqr. This shell star, with very stable emission strength over 20 years, is remarkable since it shows an extremely narrow shell core in the Fe II lines (Fig. 75d). With a half-width of 6 km s^{-1} the narrow Fe II feature in 1989 is unresolved and forms the most narrow absorption feature from a Be star disk in our sample. It indicates disk matter in front of the star at considerable distance (5−10 stellar radii) being in almost perfect Keplerian rotation (radial component $\ll$ 6 km s^{-1}).

HR 8539 = π Aqr. With short-term profile variability in 1982 (Fig. 78), this star is a candidate interacting binary system, though it is not listed in Pols et al. 1991.

HR 8773 = β Psc. This is another star with Thomson wing variability (Fig. 80).

4. Line profile shapes

Despite the apparently wild fluctuations in emission line shape, it is possible to arrange most observed line profiles into a rather simple scheme. There seem to be just three parameters: i) inclination i, ii) optical depth τ, and iii) kinematics. Firstly we will demonstrate the effect of the first two parameters.

4.1. Inclination and optical depth

All lines are expected to be shaped by the influence of large-scale Doppler (kinematical) broadening,

$$\Delta v_{\mathrm{kin}} = v_{\mathrm{K}} \sin i , \qquad (2)$$

where v_{K} denotes the Keplerian velocity at the stellar radius (= inner edge of the disk), and i the inclination angle. v_{K} is of order 400−500 km s^{-1}. It is natural to arrange line profiles along a $v \sin i$ sequence where $v \sin i$ is the *stellar* projected rotational velocity which measures the inclination if v is known (or assumed to be uniform in all Be stars which is done here).

Emission lines are also broadened by thermal broadening Δv_{th}. This is of the order of 20 km s$^{-1}/\sqrt{A}$ (with the atomic weight A) and can be neglected here.

The kinematical broadening becomes also manifest as small-scale process in thin disks, as *shear broadening*. This effect is caused by velocity shear between the upper and the lower intersection point of a certain line-of-sight and the disk (Horne & Marsh 1986). The shear increases with inclination according to

$$\Delta v_{\mathrm{sh}} = \Delta v_{\mathrm{th}} \cdot \frac{3}{4} \sin i \tan i \sin 2\varphi \qquad (3)$$

(φ is the azimuthal angle within the disk). For $i > 60°$, Δv_{sh} may exceed the thermal broadening Δv_{th} in certain directions. This causes a non-isotropic line absorption coefficient resulting in a deep V-shaped central depression.

This effect is even important for optically thin Fe II lines with their small thermal width.

In addition, optically thick lines, and especially Hα, are shaped by other broadening mechanisms induced by radiative transfer. (We will use in the following the term optical depth, τ, for the *vertical* optical depth at the innermost disk radius.)

The most important contribution to optically thick line shaping in disks is broadening by non-coherent scattering (NSB). It is caused by the effect that for optically thick lines, deeper layers of the disk become visible in the wings of the local absorption profile than in the core (Avrett & Hummer 1965; Hummel & Dachs 1992; Hummel 1994). Since the source function increases with depth, the effective local absorption profile becomes double-peaked (i.e. non-Gaussian) and somewhat broader than in the purely thermal case,

$$\Delta v_{\mathrm{nsb}} \approx 1.5 \Delta v_{\mathrm{th}} [\ln(\tau \sec i)]^{1/2} \qquad (4)$$

(Avrett & Hummer 1965) or $\approx 2.3 \ldots 3.9 \Delta v_{\mathrm{th}}$ for $\tau = 10 \ldots 10^3$ at $i = 0°$. At low inclination, it is of same magnitude as kinematical broadening and causes winebottle-type flank inflections. At very low inclination, it may produce single-peak, or in rare cases triple-peak profiles[1]. Above $i \approx 60°$, it becomes less important than shear broadening.

Another broadening effect, Thomson scattering (e.g., Poeckert & Marlborough 1978), affects only the line wings since its typical width is given by the thermal width of electrons.

Finally, at very high inclination ($i > 80°$), shell absorption of photospheric light by the disk becomes important which causes a deep central depression below the stellar continuum in both Hα and Fe II profiles.

It is obviously useful to introduce a second parameter for classification, optical depth τ, since NSB broadening depends on τ. Since we are not intending to actually measure τ, we simply use the terms $\tau \gg 1$ for Hα lines, and $\tau \lesssim 1$ for Fe II lines here.

In Fig. 1 we have collected four sets of Hα/Fe II profiles with typical shapes. The leftmost profile arises from a nearly face-on disk, with $\Delta v_{\mathrm{nsb}} \approx \Delta v_{\mathrm{kin}} \approx \Delta v_{\mathrm{th}} \gg \Delta v_{\mathrm{sh}}$. The H$\alpha$ profile exhibits a single peak (caused by overlap of the two innermost peaks of the convolved kinematical and NSB broadening functions, resp.) plus strong winebottle-type inflections (due to the two outermost peaks of the convolved functions). The Fe II profile reflects the pure kinematical profile which is known to be double-peaked for thin disks (Huang 1972; Smak 1981; Hanuschik 1988).

The next profile set is typical of low to intermediate-inclination disks. Now $\Delta v_{\mathrm{kin}} > \Delta v_{\mathrm{nsb}} \gg \Delta v_{\mathrm{th}} > \Delta v_{\mathrm{sh}}$,

---

[1]The original interpretation of winebottle inflections as evidence for "two-component structure" (Hanuschik 1986, HKK88) is not maintained anymore.
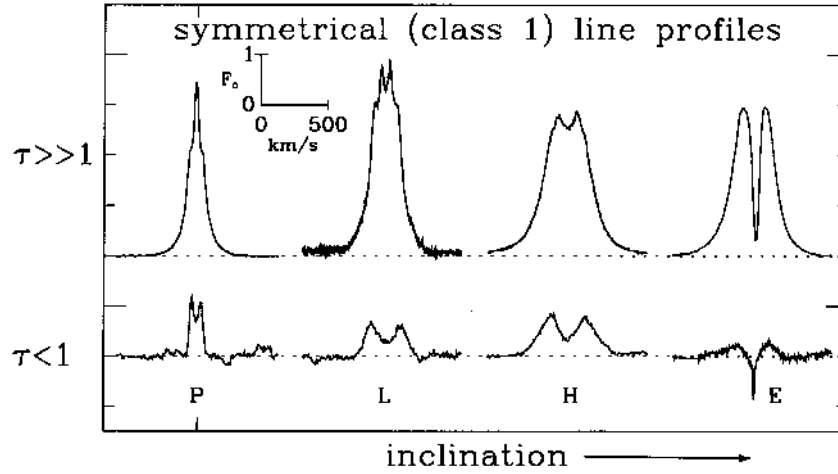
Fig. 1. Typical emission line shapes for symmetrical (class 1) profiles. We show four sets of Hα (top) and Fe II (bottom) profiles, plotted on a radial velocity vs. flux scale and assorted according to the inclination indicators in Sect. 4.3. The Fe II profiles are expanded by a factor $k = 10$, see Eq. (1). The four stars are, from left to right: HR 2825, measured in 1992 March 24 = 920324 ($v \sin i \leq 40$ km s^{-1}; full set of profiles in Fig. 34); 56 Eri = HR 1508, 820816 (180 km s^{-1}, Fig. 11); α Ara = HR 6510, 890926 (250 km s^{-1}, Fig. 67); o Aqr = HR 8402, 891001 (300 km s^{-1}, Fig. 75)
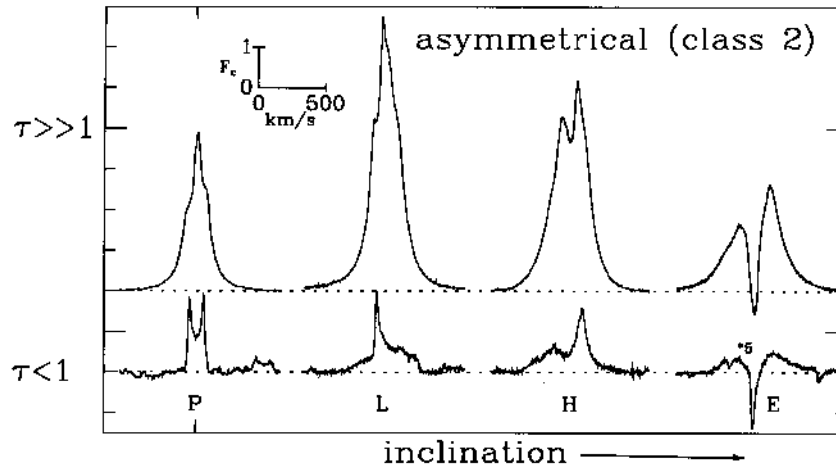
Fig. 2. Typical emission line shapes for asymmetrical (class 2) profiles. As in Fig. 1, we show four sets of Hα and Fe II profiles; from left to right: HR 5223, 920324 ($v \sin i = 70$ km s^{-1}; full set of profiles in Fig. 56); δ Cen = HR 4621, 850228 (220 km s^{-1}, Fig. 50); Pleione = HR 1180, 930909 (320 km s^{-1}, Fig. 9); 48 Lib = HR 5941 (400 km s^{-1}, Fig. 63)

and the two innermost peaks of the convolved kinematical and NSB profile are resolved.

The third profile set is representative of large inclinations, with $\Delta v_{\rm kin} \gg \Delta v_{\rm sh} > \Delta v_{\rm nsb} > \Delta v_{\rm th}$. NSB broadening is unimportant now (the winebottle shoulders have disappeared), while shear broadening deepens the central part of both Hα and Fe II profiles. Note especially the V-shape of the central depression in the Fe II profile.

Finally, the last set represents an edge-on disk ($i > 80°$) where shear broadening and shell absorption act together to produce a deep central depression.

It is well known that the shape of the kinematical profile furthermore depends on the outer radius of the

disk (peak separation) and on the emissivity law (slope of flanks). Since we are only interested here in a qualitative description of profile shapes, we neglect these influences. Fits to Fe II emission lines may be found in Hanuschik (1988).

4.2. Kinematics

Up to now we have only treated symmetric line profiles. Implicitely we have thus restricted ourselves to disks with an axisymmetrical velocity field and density distribution, which most likely corresponds to a quasi-Keplerian disk in hydrostatic equilibrium. HKK88 have coined the term
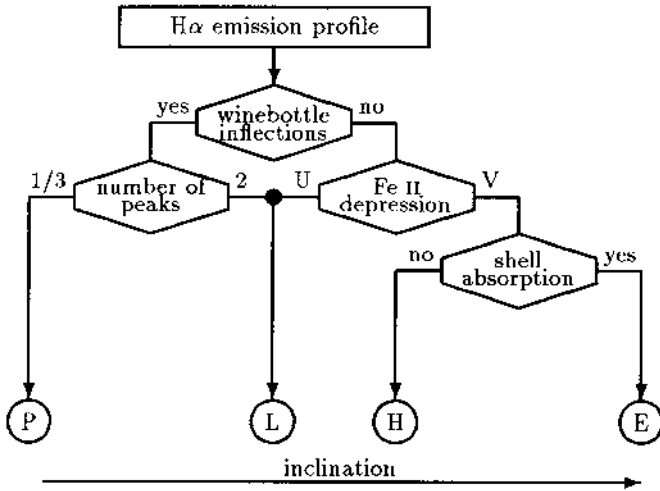
Fig. 3. Classification scheme for Be emission line shapes
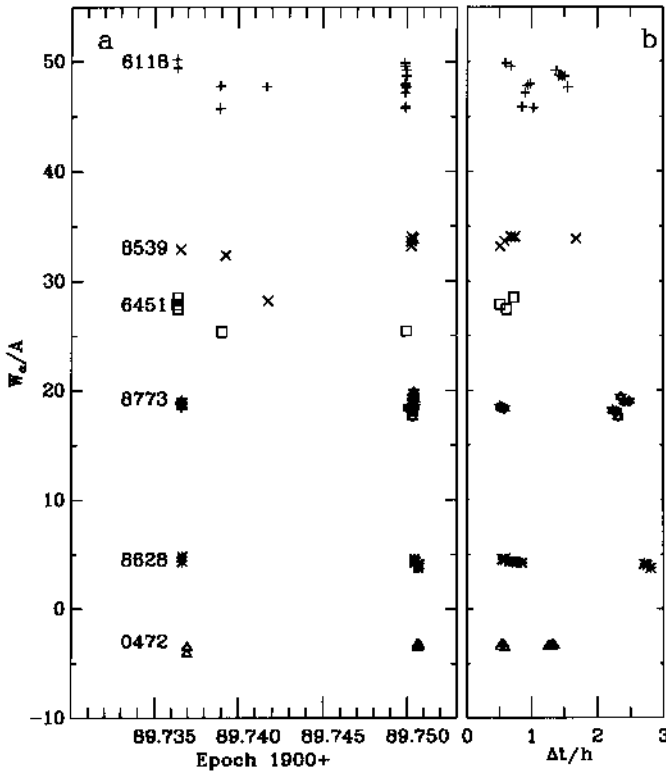
Fig. 4. Investigation of short-term variability. We have plotted here W_α for 6 programme stars which have been frequently measured between 1989 Sep. 26 (= 1989.736−7) and Oct. 1 (= 1989.750−1). The left panel shows all data of this epoch, the right panel a blow-up of the data for Oct. 1 (for HR 6451: Sep. 26), sorted on a timescale Δt measured in hours, with arbitrary zero-point

class 1 for this type of profiles. A second major class exists which collects all profiles which are asymmetric in a certain typical sense: they are cyclically variable, and they exhibit, in case of Fe II lines, a typical "steeple-like" shape in phases of strong asymmetry. Hanuschik et al. (1995a) interpret these *class 2* profiles as being due to a *distorted* Keplerian disk hosting a global density wave.

Figure 2 shows a selection of line profiles typical of class 2 shapes. For pole-on disks, we have found only mildly asymmetric examples in our atlas. For $i \approx 30°$, the typical steeple-type shape for the kinematical profile is visible in the Fe II line, with a very steep and narrow dominating peak, and an almost suppressed secondary peak. Around the corresponding radial velocity position in Hα, a strong flank inflection and a single peak are visible, both caused by the convolution of the NSB function and the dominating kinematical peak. On the red side of Hα, no pronounced structure is visible, corresponding to the fact that the secondary kinematical peak is suppressed.

At high inclinations, the flank inflections disappear like in class 1 profiles. Finally shell absorption arises in edge-on disks, with the asymmetry of the velocity field reflected in the asymmetry of the absorption trough.

4.3. Classification

We have classified the profile shapes observed in our programme stars with the scheme proposed in the previous section. Since essentially all Hα profiles in our atlas are optically thick (winebottle structure becomes visible if $F_\alpha/F_c \gtrsim 1.5$, see HR 5193 in Fig. 55), and Fe II profiles are optically thin (they never show winebottle inflections), only two dimensions remain for each observed Hα or Fe II profile. These are (inclination parameter) × (kinematical parameter).

The inclination indicator is coded as (see Fig. 3)

- *P* for profiles from pole-on disks (single [merged] NSB peak and winebottle-type shoulders which may form together triple peaks in extreme cases),
- *L* for low to intermediate inclinations (double NSB/kinematical peaks plus weaker shoulders),
- *H* for high inclinations (double kinematical peaks, no shoulders, V-shaped central depression in Fe II lines),
- *E* for edge-on disks (deep central depression, below continuum in Fe II lines).

An example for triple peaks is provided by χ Oph (Fig. 62). In one single case, a P-type profile is optically thick enough to show *NSB peak splitting*, i.e. $\Delta v_{\rm nsb} > \Delta v_{\rm kin}$ (HR 2825 in 1985, see Fig. 34). We classify the profiles merely from their shape, the stellar $v \sin i$ value does not enter. We therefore provide an independent (though not very precise) measure for inclination here. The estimated inclination angles are $i \lesssim 10°$ for P-type profiles, $10° \lesssim i \lesssim 60°$ for L-type profiles, $60° \lesssim i \lesssim 80°$ for type-H, and $i \gtrsim 80°$ for type-E.

Table 4. Short-term variations (Sep. 26-Oct. 1, 1989)

Star HR	$\Delta t \leq 3$ hours (Oct. 1)				$\Delta t = 5$ days (Sep.26–Oct.1)		
	N	mean W_α/Å	ΔW_α/Å	$\Delta W_\alpha/W_\alpha$	mean W_α/Å	ΔW_α/Å	$\Delta W_\alpha/W_\alpha$
472	9	-3.40	0.13	4%	-3.60	0.20	6%
6118	12	48.1	1.9	4%	48.1	2.0	4%
6451	3[a]	27.9	0.5	2%	26.2	1.2	5%
8539	5	33.8	0.3	1%	31.8	1.4	4%
8628	9	4.26	0.27	6%	4.44	0.25	6%
8773	13	18.7	0.7	4%	18.7	0.05	< 1%

[a] Sep. 26, 1989

The kinematical state is indicated by "1" for class 1 profiles, and by "2" for class 2 profiles.

The last column of Table 2 contains the shape coding. Uncertain coding is indicated by a colon, ... denotes profiles which do not fit in our system (due to short-term variability or irregular profile shape), and "abs" indicates a pure absorption line. Symbols in brackets denote weak Hα emission lines which do not show flank inflections due to low optical depth.

5. Short-term variability of emission lines

5.1. Days or shorter

It is well known that Be stars may show at times line profile variability on short timescales (e.g., Harmanec 1991). Most such observations concern *photospheric absorption lines* where low-amplitude bumps have been found, moving across the line profile and interpreted as evidence for pulsations. The observations of Smith (1989) of faint emission bumps in λ Eri are another type of short-term phenomenon, indicating photosphere-disk interaction.

Usually we have covered in our atlas typical timescales of months up to years. In September/October 1989, we have furthermore systematically searched for *short-term* Hα variability in six programme stars: HR 472, HR 6118, HR 6451, HR 8539, HR 8628, and HR 8773. We have covered timescales Δt of five days, one day, a few hours, and a few minutes.

We have measured the equivalent width of Hα, W_α, by interpolation of the local stellar continuum across the line profile. The results of this search are collected in Table 4 and plotted in Fig. 4.

– $\Delta t \lesssim$ *hours:* All these six stars show scattering in W_α on a relative scale $\leq$ 6%, typically 4%. As a careful check shows, no variability in line profile shape (finestructure) is found. The scatter affects the whole line profile.

– $\Delta t \sim$ *days:* We find the same scattering behaviour with a typical value of 4%. Again no finestructure variability is found.

It follows that the scatter found on both timescales is not physical, but entirely or mostly due to reduction and measuring uncertainties caused by insecure definition of the interpolated stellar continuum. This conclusion is supported by the facts that the scatter found i) is the same on timescales of minutes, hours and days, ii) is not accompanied by finestructure variability, iii) is the same for Hα absorption lines (in α Eri), faint Hα emission (ε PsA), or strong emission.

We conclude that we have found no indication of short-term variability in emission lines on timescales of one day or shorter. Contentions sometimes found in the literature (e.g. Ghosh 1988; Hubert et al. 1988) are not supported by data in our atlas. This is at least true for disk-induced variability (i.e. variability of emission strength) which should not be confused with photosphere-induced variability (variations of the underlying stellar absorption line).

5.2. Few days

The shortest timescale of emission line variability found here is established by two different types of finestructure variability, "binary-type" and "flickering emission-type".

Binary-type. In the stars ζ Tau, HR 2142, and π Aqr, timescales of $< 24^d$ (ζ Tau), few days (HR 2142) and $< 12^d$ (π Aqr) have been found (see Figs. 17d, 22d, 78d). Two of these stars are known as binaries ($P = 132.91^d$ and 80.86^d for ζ Tau and HR 2142, resp., Pols et al. 1991). In case of HR 2142, the emission line shape furthermore varies with the orbital period (Fig. 22d). This demonstrates that the Be disk is at least distorted by the companion star. In case of π Aqr, no evidence for duplicity is known at present. Its rapid line profile variability, however, could be an indicator for binarity.

Flickering emission. For stars showing flickering emission, timescales of a day are well established and identified with the *dynamical (= orbital)* period in the disk close to the stellar surface. The density distribution in these disks is still inhomogeneous if they are observed in the process of formation. After a few such timescales, cir-

cularization of orbits is achieved and line profile shapes remain constant (with, however, still varying equivalent width). From our atlas, the stars α Eri, λ Eri, HR 3498 (?), and, as prototype, μ Cen (Hanuschik et al. 1993) belong to this subclass.

References

Andrillat Y., 1983, A&AS 53, 319

Andrillat Y., Fehrenbach C., 1982, A&AS 48, 93

Andrillat Y., Jaschek M., Jaschek C., 1988, A&AS 72, 129

Andrillat Y., Jaschek M., Jaschek C., 1990, A&AS 84, 11

Andrillat Y., Jaschek M., Jaschek C., 1994, A&AS 103, 135

Avrett E.H., Hummer D.G., 1965, MNRAS 130, 295

Baade D., 1987, in: Slettebak A., Snow T.P. (eds.), Physics of Be stars, IAU Coll. 92. Cambridge Univ. Press, p. 361

Baade D., Dachs J., van de Weygaert R., Steeman F., 1988, A&A 198, 211

Ballereau D., Alvarez M., Chauville J., Michel R., 1987, Rev. Mex. A&A 15, 29

Barker P., 1986, PASP 98, 44

Dachs J., Eichendorf W., Schleicher H., Schmidt-Kaler Th., Stift M., Tüg H., 1981, A&AS 43, 427

Dachs J., Hanuschik R.W., Kaiser D., et al., 1986, A&AS 63, 87

Dachs J., Hummel W., Hanuschik R.W., 1992, A&AS 95, 437

Doazan V., Sedmak G., Barylak M., Rusconi L., 1991, A Be Star Atlas, esa SP-1147

Ghosh K.K., 1988, Vistas Astron. 31, 281

Ghosh K.K., Kuppuswamy K., Pukalenthi S., Selvakumar G., 1991, AJ 102, 1191

Gies D.R., Willis C.Y., Penny L.R., 1993, PASP 105, 281

Guo Yulian, 1994, Inf. Bull. Var. Stars, No. 4112

Hanuschik R.W., 1986, A&A 166, 185

Hanuschik R.W., 1987, A&A 173, 299

Hanuschik R.W., 1988, A&A 190, 187

Hanuschik R.W., Kozok J., Kaiser D., 1988, A&A 189, 147 (= HKK88)

Hanuschik R.W., Dachs J., Baudzus M., Thimm G., 1993, A&A 274, 356

Hanuschik R.W., Hummel W., Dietle O., Sutorius E., 1995a, A&A 300, 163

Hanuschik R.W., Hummel W., Štefl S., Vrancken M., 1995b, Inf. Bull. Var. Stars No. 4174

Harmanec P., 1991, in: Baade D. (ed.), ESO Workshop on Rapid Variability of OB stars: Nature and Diagnostic Value. ESO Garching, p. 265

Horne K., Marsh T., 1986, MNRAS 218, 761

Huang S.-S., 1972, ApJ 171, 549

Hubert A.M., Hubert H., Dagostinoz B., Floquet M., 1988, in: Cayrel de Strobel G., Spite M. (eds.), Impact of very high S/N spectroscopy on stellar physics, IAU Symp. 132. Kluwer, p. 131

Hummel W., Dachs J., 1992, A&A 262, L17

Hummel W., 1994, A&A 289, 458

Jarad M.M., Hilditch R.W., Skillen I., 1989, MNRAS 238, 1085

Peters G., 1979, ApJS 39, 175

Peters G., 1983, PASP 95, 311

Peters G., 1986, ApJ 301, L61

Peters G., 1988, PASP 100, 207

Poeckert R., Marlborough M., 1978, ApJ 220, 940

Pols O.R., Coté J., Waters L.B., Heise J., 1991, A&A 241, 419

Porri A., Stalio R., 1988, A&AS 75, 371

Slettebak A., 1982, ApJS 50, 55

Slettebak A., Collins G.W., Truax R., 1992, ApJS 81, 335 (= Sl92)

Smak J., 1981, Acta Astron. 31, 395

Smith M., 1989, ApJS 71, 357

Štefl S., 1994, IAU Circ. 6098

Struve O., 1931, ApJ 73, 94
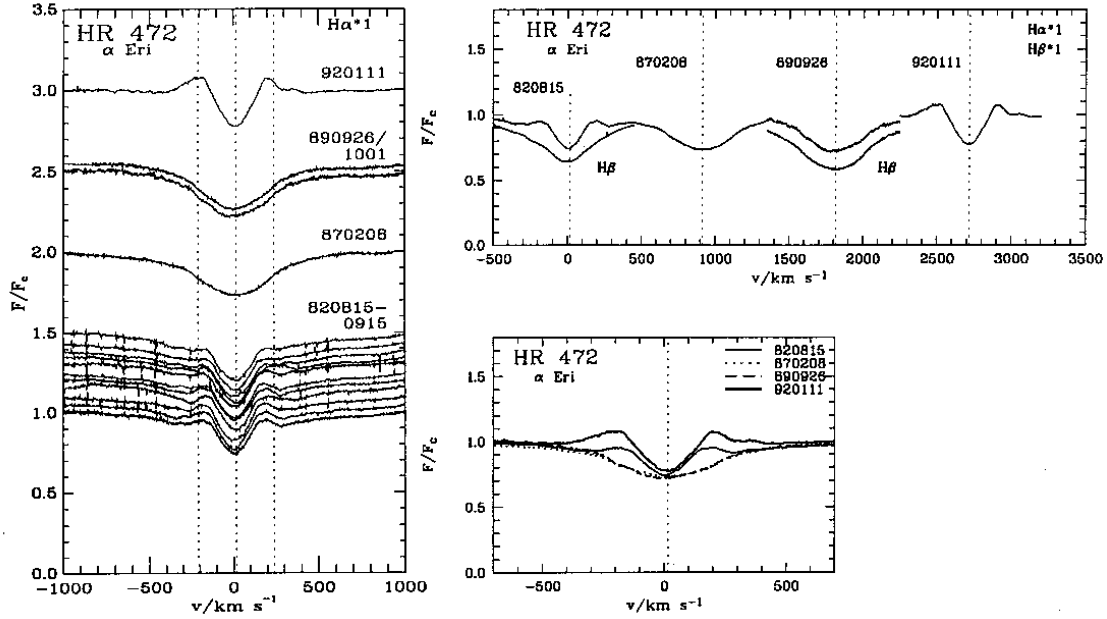
Fig. 5. High-resolution Hα and Hβ profiles for HR 472 = α Eri. All profiles are on a heliocentric radial velocity scale. The peculiar velocity $v_{\rm pec}$ of the star, as taken from the Bright Star Catalogue, is plotted as dotted central vertical line in **a)**, and dotted lines in **b)** and **c)**. The other two vertical lines in **a)** mark $v_{\rm pec} \pm v \sin i$. **a)** shows a vertical time sequence; profiles are shifted by arbitrary amounts, where – if possible – an attempt has been made to indicate the time shift by corresponding vertical shifts. Dates are given in the format 820815 = August 15, 1982. Profiles from 1982 (bottom to top): 0815, 16, 17, 18, 19, 20, 29, 30, 0913, 14, 15. **b)** usually shows the profile set from **a)** in a horizontal display (here: only a subset). The radial velocity shift is indicated by the distance between two dotted lines. **c)** compares all Hα profiles plotted on top of each other
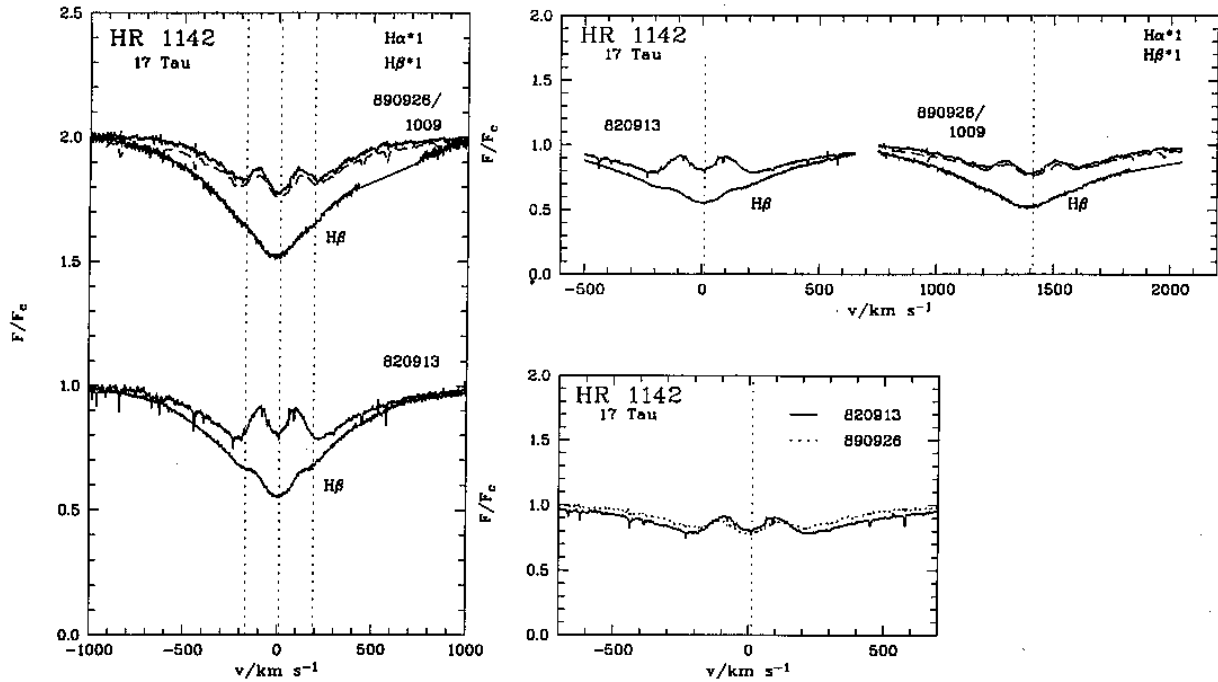
Fig. 6. Same as Fig. 5, for HR 1142 = 17 Tau. Here, and in all following plots, the convention is that profiles plotted as *broken* line have been measured on the date given *behind* the slash (here: 891009 in **a)**)
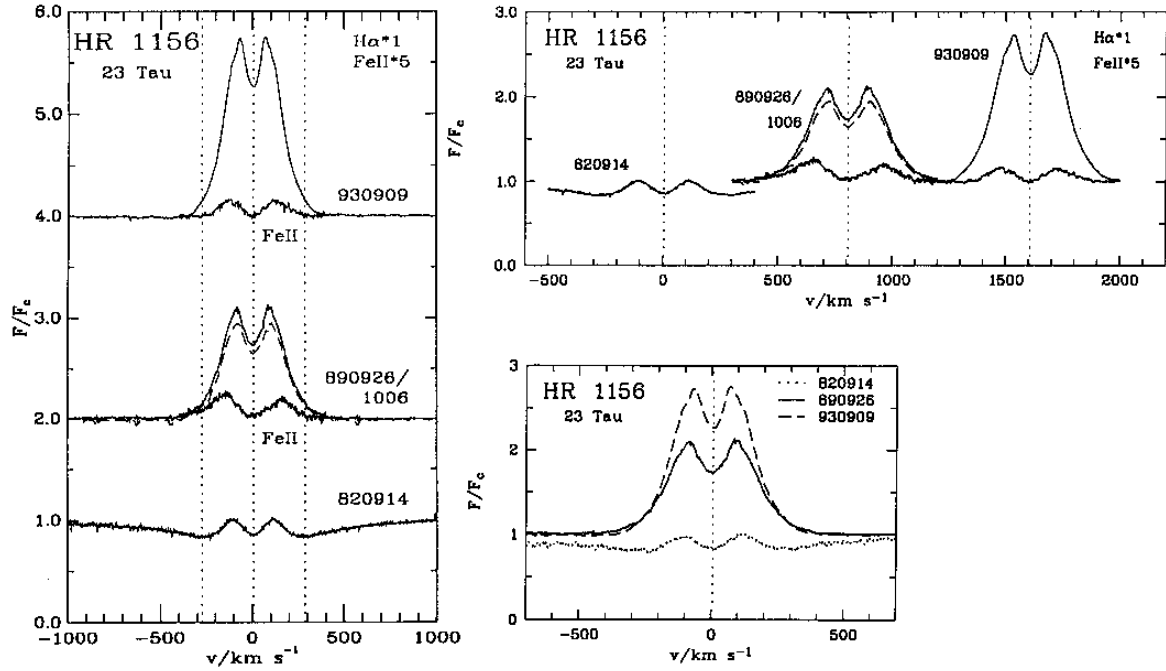
Fig. 7. As Figs. 5 and 6, for HR 1156 = 23 Tau. Here, and in most other following plots, we show in **a)** and **b)** a comparison of quasi-simultaneously measured Hα and Fe II lines. If not otherwise noted, we have plotted the Fe II λ5317 line. The scaling factor for the flux enhancement (Eq. 1) is given in the figure
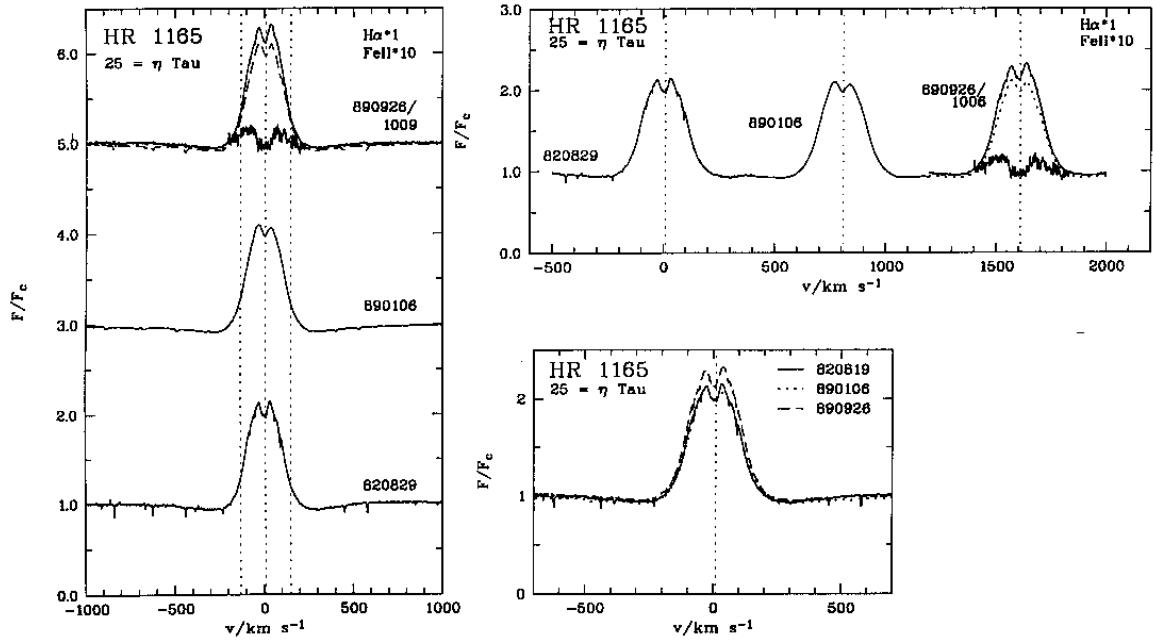
Fig. 8. Hα and Fe II profiles for HR 1165
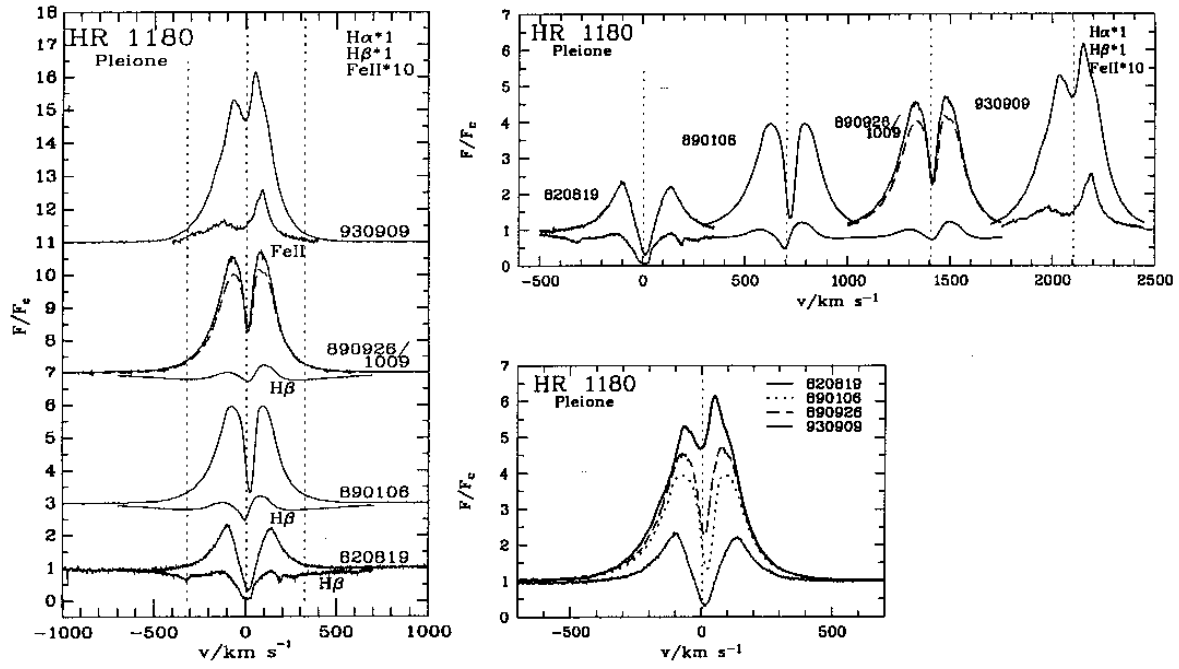
Fig. 9. Hα, Hβ and Fe II profiles for HR 1180. Note the transition from Be-shell spectrum (until 1989) to Be spectrum (1993)
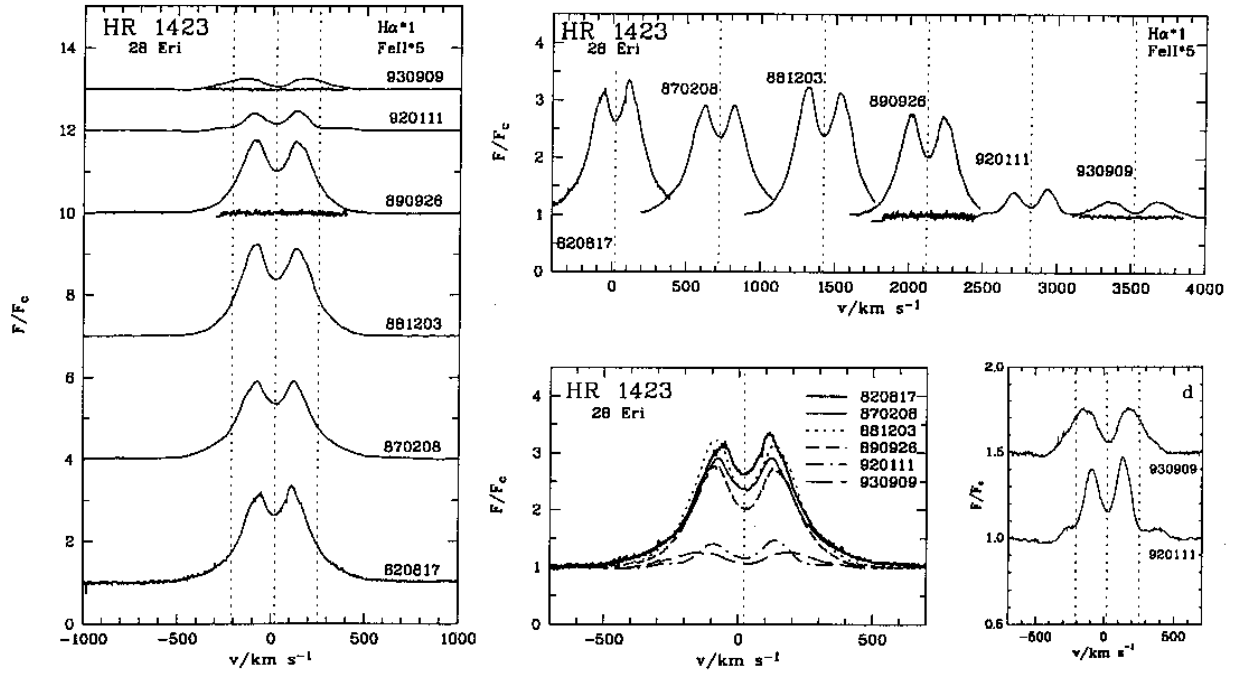
Fig. 10. Hα profiles and Fe II measurements for HR 1423. A close-up of the unusual Hα profile from 1992 is shown in panel d
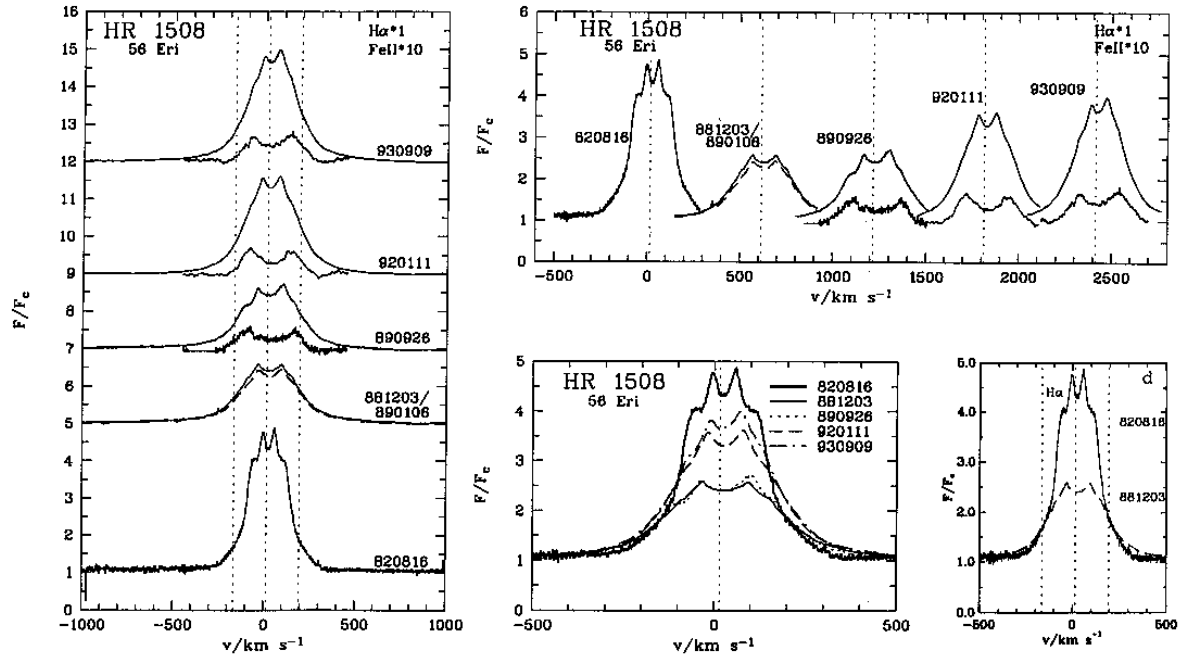
Fig. 11. Hα and Fe II profiles for HR 1508. Panel d shows the change of line width in Hα between 1982 and 1988
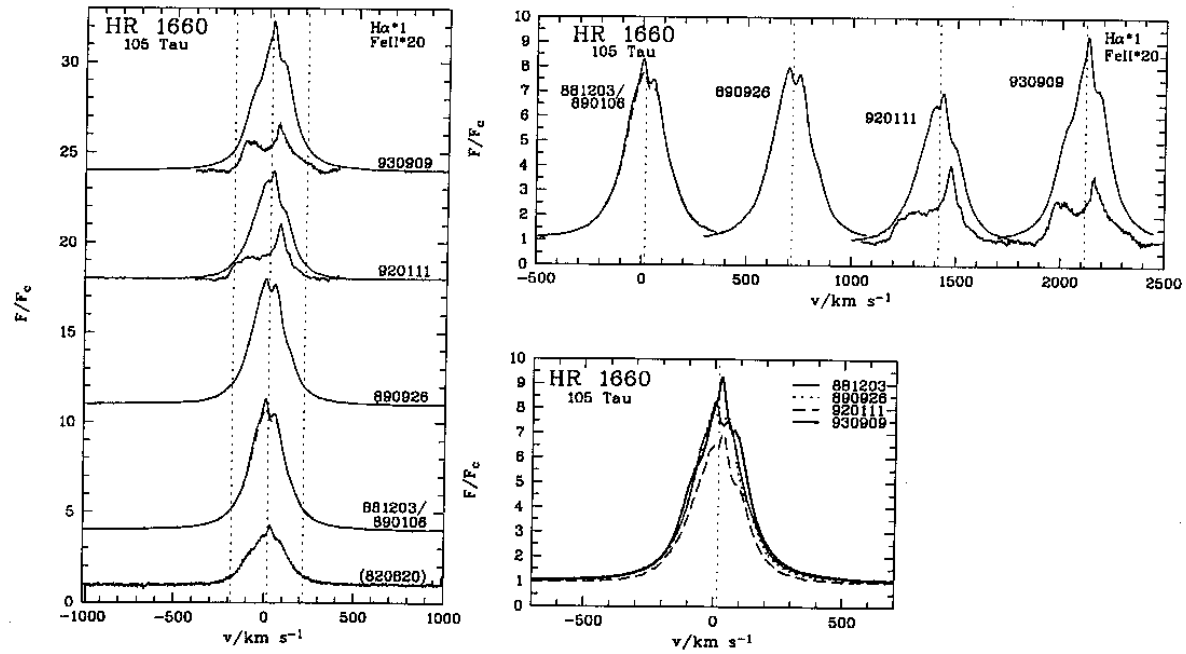
Fig. 12. Hα and Fe II profiles for HR 1660. The 820820 profile has an unknown flux scale, only the profile shape is usable for interpretation
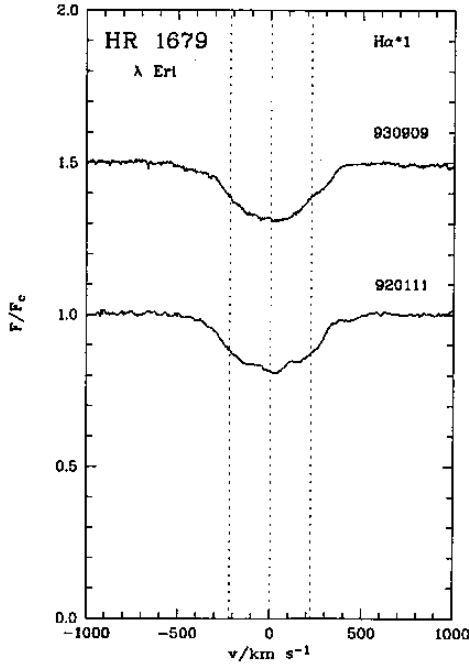
Fig. 13. Hα profiles for HR 1679
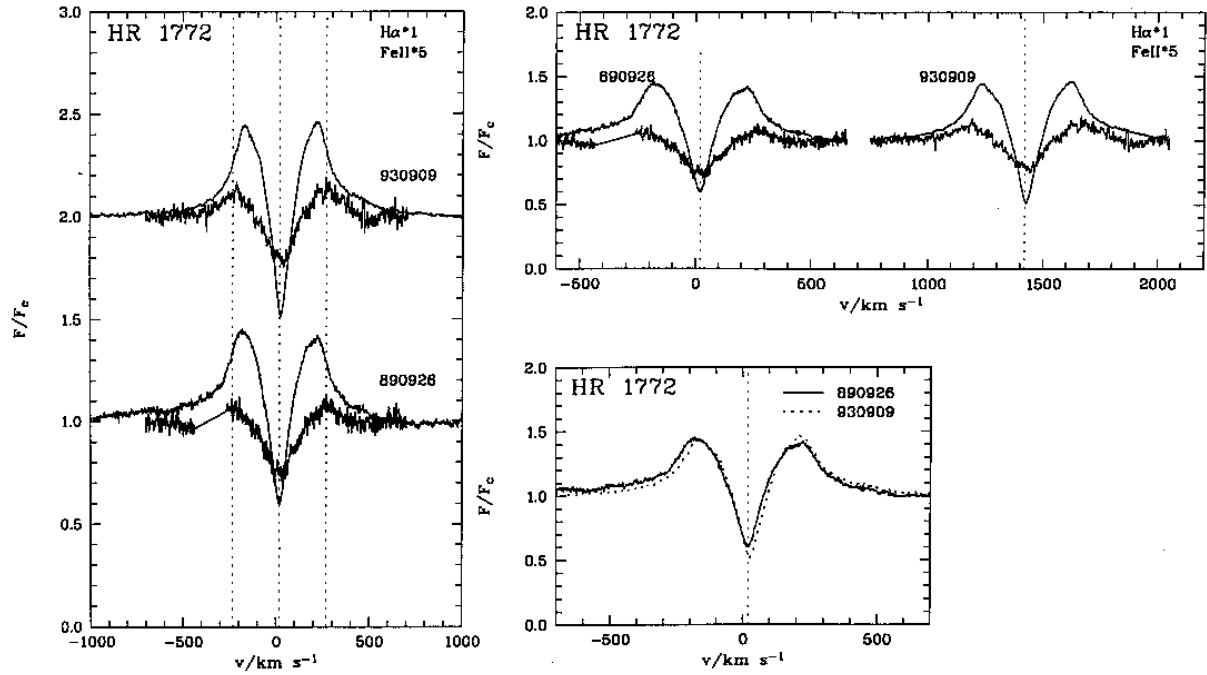
Fig. 14. Hα and Fe II profiles for HR 1772
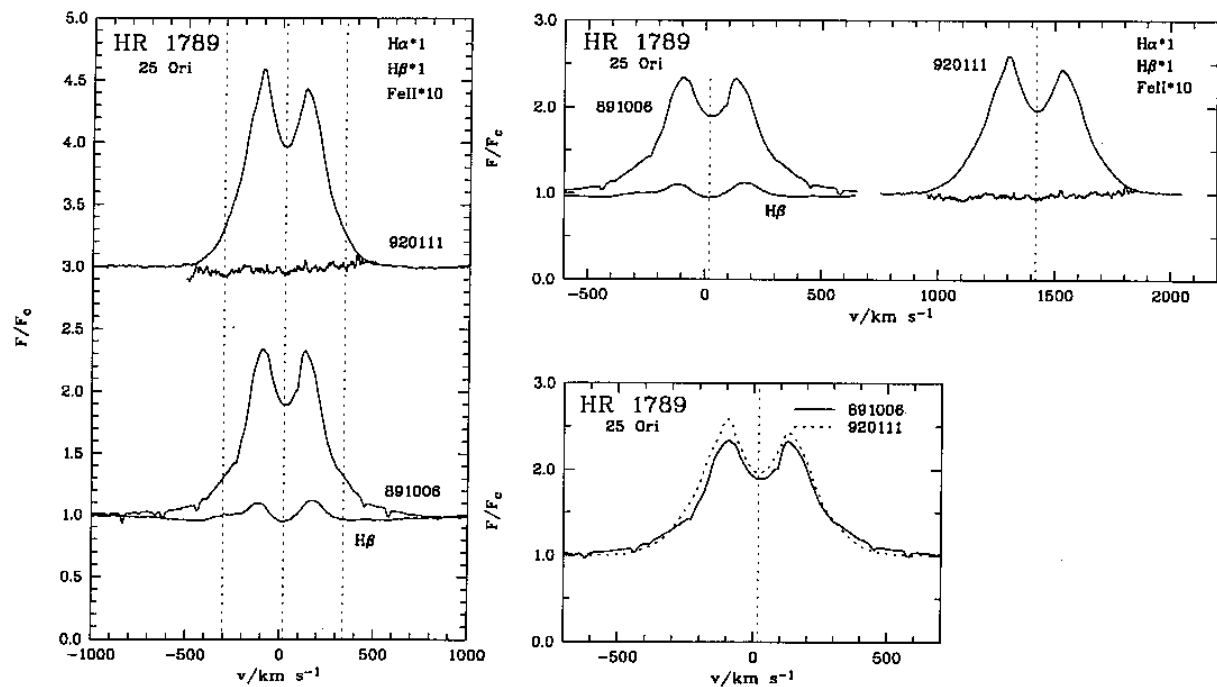
Fig. 15. Hα, Hβ and λ5317 profiles for HR 1789 (no emission visible in Fe II)
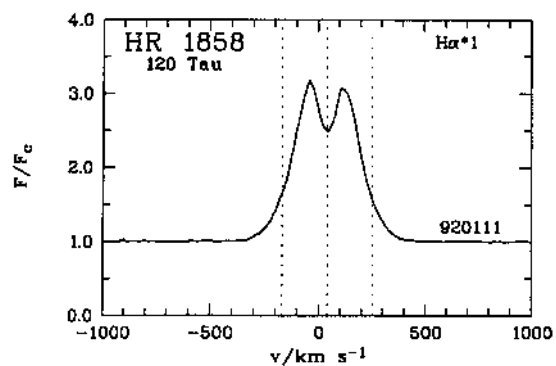
Fig. 16. Hα profile for HR 1858
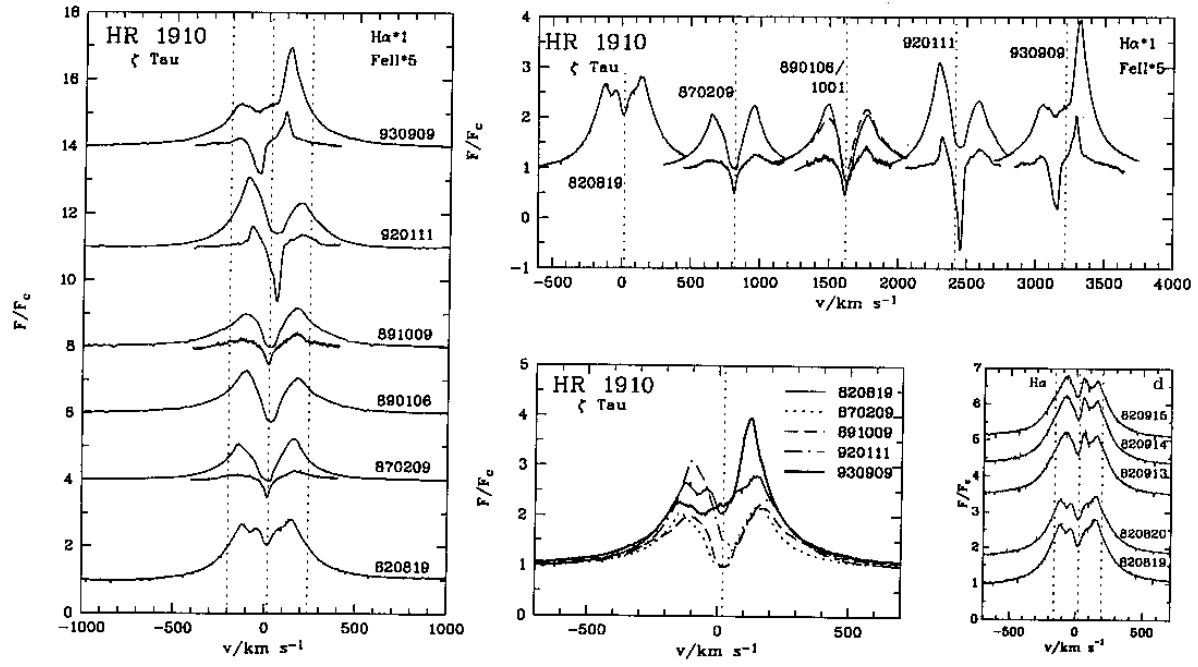
Fig. 17. Hα and Fe II profiles for HR 1910. Note that by the expansion of the Fe II profiles also the shell troughs are affected
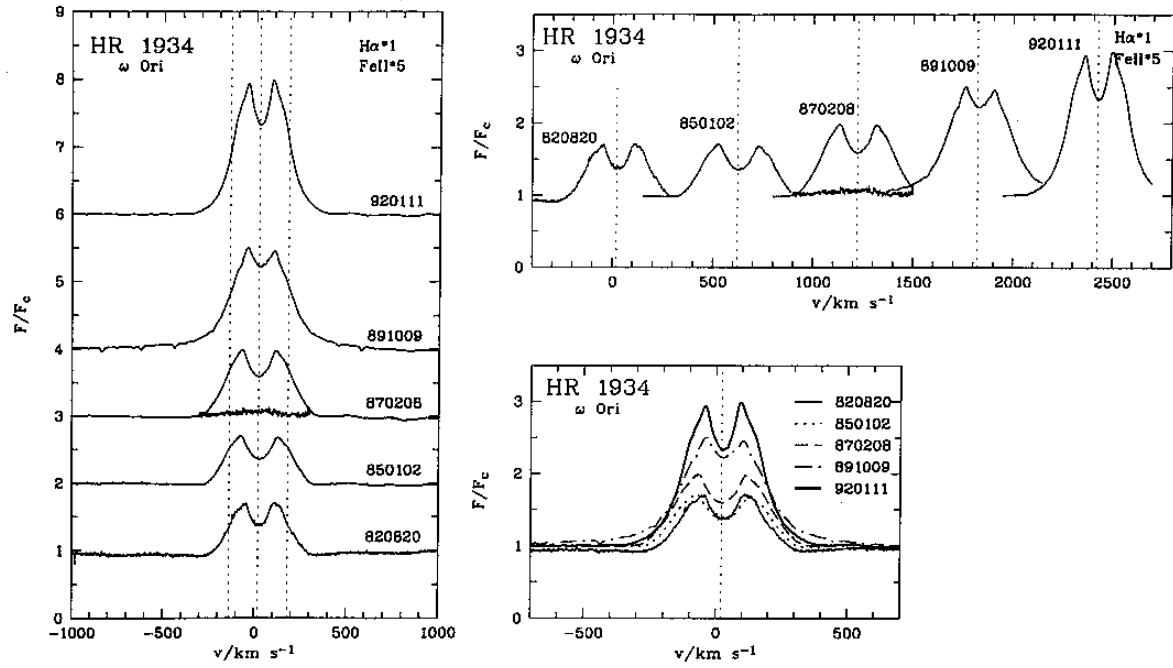
Fig. 18. Hα and λ5317 profiles for HR 1934 (no emission visible in Fe II)
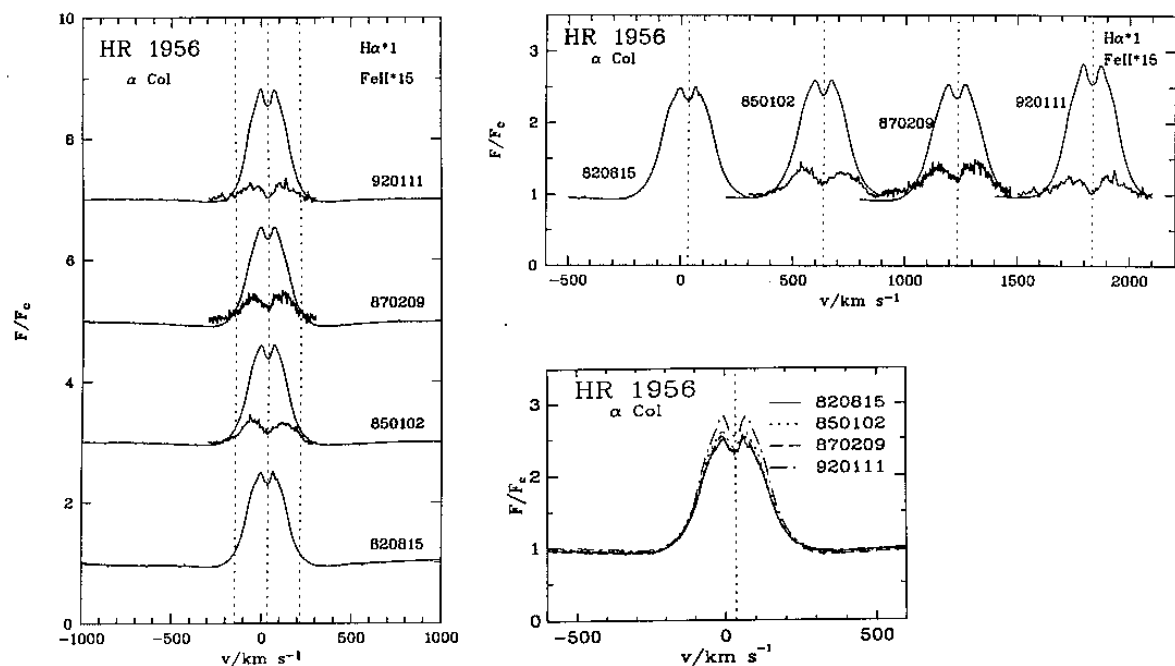
Fig. 19. Hα and Fe II profiles for HR 1956
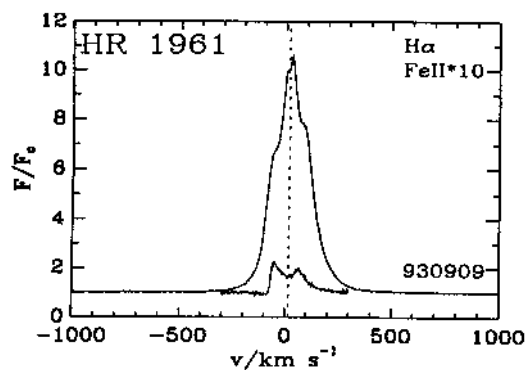
Fig. 20. Hα and Fe II profile for HR 1961
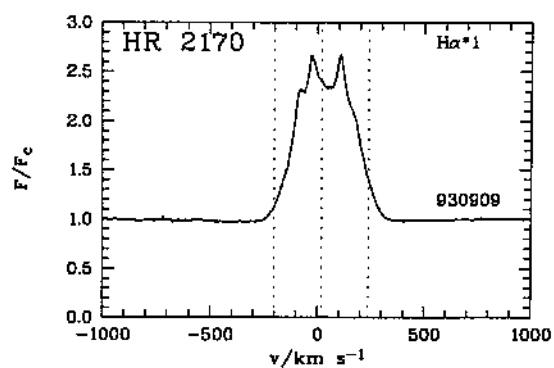
Fig. 21. Hα profile for HR 2170
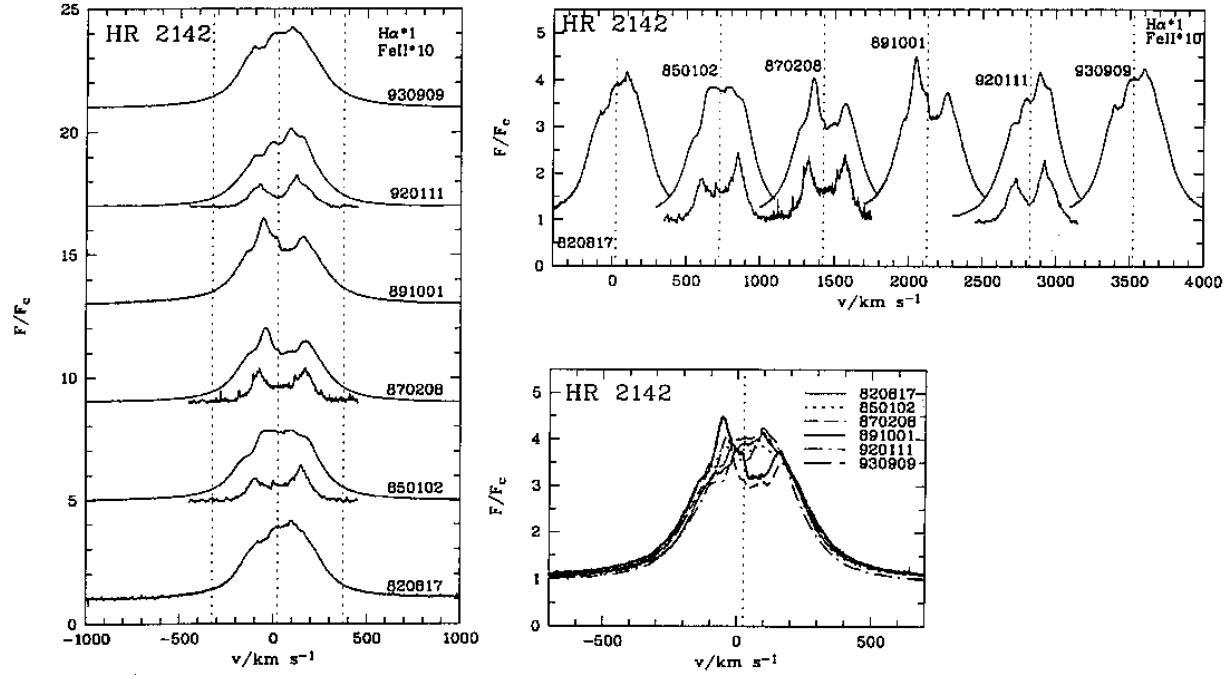
Fig. 22. Hα and Fe II profiles for HR 2142
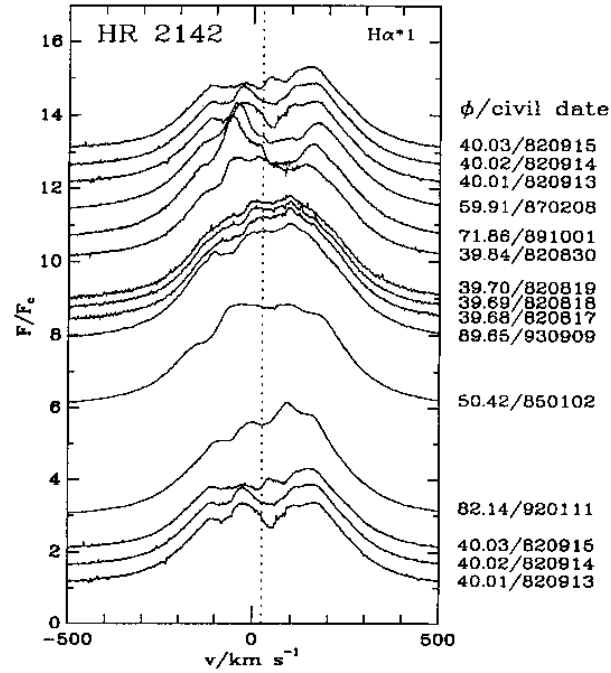
Fig. 23. Phase-binned Hα profiles for HR 2142, using $P_{orb} = 80.860$ days and $T_0 = $ JD 2 441 990.5 (Peters 1983)
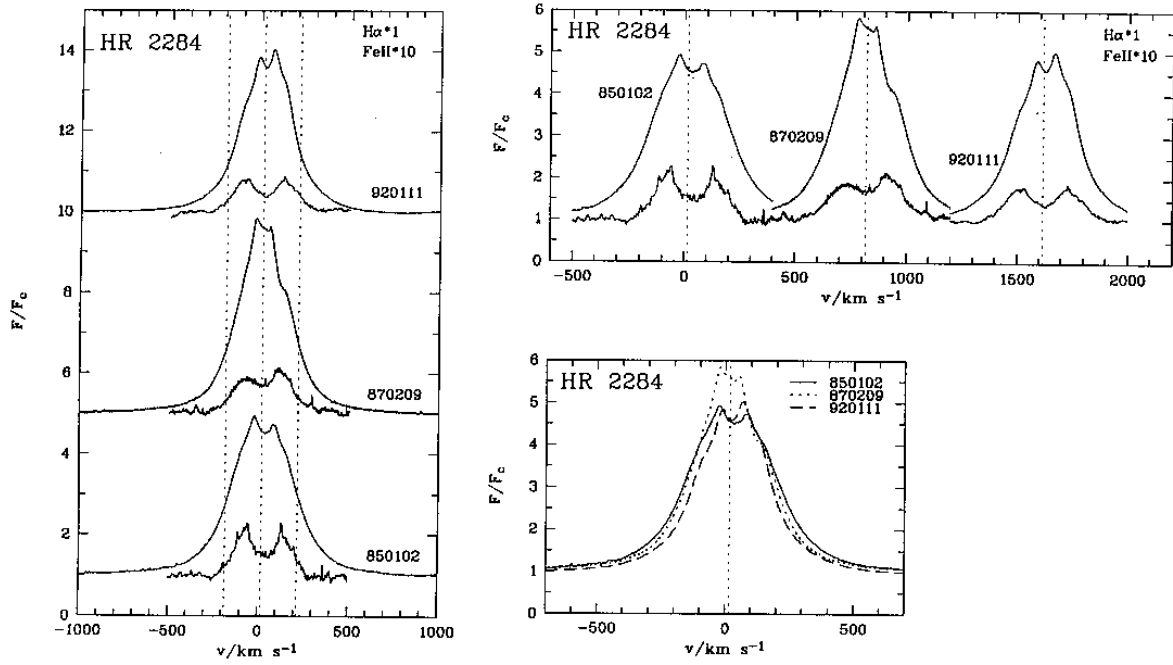
Fig. 24. Hα and Fe II profiles for HR 2284
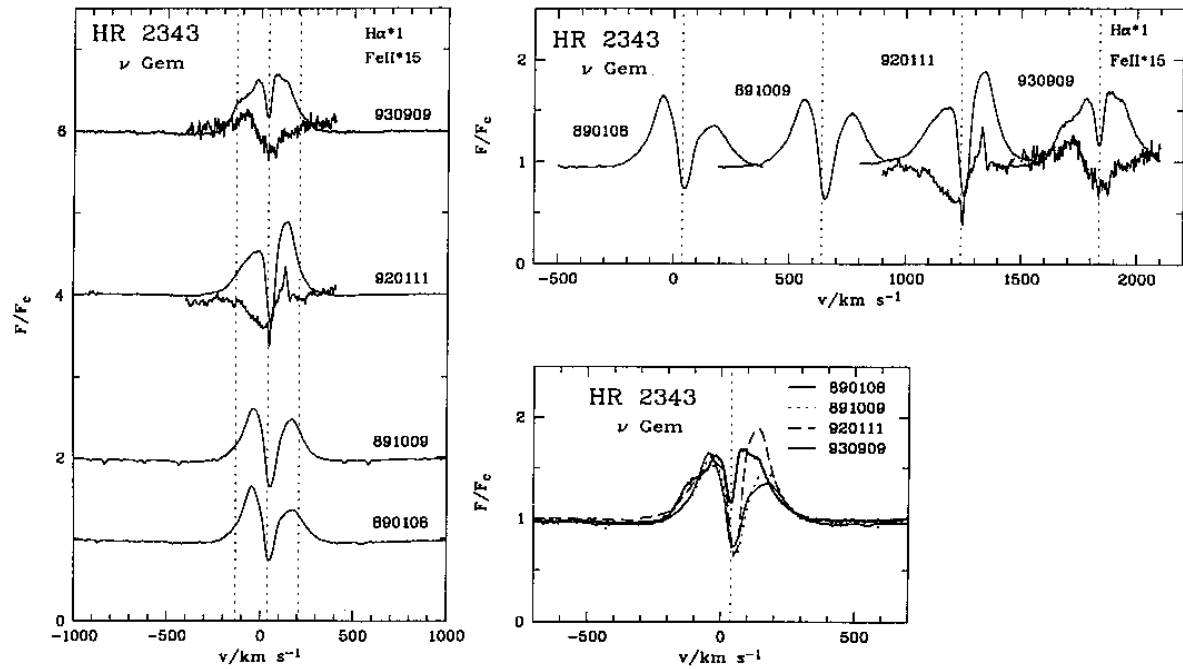
Fig. 25. Hα and Fe II profiles for HR 2343. Note that by the expansion of the Fe II profiles also the shell troughs are affected
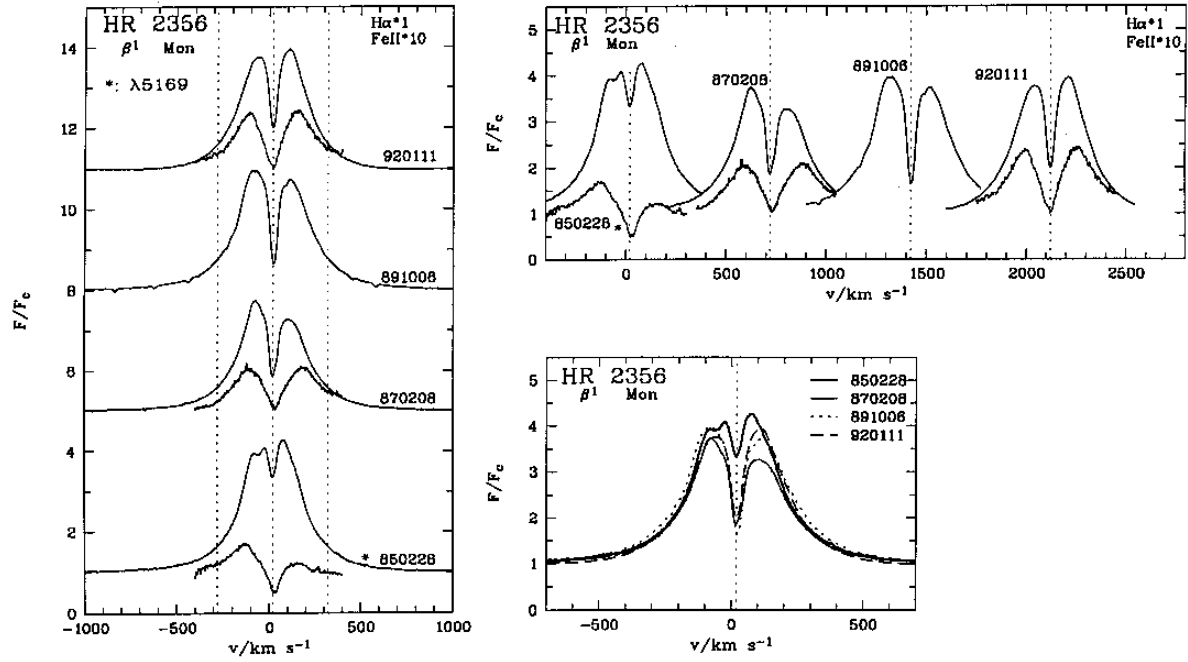
Fig. 26. Hα and Fe II profiles for HR 2356. In 1985, the Fe II λ5169 line has been measured instead of λ5317 (marked by an asterisk)
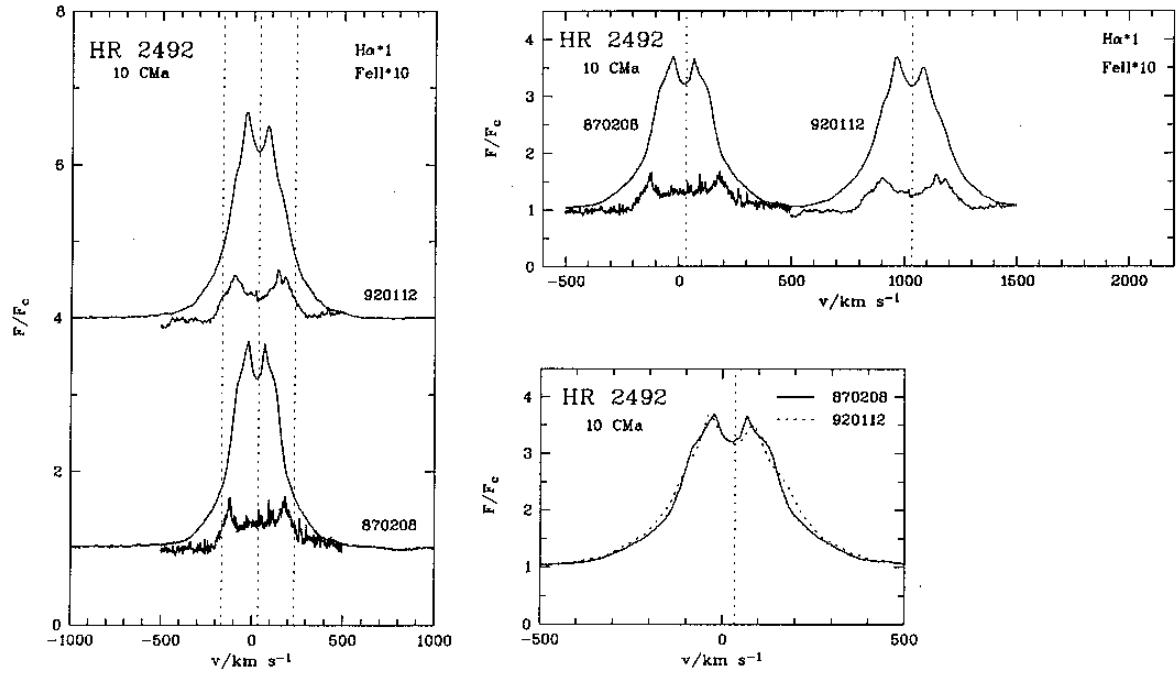
Fig. 27. Hα and Fe II profiles for HR 2492
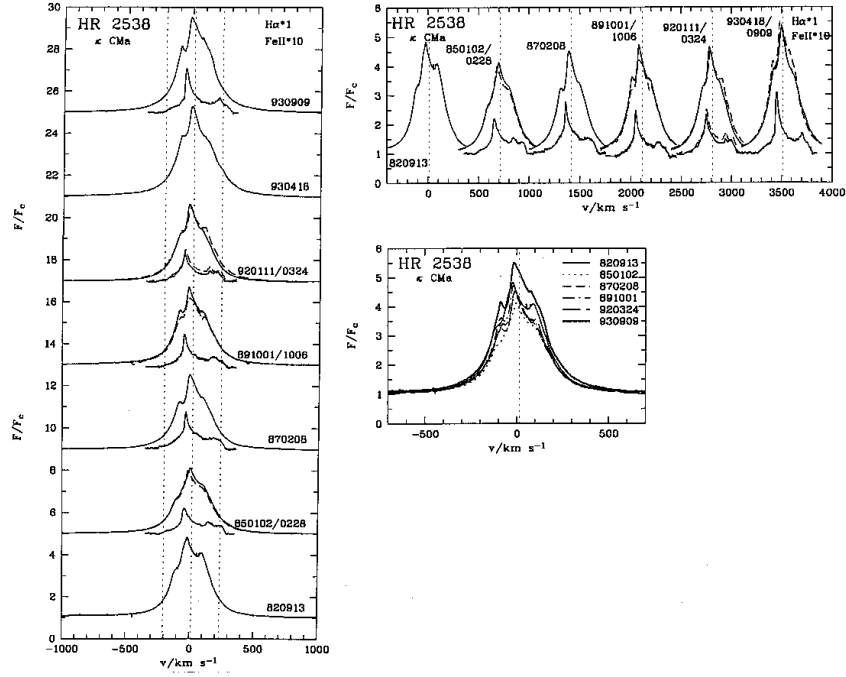
Fig. 28. Hα and Fe ɪɪ profiles for HR 2538
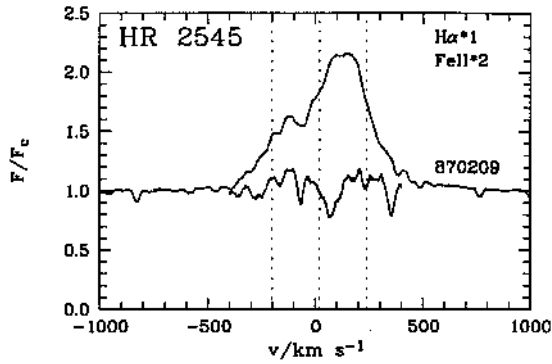
Fig. 29. Hα and Fe ɪɪ profile for HR 2545; the A-type
companion star produces the narrow absorption features
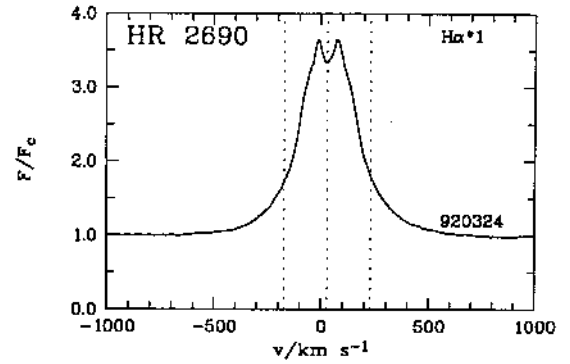
Fig. 30. Hα profile for HR 2690
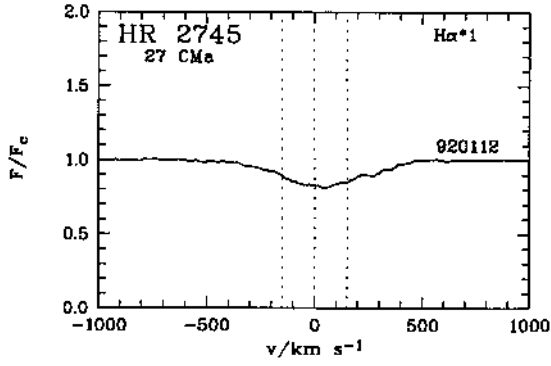
Fig. 31. Hα profile for HR 2745
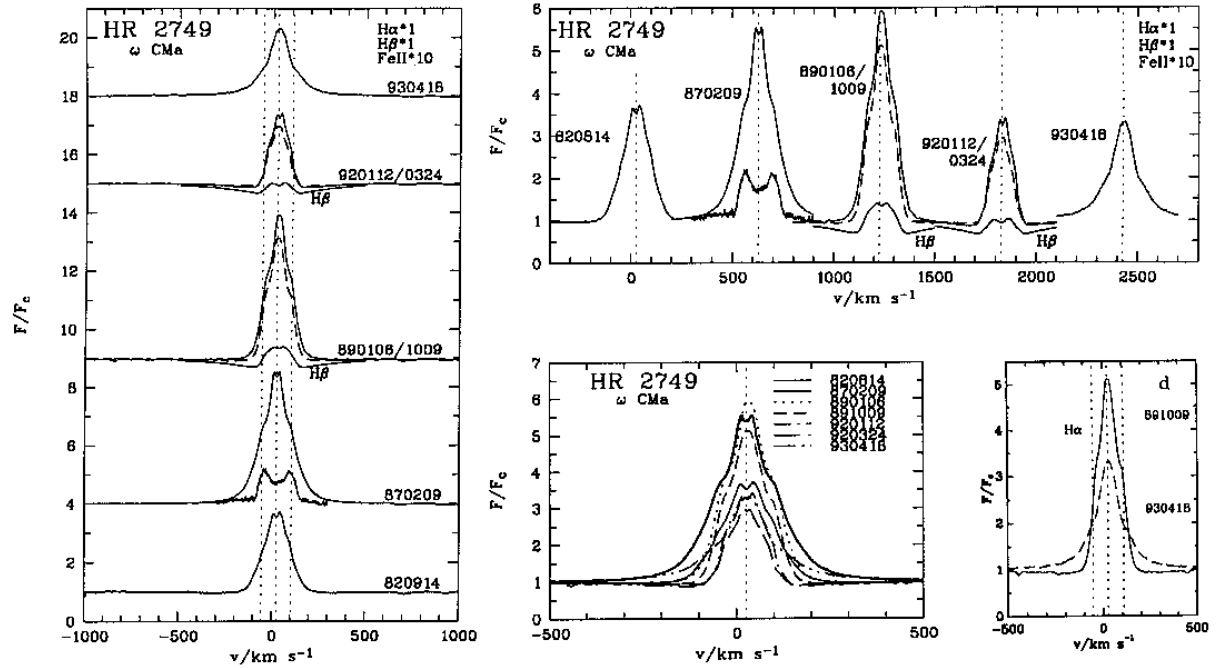
Fig. 32. Hα, Hβ and Fe ɪɪ profiles for HR 2749. Panel d demonstrates the dramatical change in width and height of the Hα line between 1989 and 1992
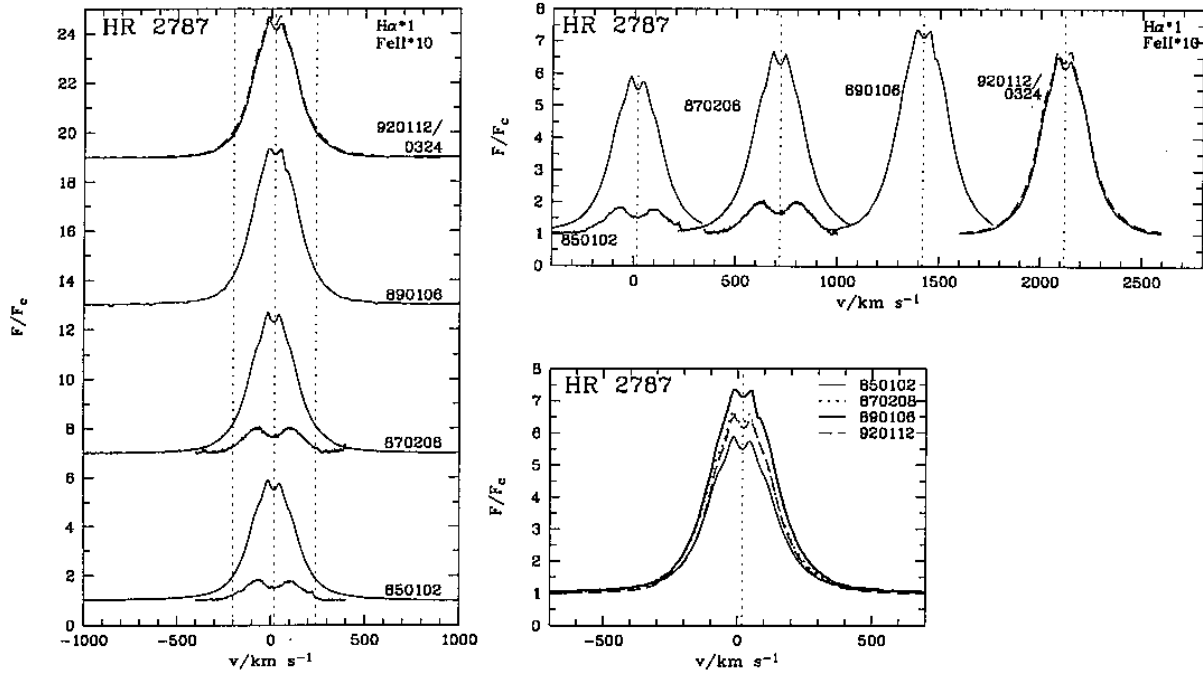
Fig. 33. Hα and Fe II profiles for HR 2787
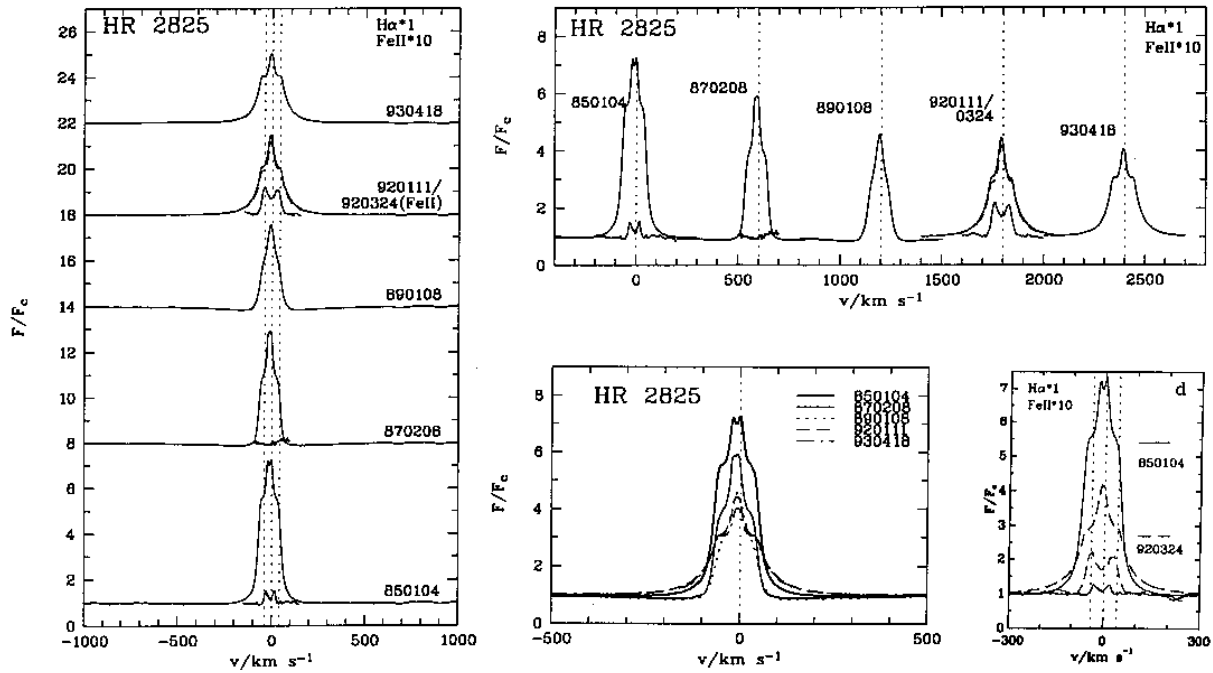
Fig. 34. Hα and Fe II profiles for HR 2825. The Hα profile from 1985 is the only one known to us showing peak splitting due to NSB broadening. Panel d shows the variation of line width and intensity both of Hα and Fe II (anti-correlation)
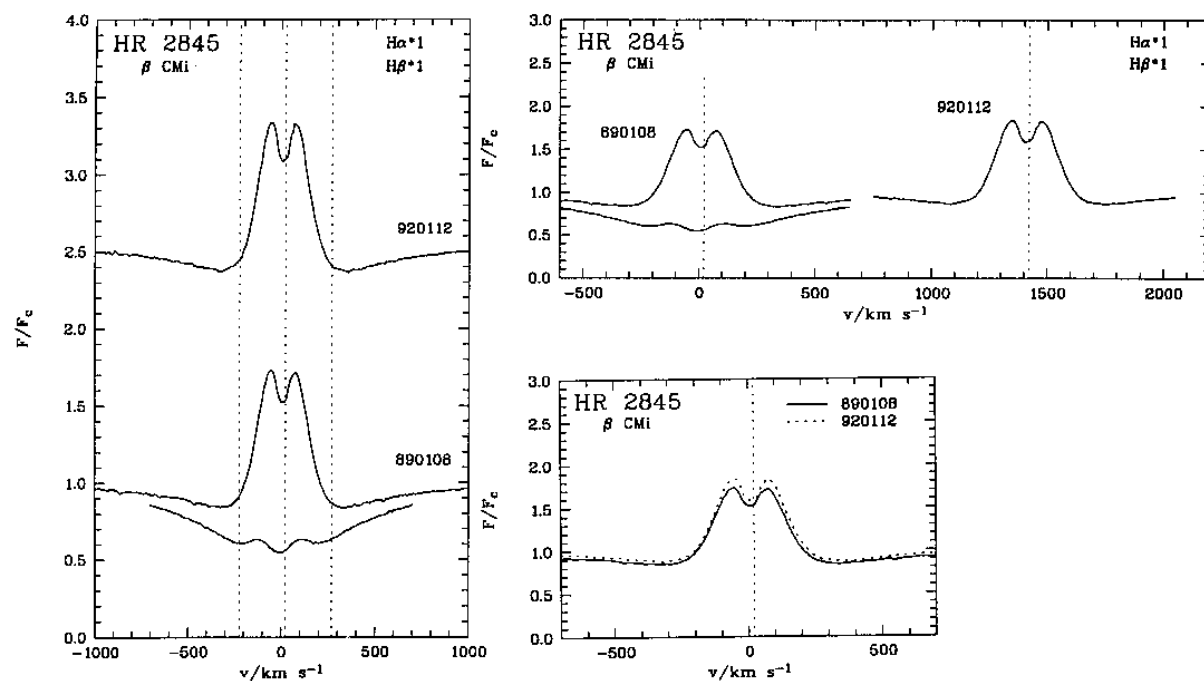
Fig. 35. Hα and Hβ profiles for HR 2845
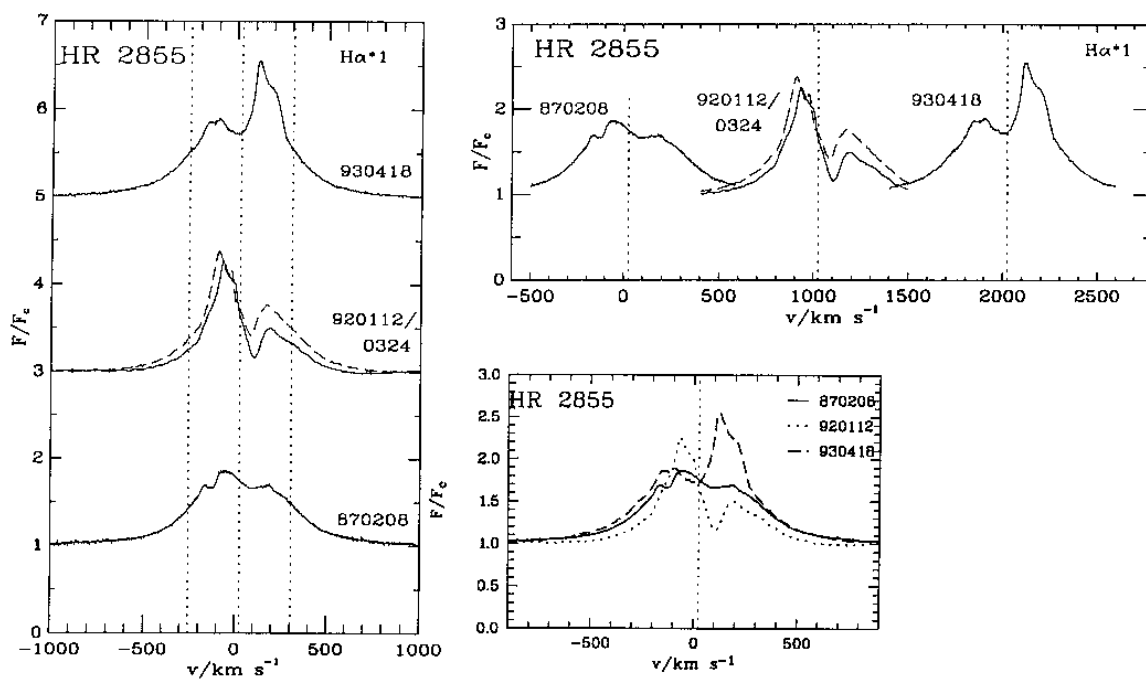
Fig. 36. Hα profiles for HR 2855 (Fe II emission was present in 1992, but profile has been lost)
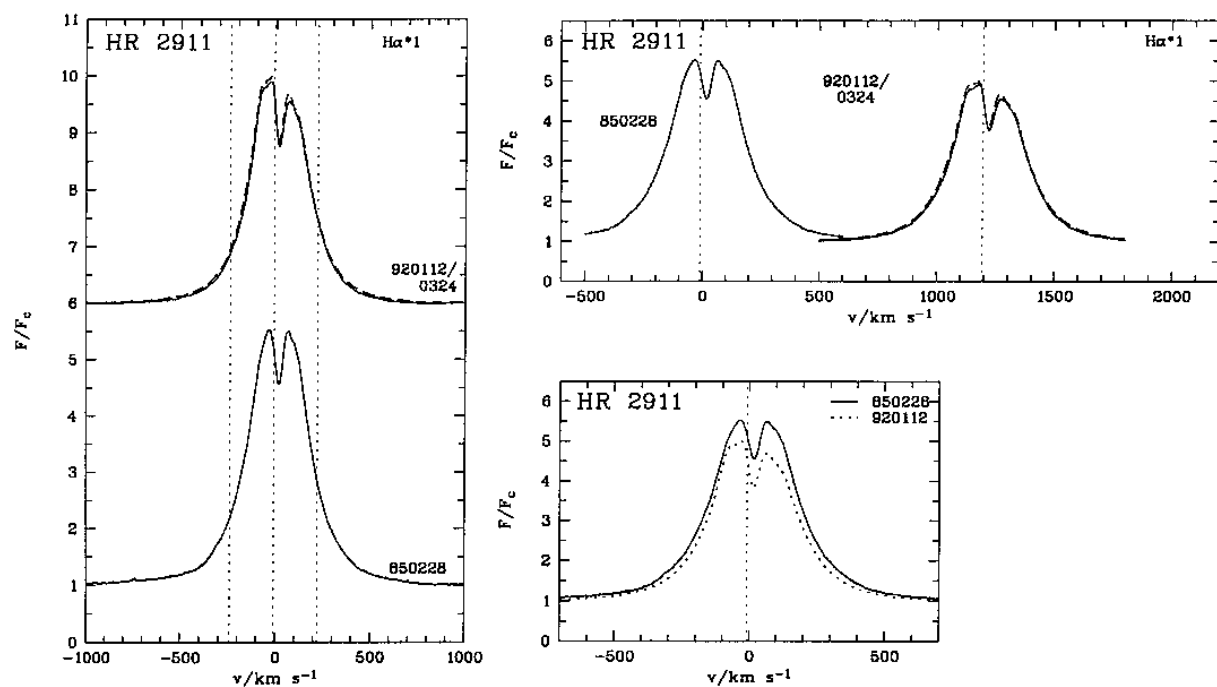
Fig. 37. Hα profiles for HR 2911
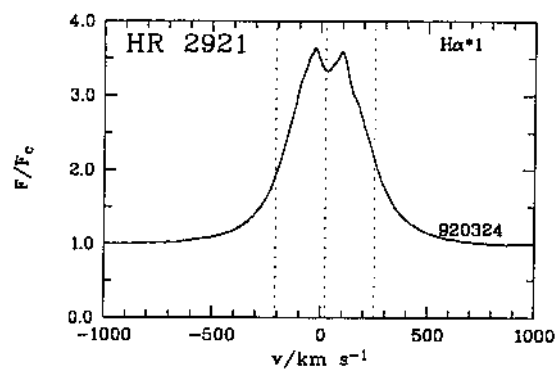
Fig. 38. Hα profile for HR 2921
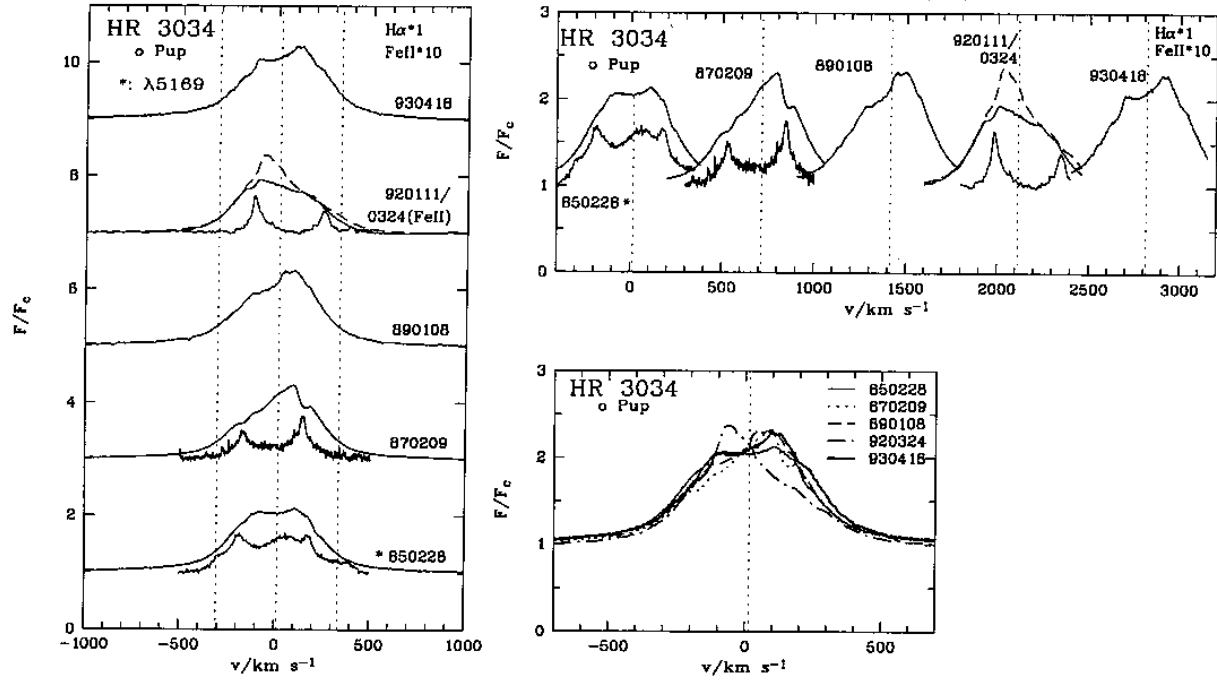
Fig. 39. Hα and Fe II profiles for HR 3034. The complex structure of the Fe II λ5169 line is due to faint blends
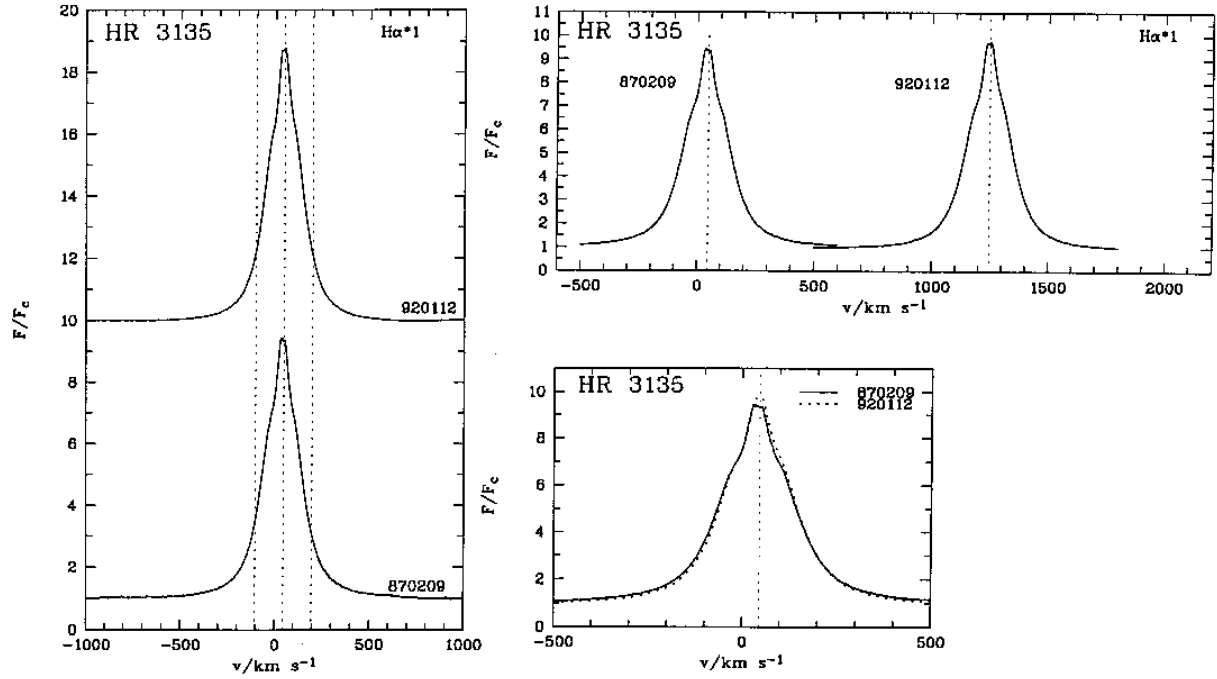
Fig. 40. Hα profiles for HR 3135
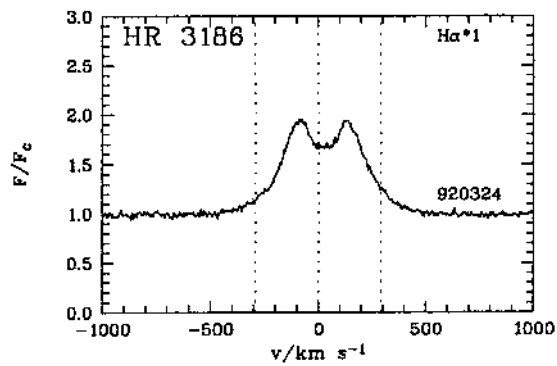
Fig. 41. Hα profile for HR 3186
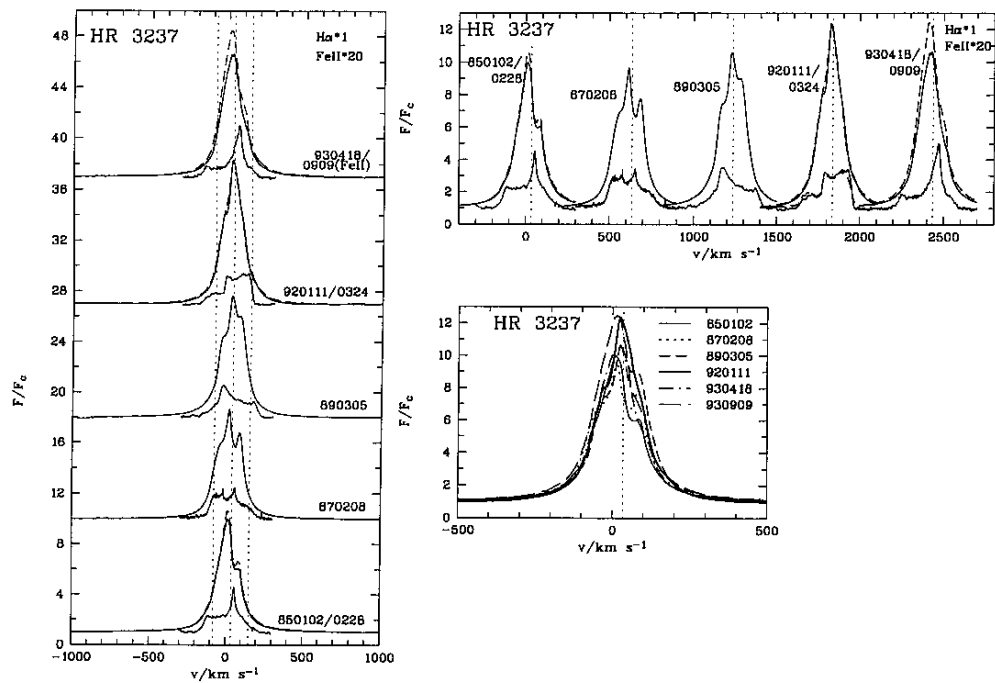
Fig. 42. Hα and Fe II profiles for HR 3237
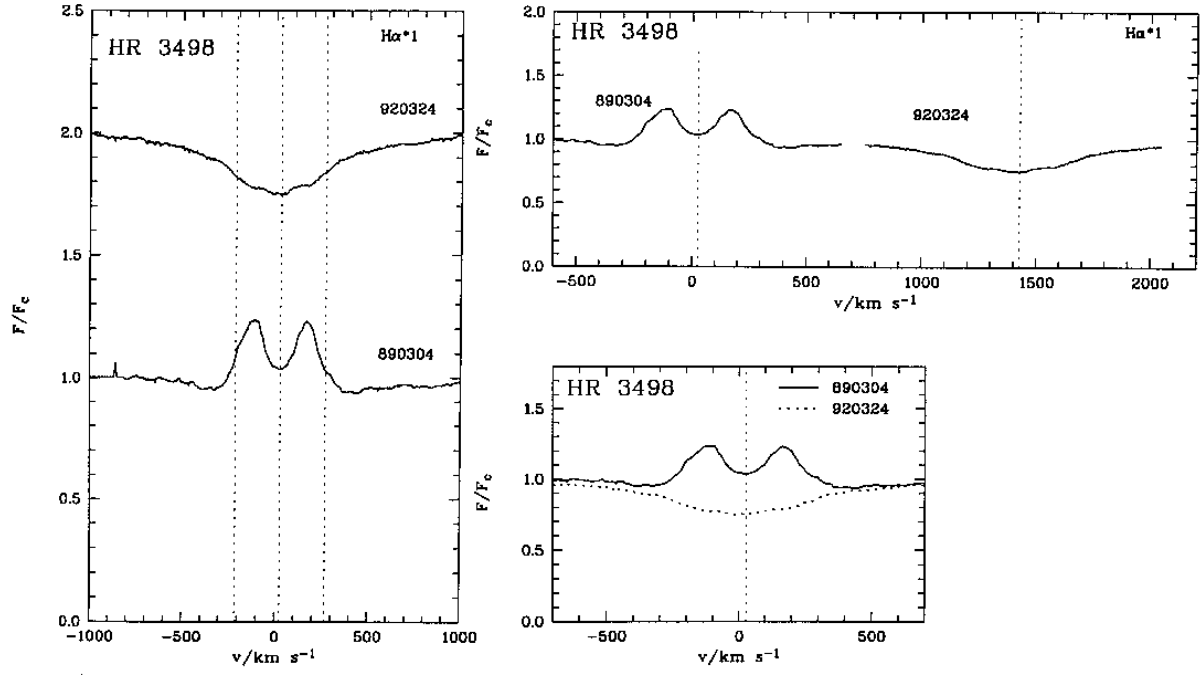
Fig. 43. Hα profiles for HR 3498
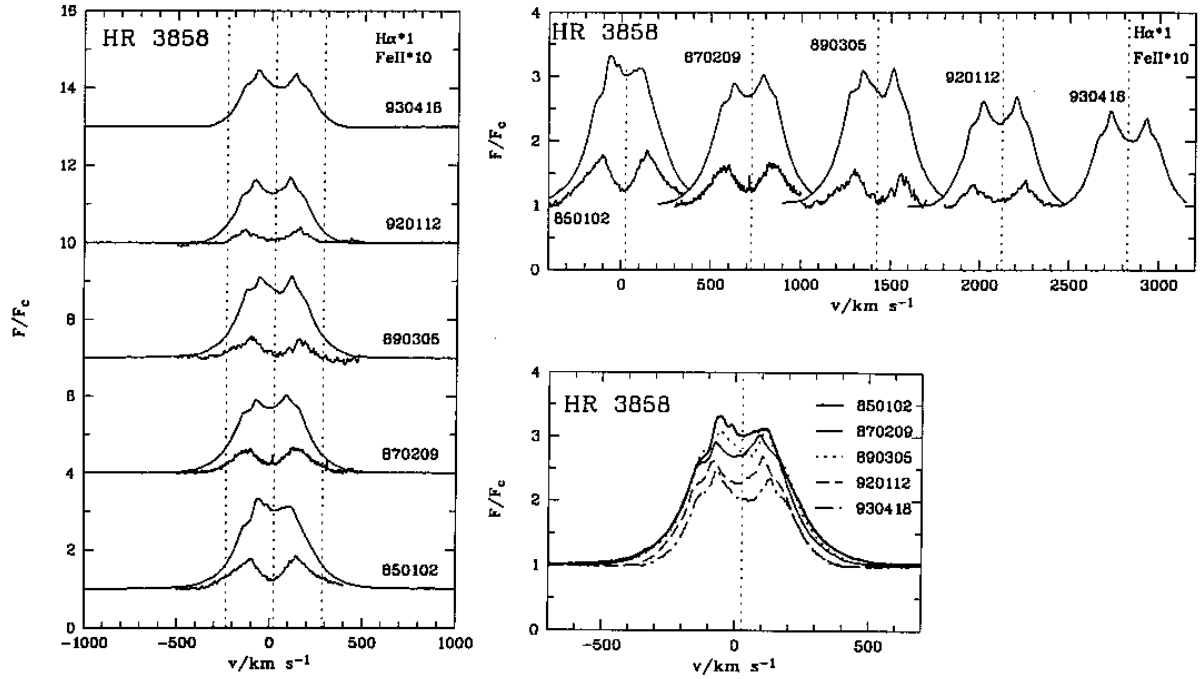
Fig. 44. Hα and Fe II profiles for HR 3858
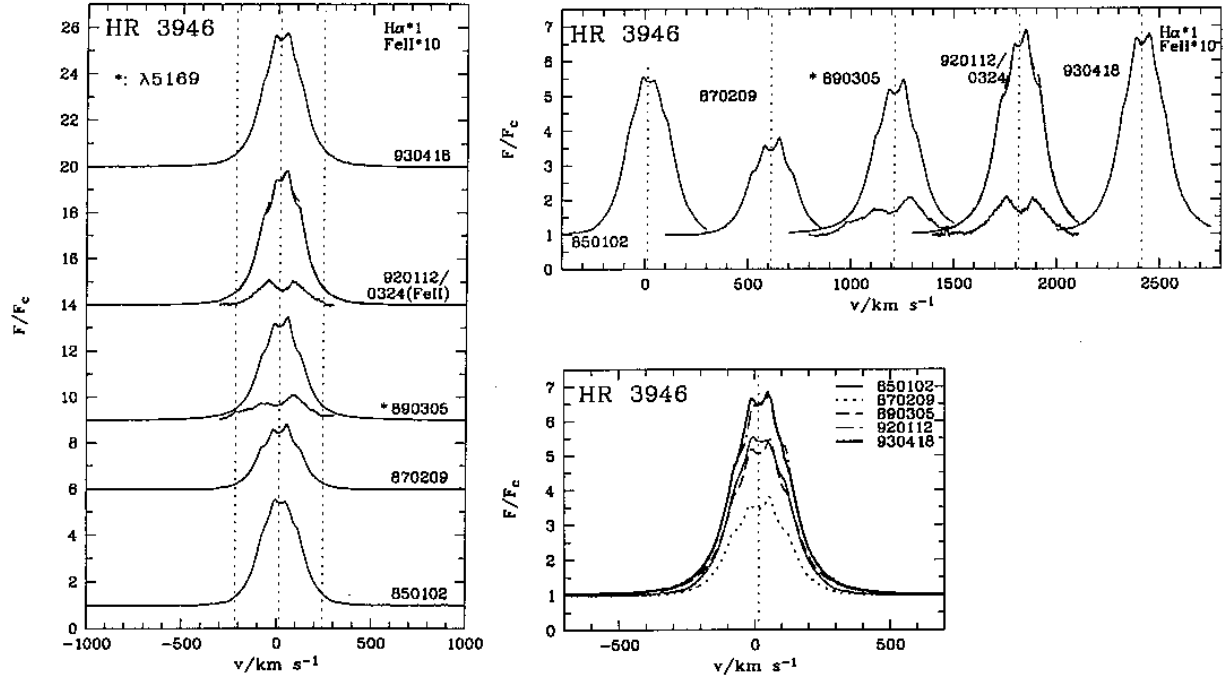
Fig. 45. Hα and Fe II profiles for HR 3946
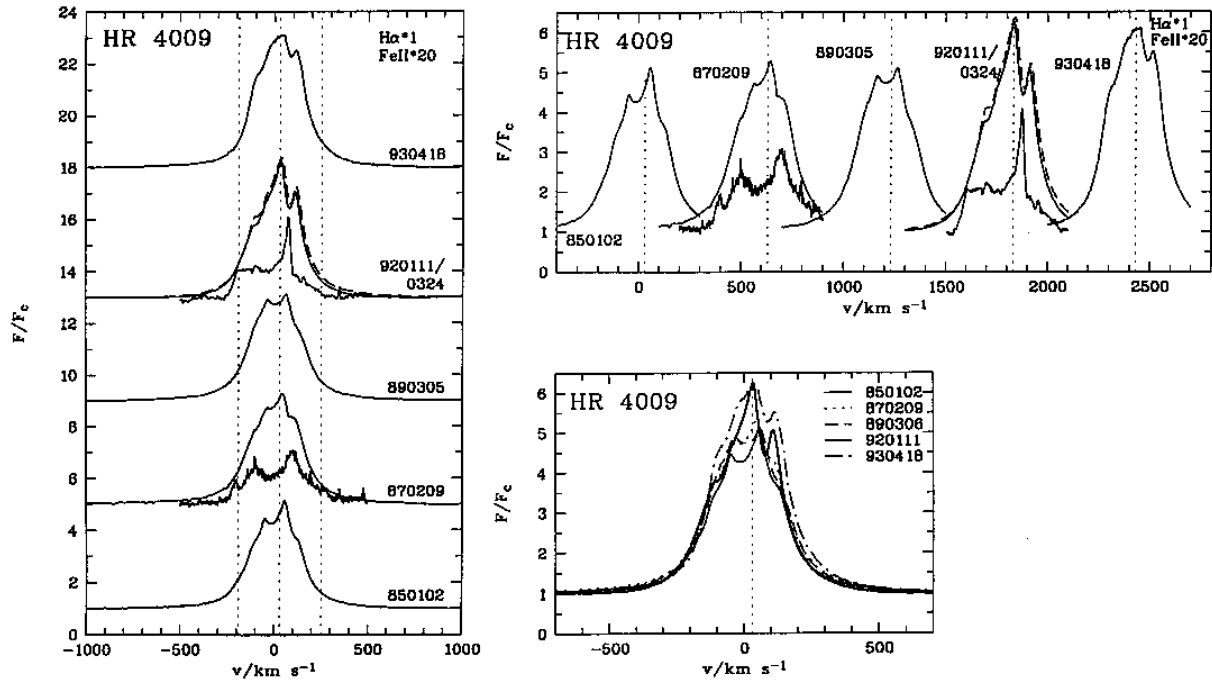
Fig. 46. Hα and Fe II profiles for HR 4009
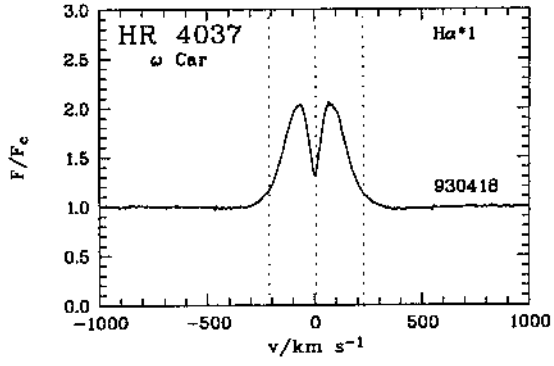
Fig. 47. Hα profile for HR 4037
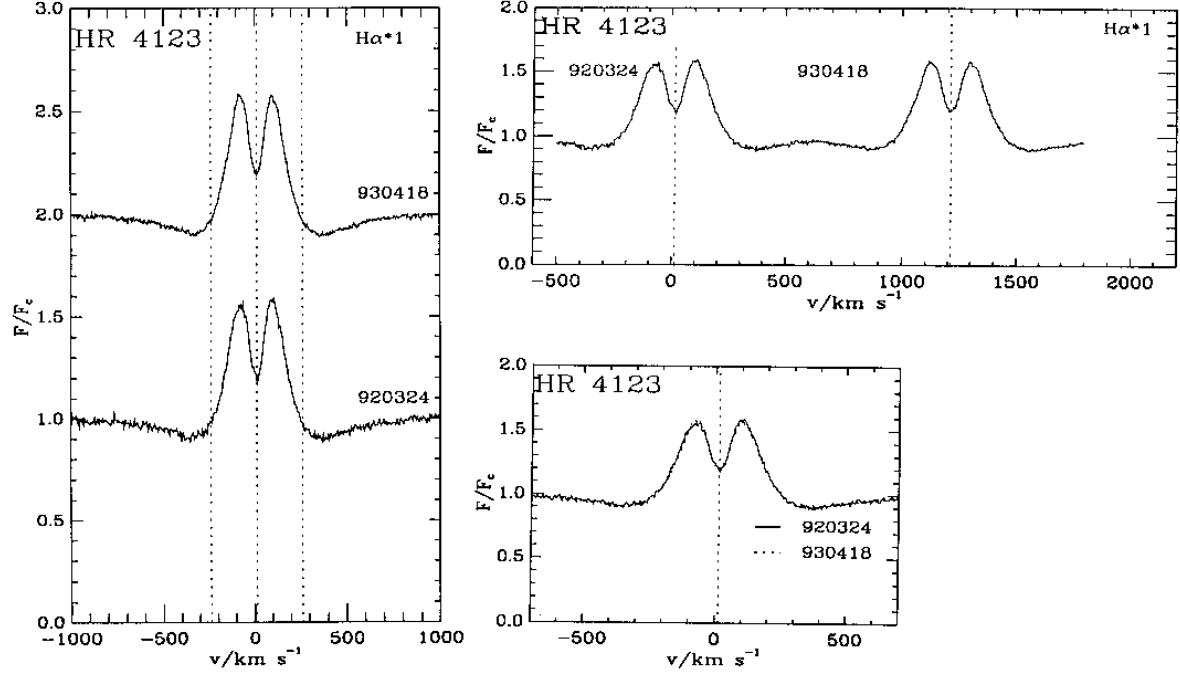
Fig. 48. Hα profiles for HR 4123. The two Hα profiles almost fall together in panel c
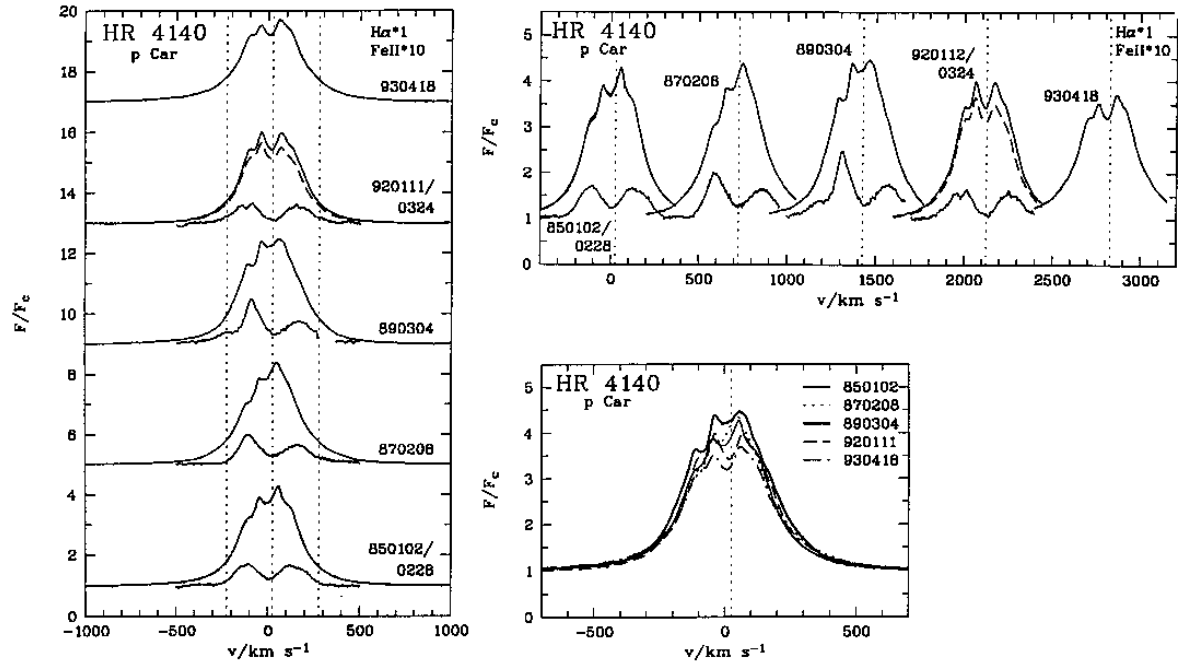
Fig. 49. Hα and Fe II profiles for HR 4140
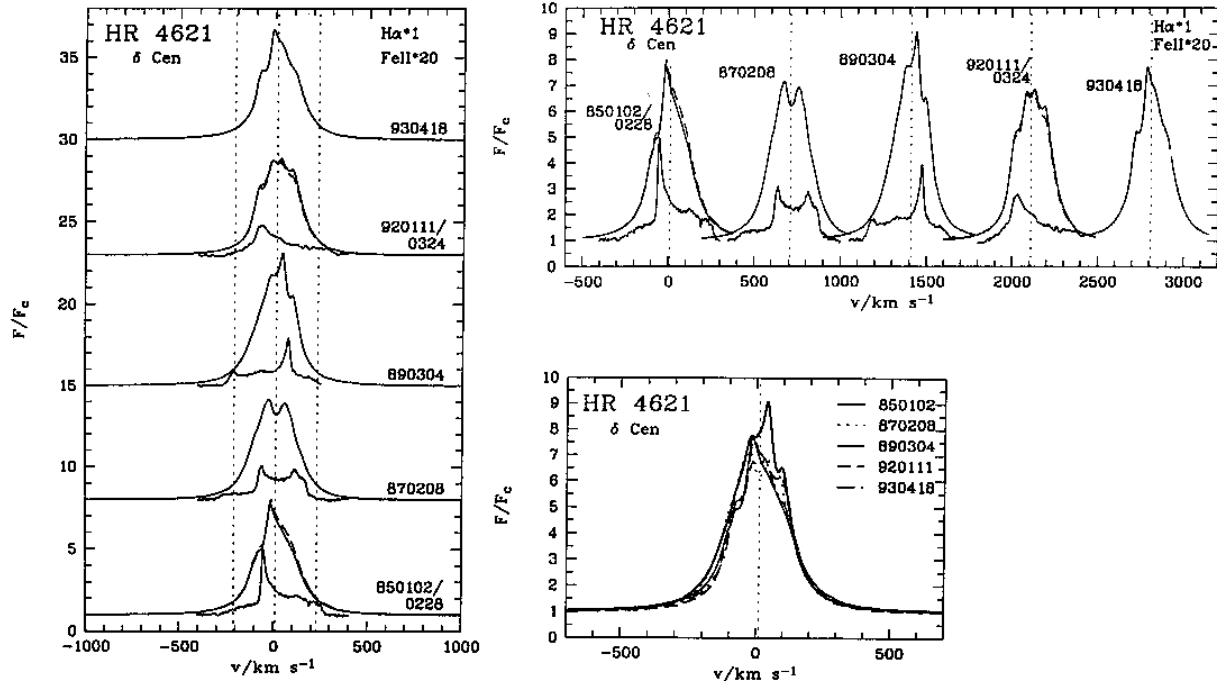
Fig. 50. Hα and Fe II profiles for HR 4621. Note the prototype "steeple" shape of the Fe II profiles in 1985 and 1989
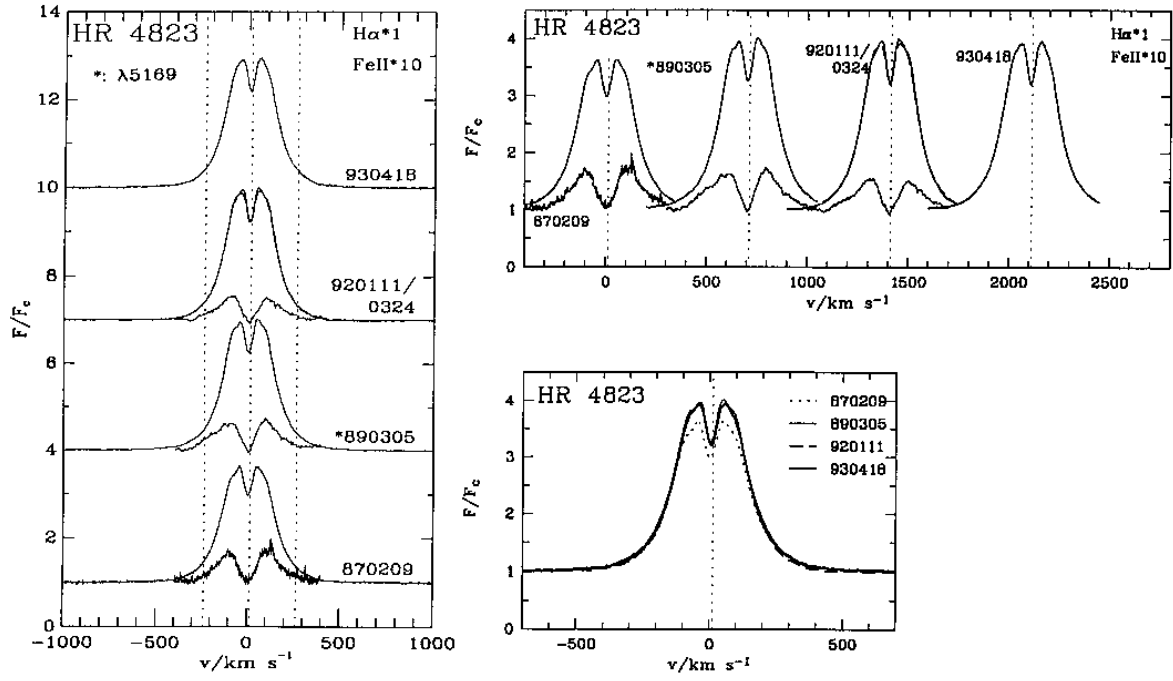
Fig. 51. Hα and Fe II profiles for HR 4823
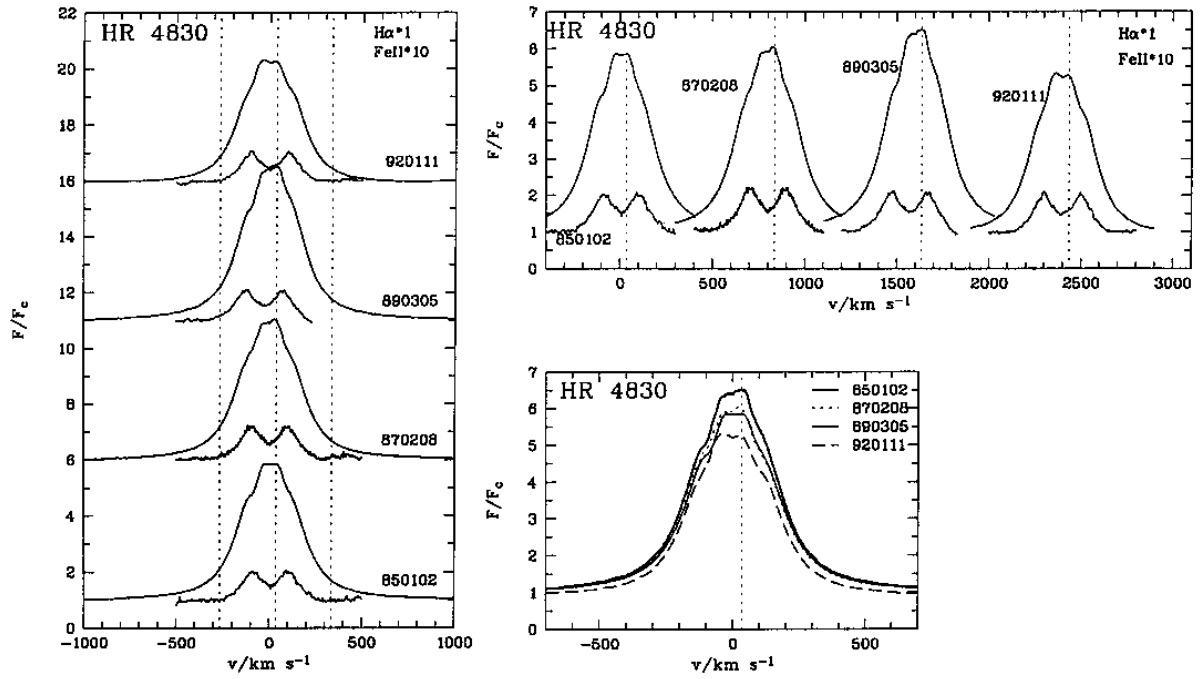
Fig. 52. Hα and Fe II profiles for HR 4830
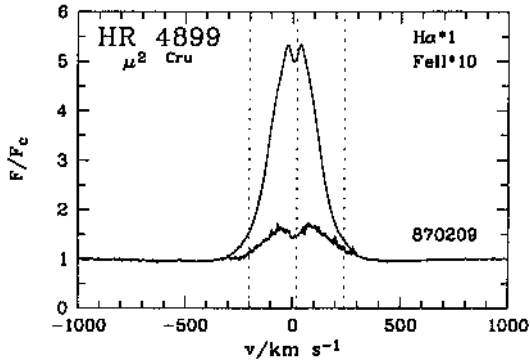
Fig. 53. Hα and Fe II profile for HR 4899 (a further Fe II measurement in 920324 did not yield any emission)
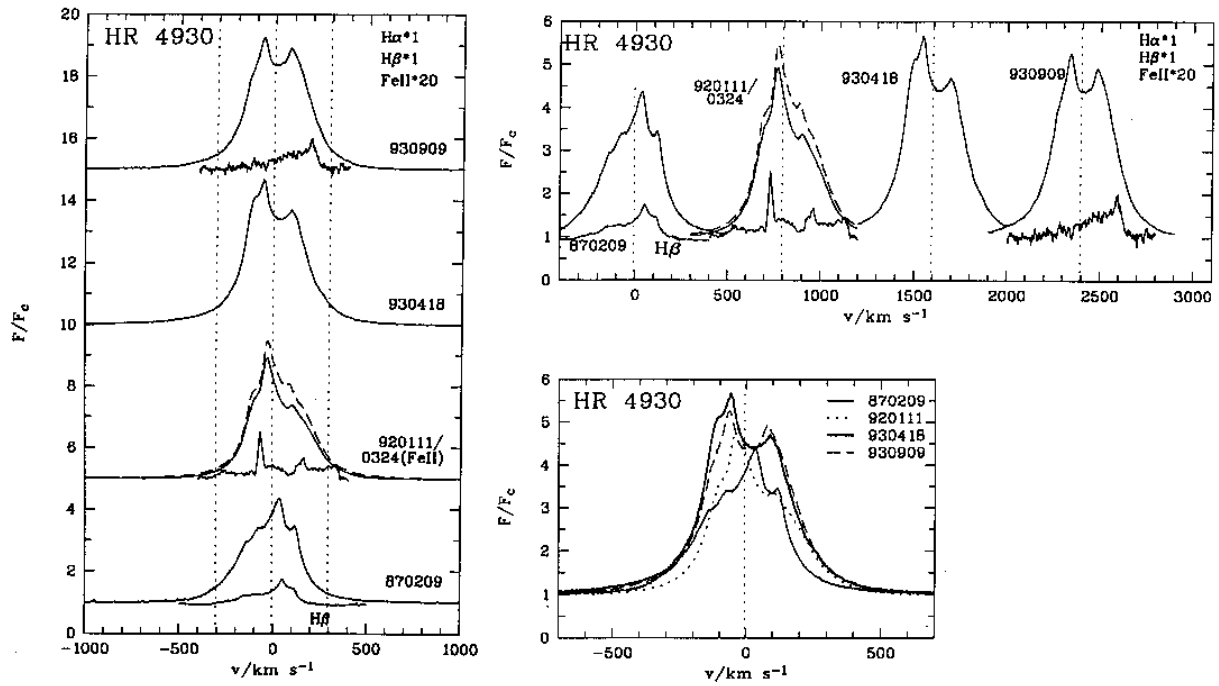
Fig. 54. Hα, Hβ and Fe II profiles for HR 4930. Note that the complex substructure in the 1992 Fe II profile might be spurious (within the uncertainty of the normalization procedure)
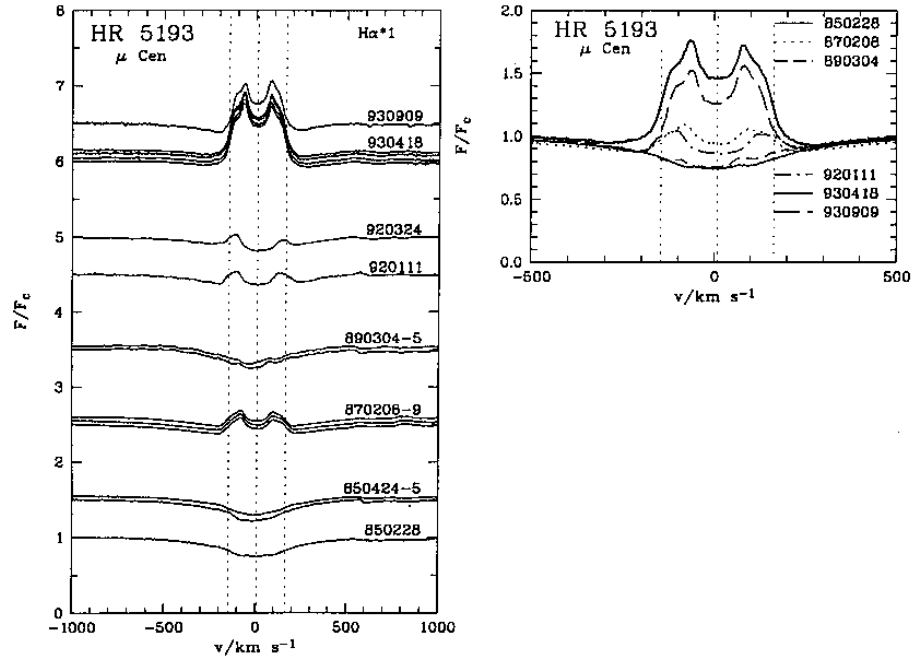
Fig. 55. Hα profiles for HR 5193. This star is building up a new permanent disk since 1993
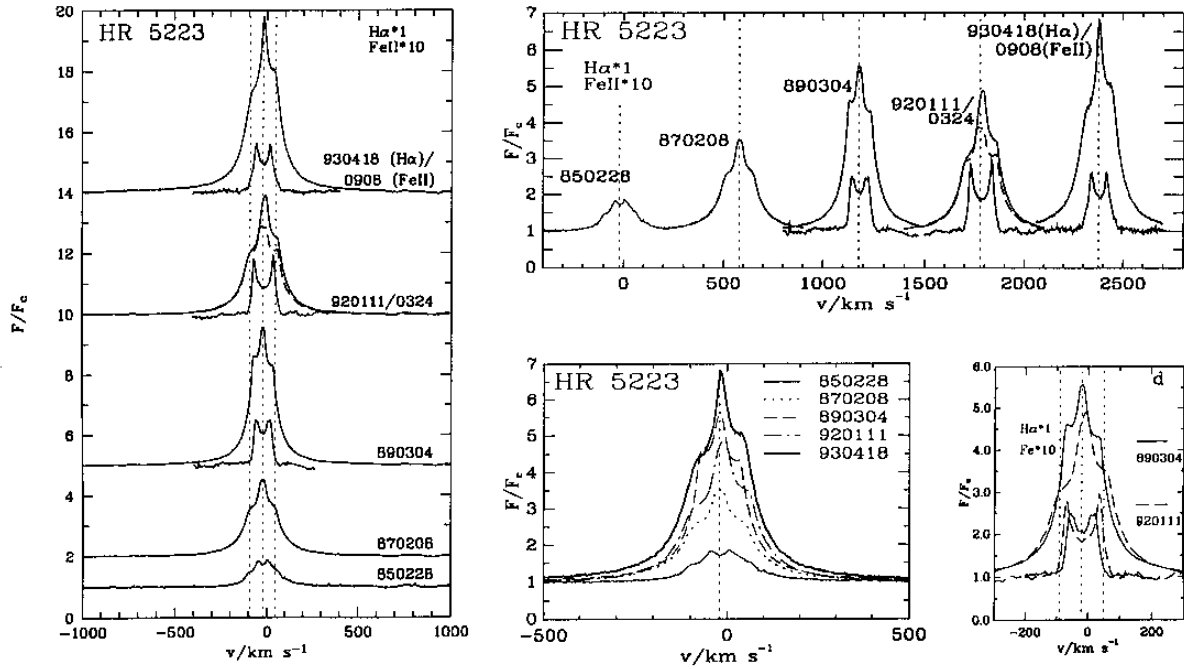
Fig. 56. Hα and Fe II profiles for HR 5223. Note the anticorrelation of Hα and Fe II strength and width in 1989 and 1992
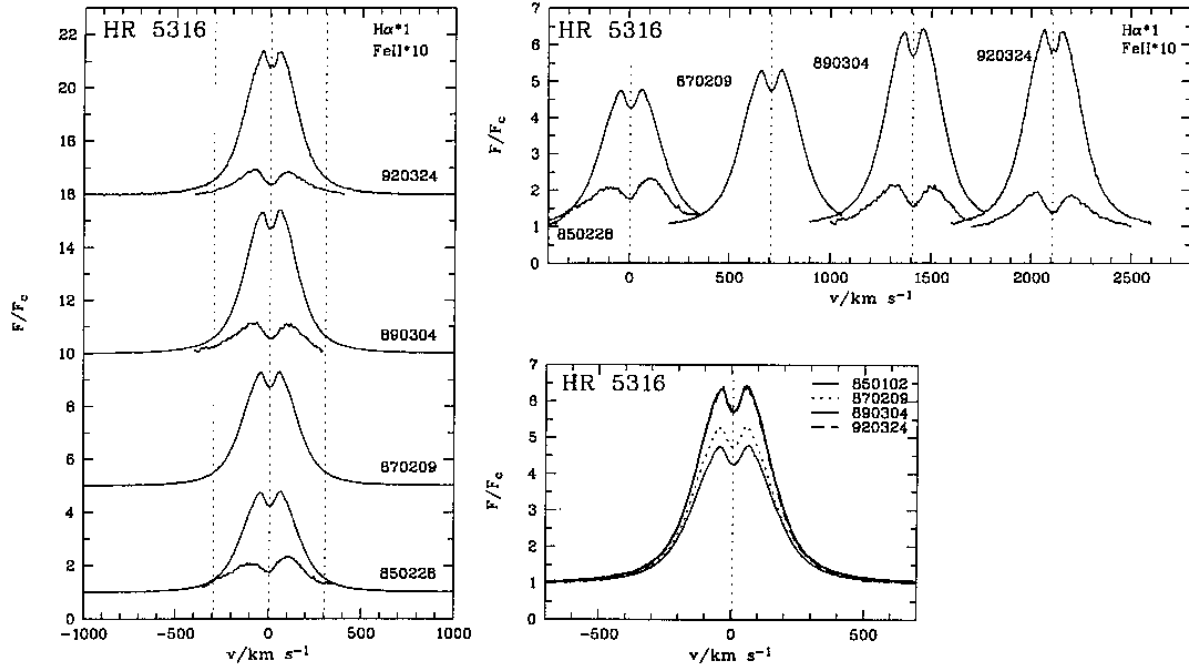
Fig. 57. Hα and Fe II profiles for HR 5316
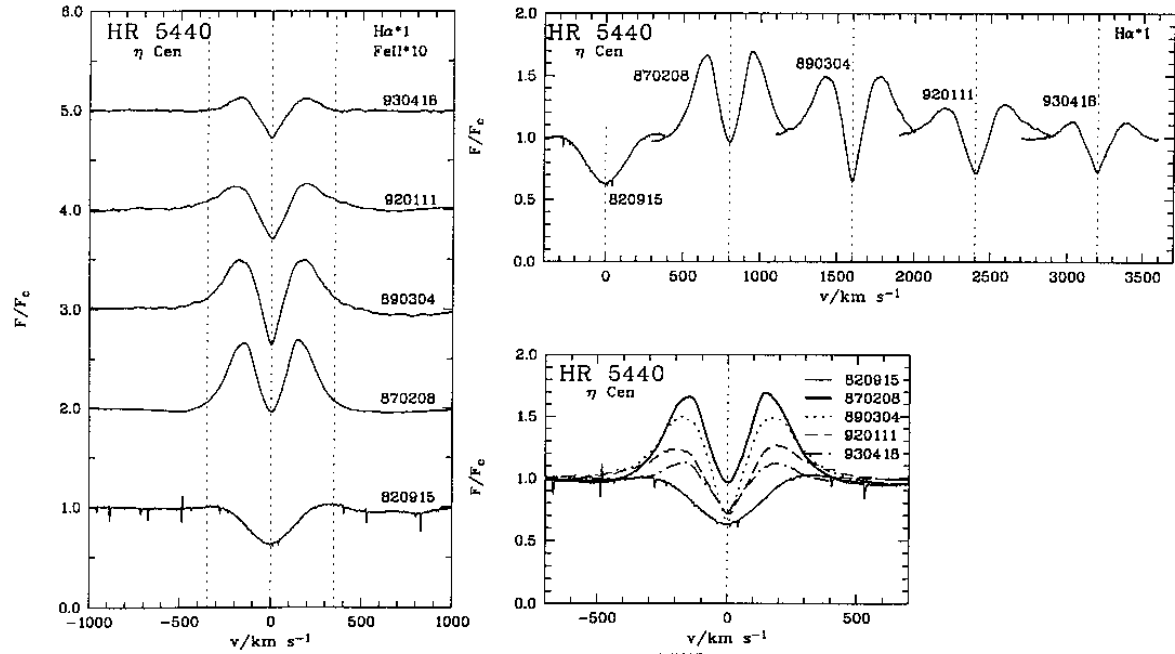
Fig. 58. Hα profiles for HR 5440
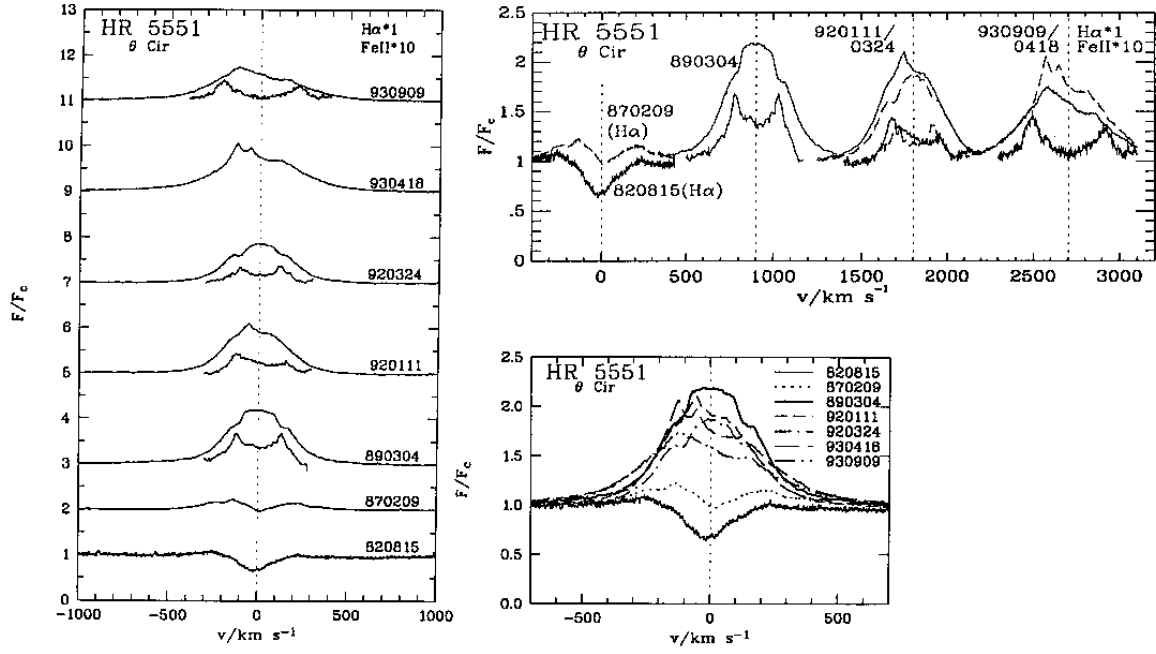
Fig. 59. Hα and Fe II profiles for HR 5551. Vertical $v \sin i$ lines have been omitted here since Slettebak's (1982) value (100 km s^{-1}) seems dramatically underestimated
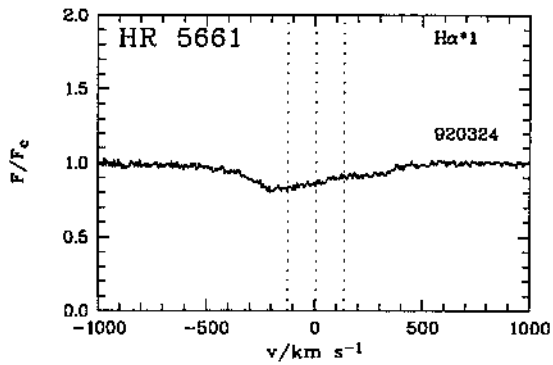
Fig. 60. Hα profile for HR 5661
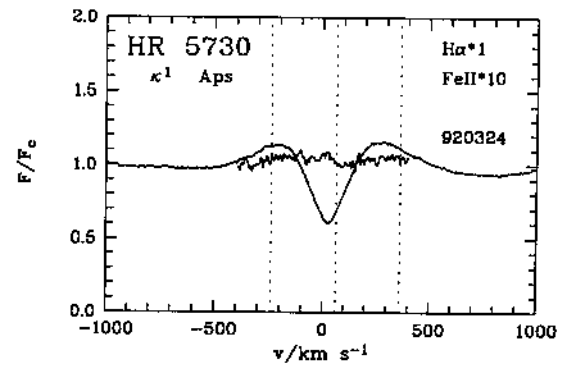
Fig. 61. Hα and Fe II profile for HR 5730
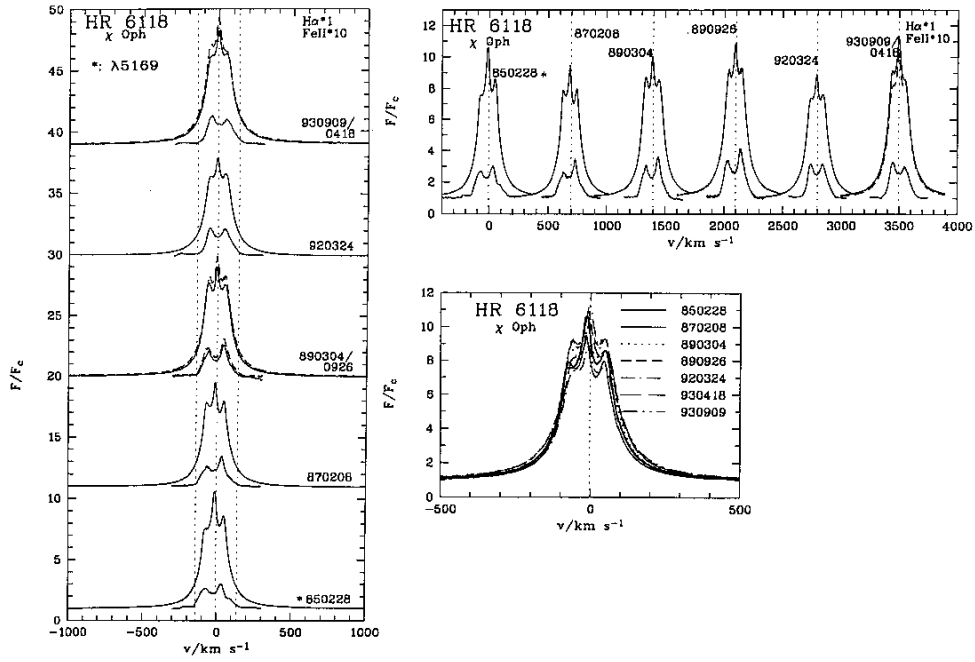
Fig. 62. Hα and Fe II profiles for HR 6118
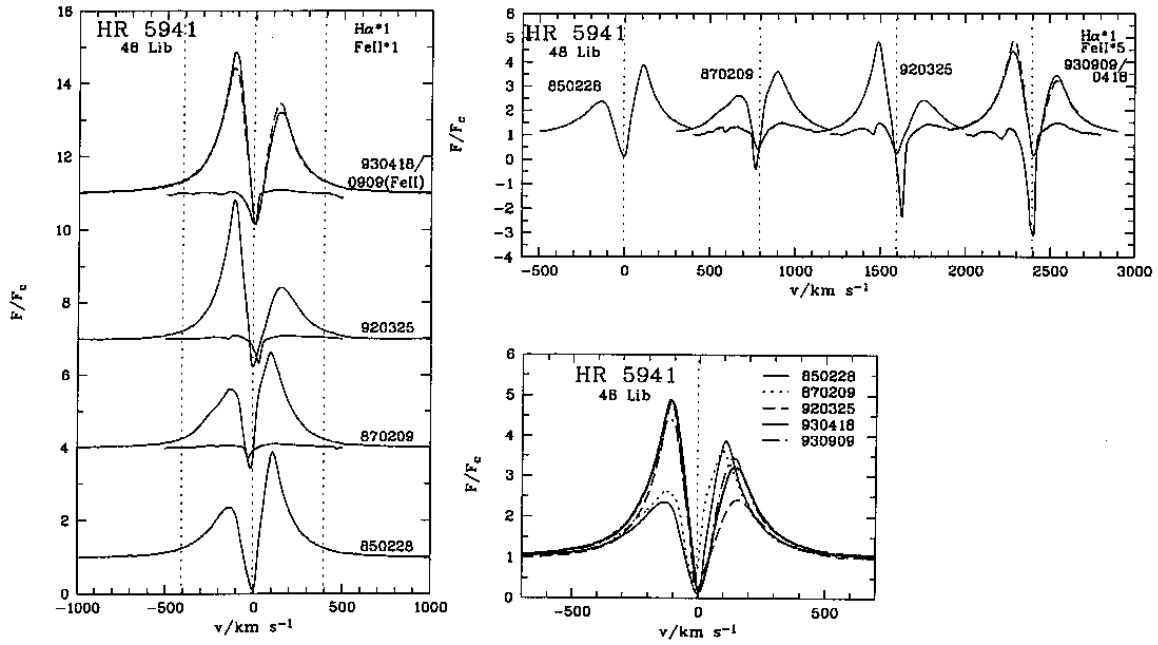
Fig. 63. Hα and Fe II profiles for HR 5941. Note that the scaling for Fe II lines is different in panels a and b, and that the depth of the Fe II troughs in panel b is affected by the expansion
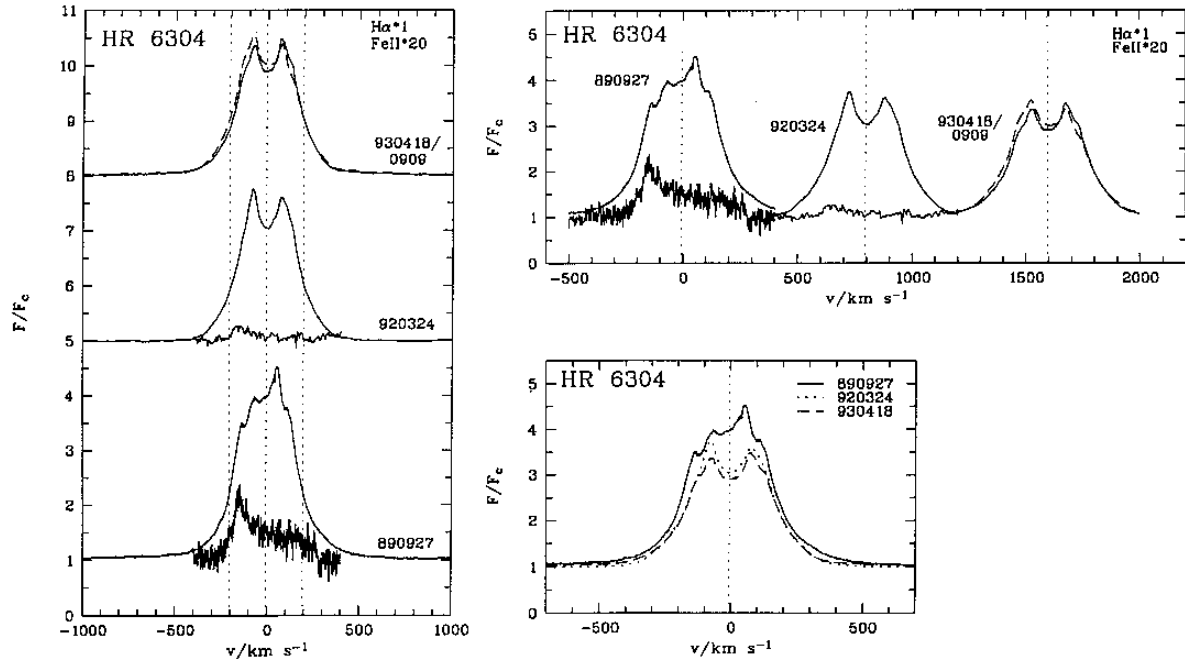
Fig. 64. Hα and Fe ɪɪ profiles for HR 6304
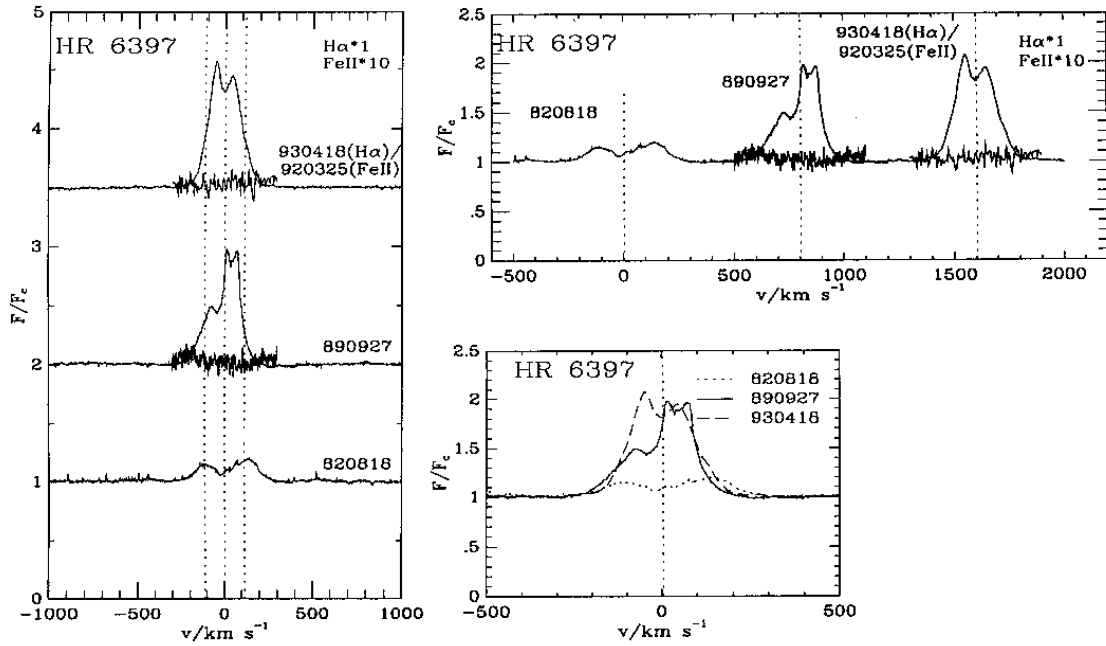
Fig. 65. Hα and λ5317 profiles for HR 6397. No trace of Fe ɪɪ was visible in 1989 and 1992
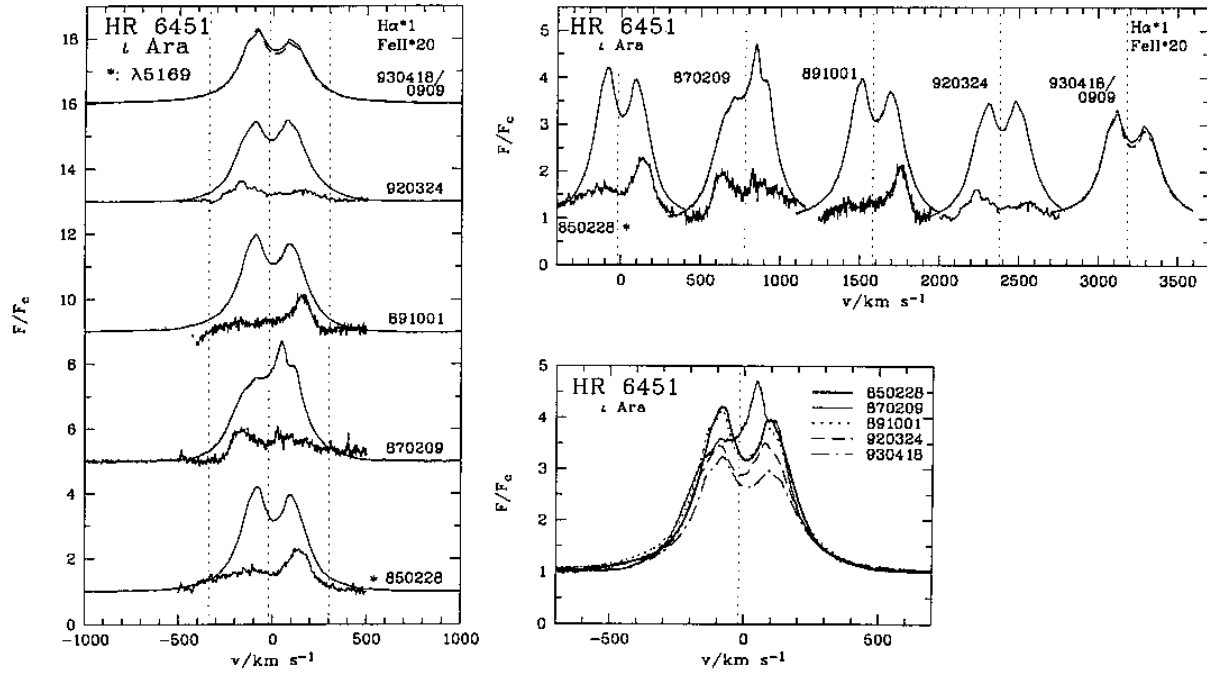
Fig. 66. Hα and Fe II profiles for HR 6451
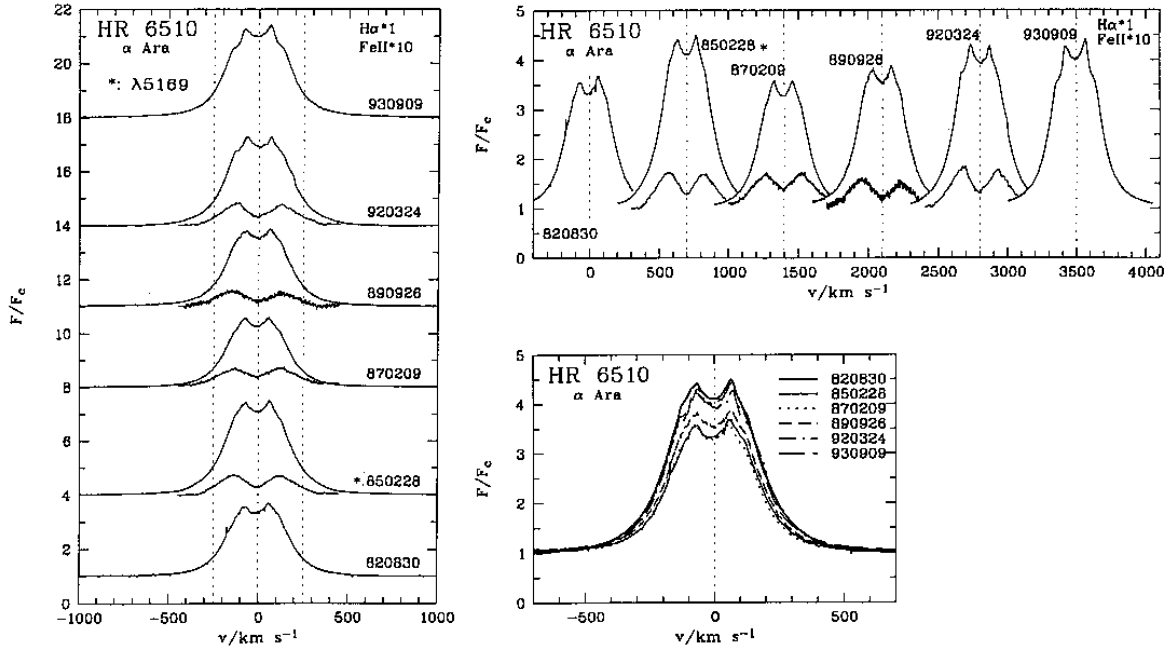
Fig. 67. Hα and Fe II profiles for HR 6510
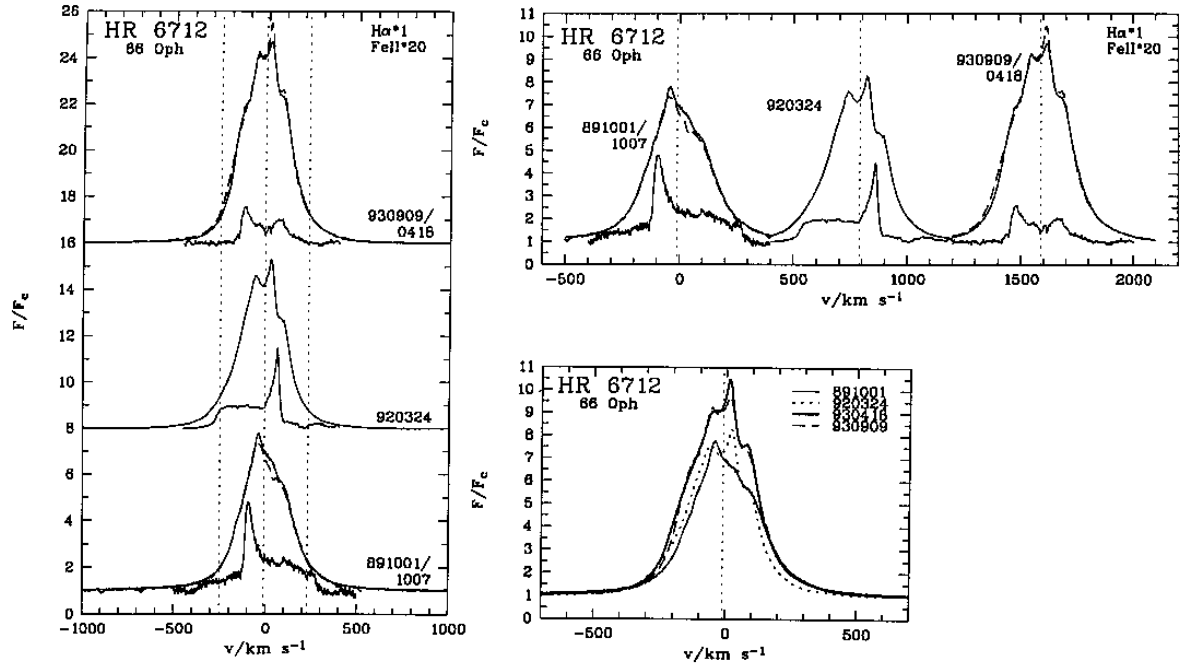
Fig. 68. Hα and Fe II profiles for HR 6712
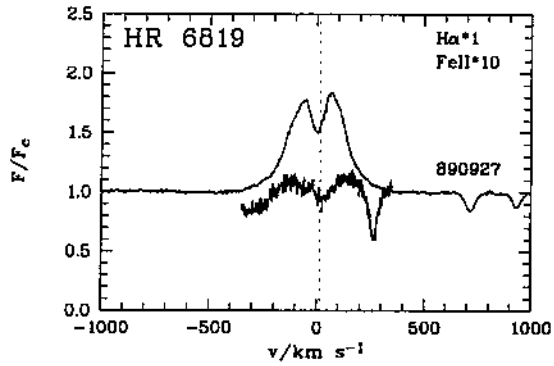
Fig. 69. Hα and Fe II profile for HR 6819
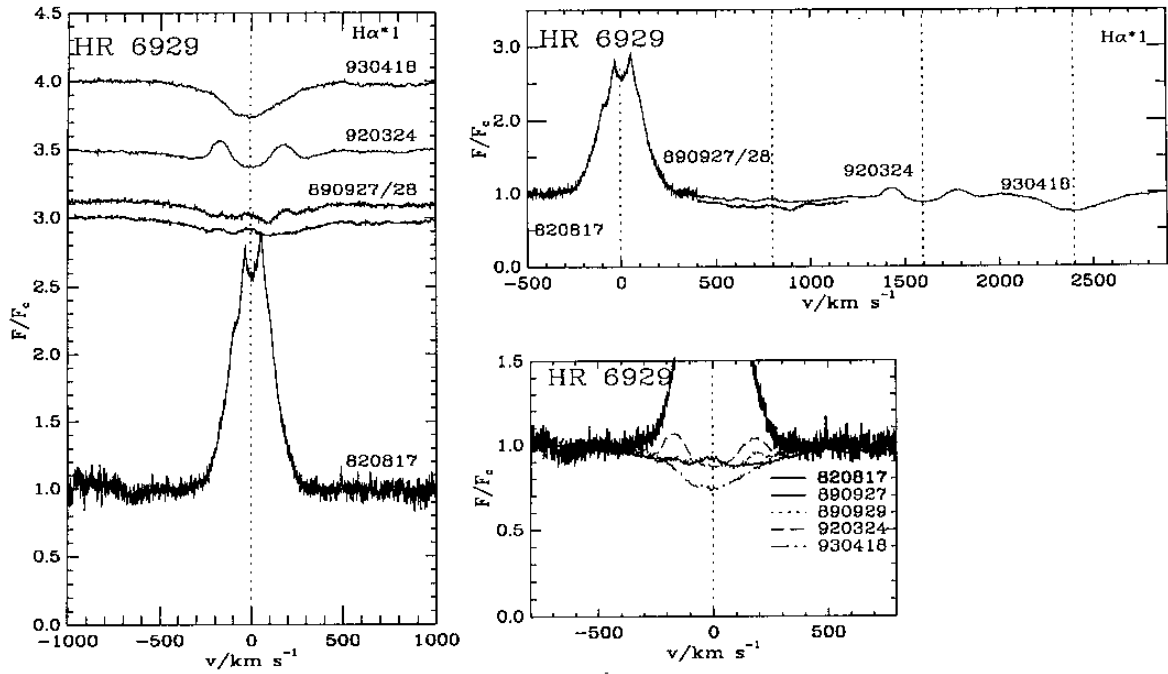
Fig. 70. Hα profiles for HR 6929. Note that the Hα profile from 820817 has been cut off in panel c
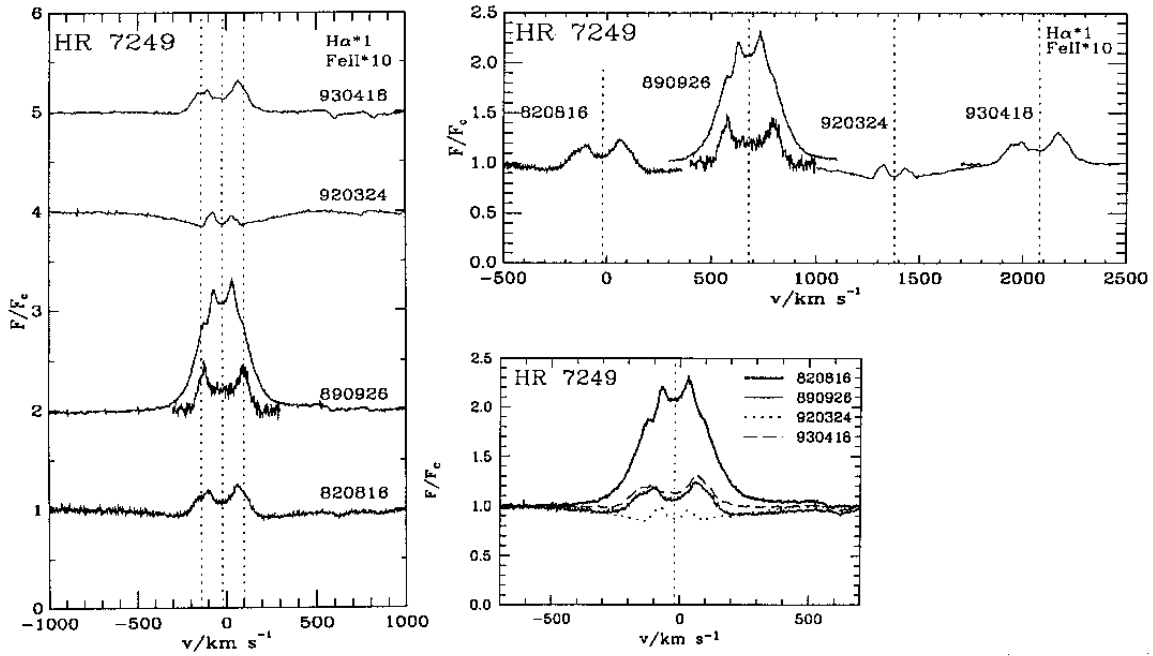
Fig. 71. Hα and Fe II profiles for HR 7249
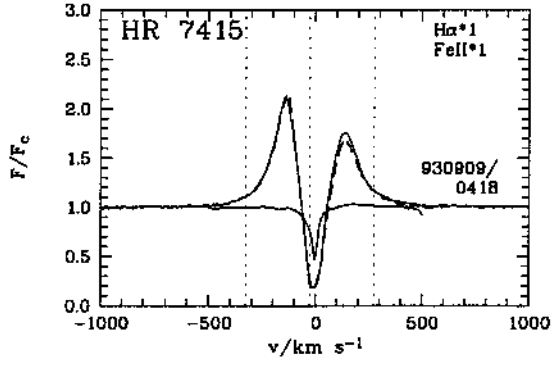
Fig. 72. Hα and Fe ɪɪ profiles for HR 7415
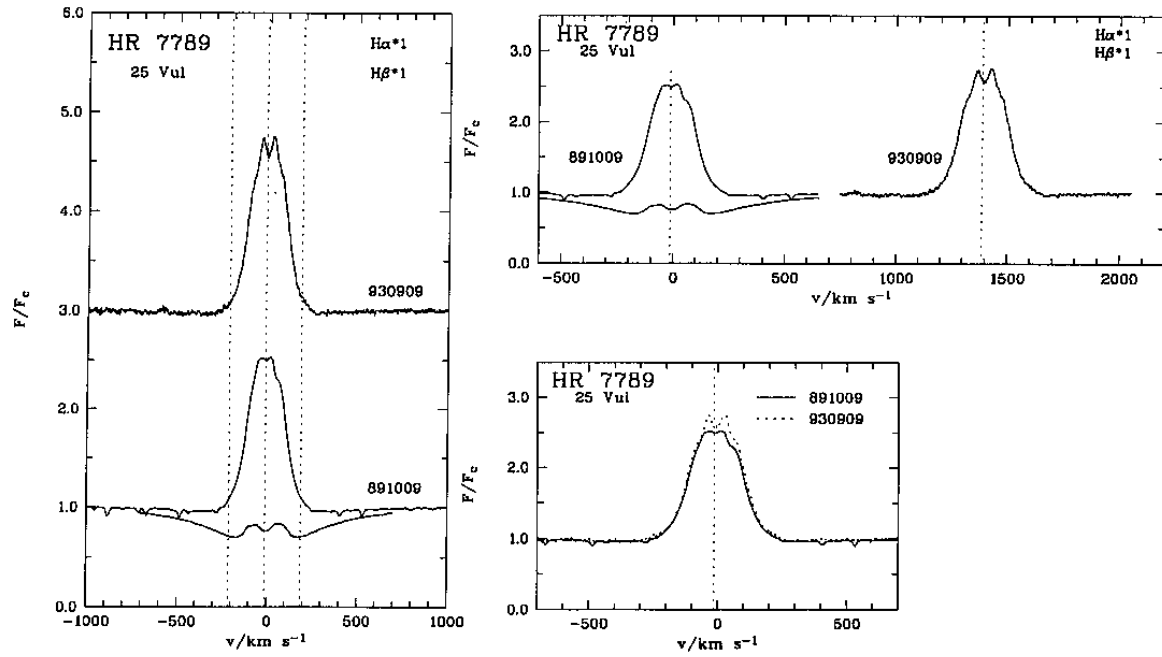
Fig. 73. Hα and Hβ profiles for HR 7789. Note that the 891009 profiles (from Sl92) are not fully resolved
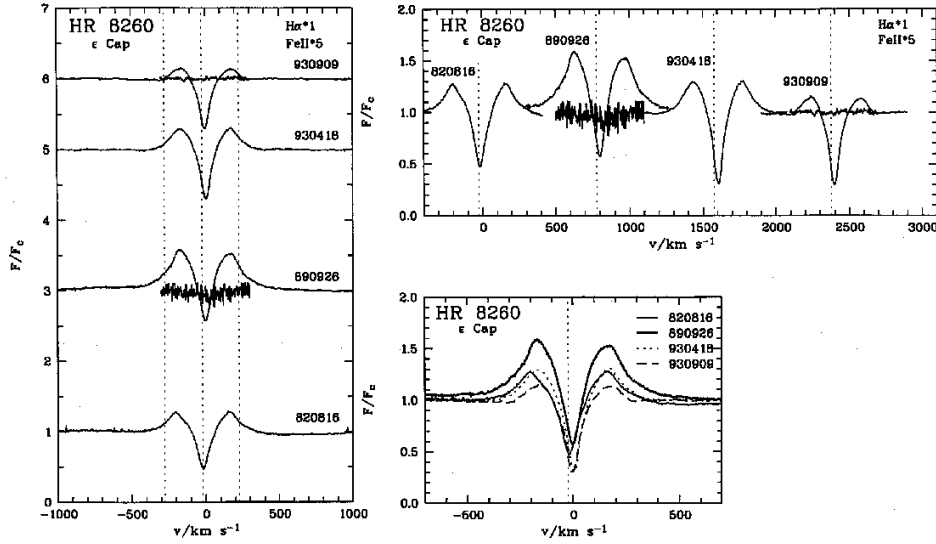
Fig. 74. Hα and λ5317 profiles for HR 8260. There is no trace of Fe II emission or shell absorption in the 1989 and 1993 data
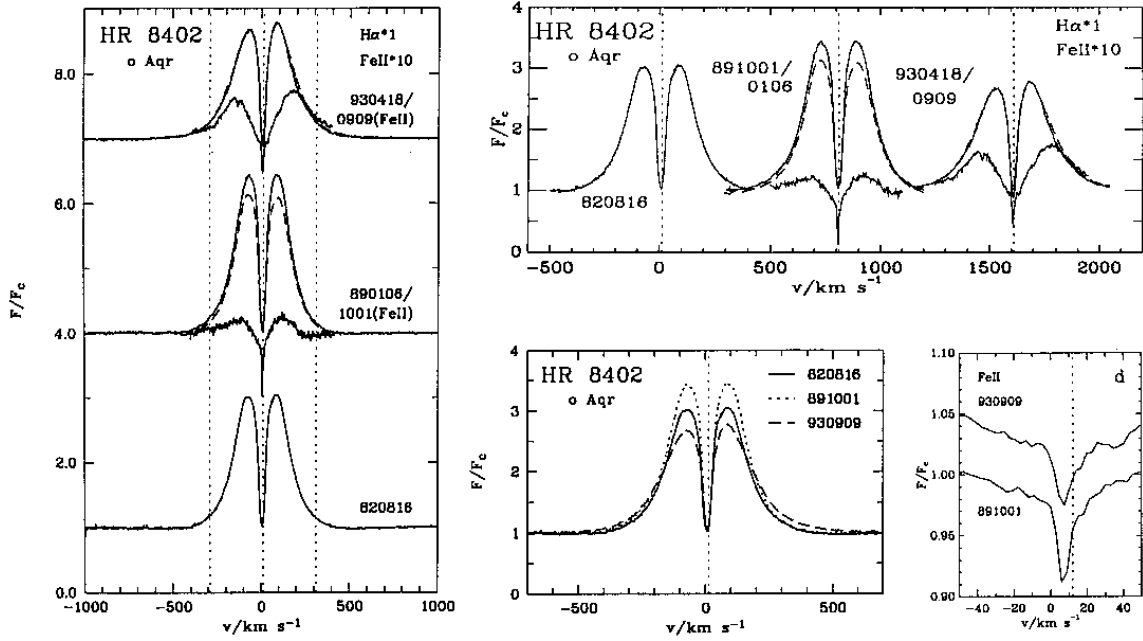
Fig. 75. Hα and Fe II profiles for HR 8402. Panel **d** shows a blow-up of the extremely narrow Fe II lines. Note that in panels a and b, the depth of the Fe II lines is affected by the expansion
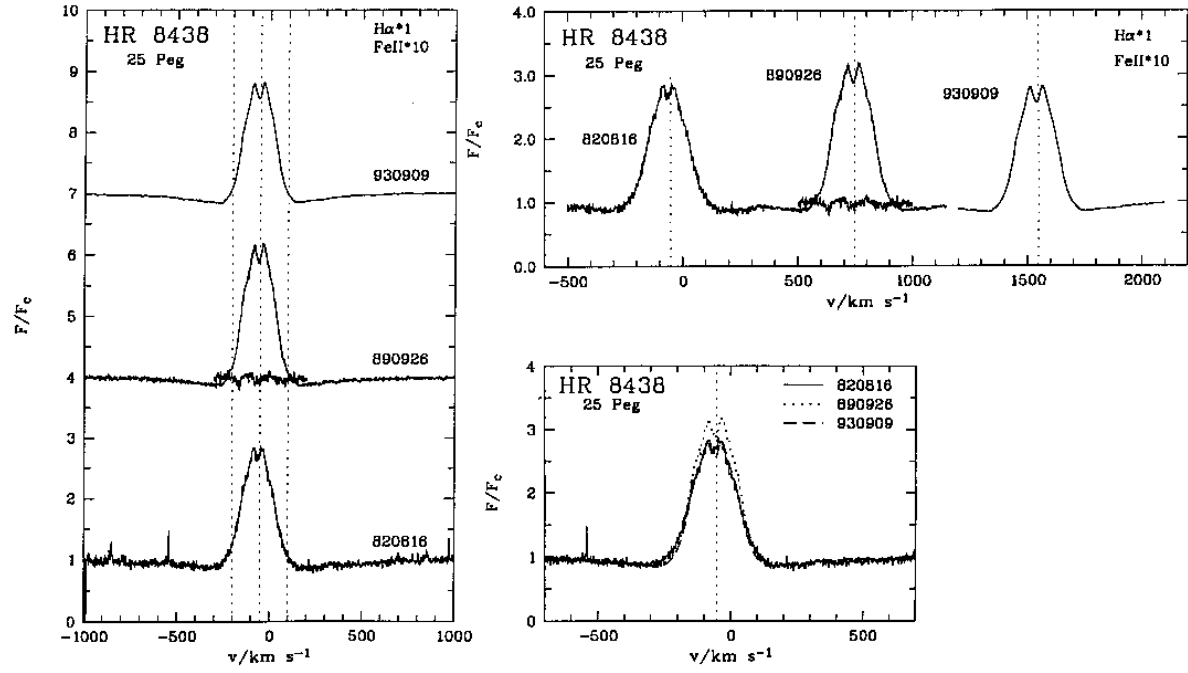
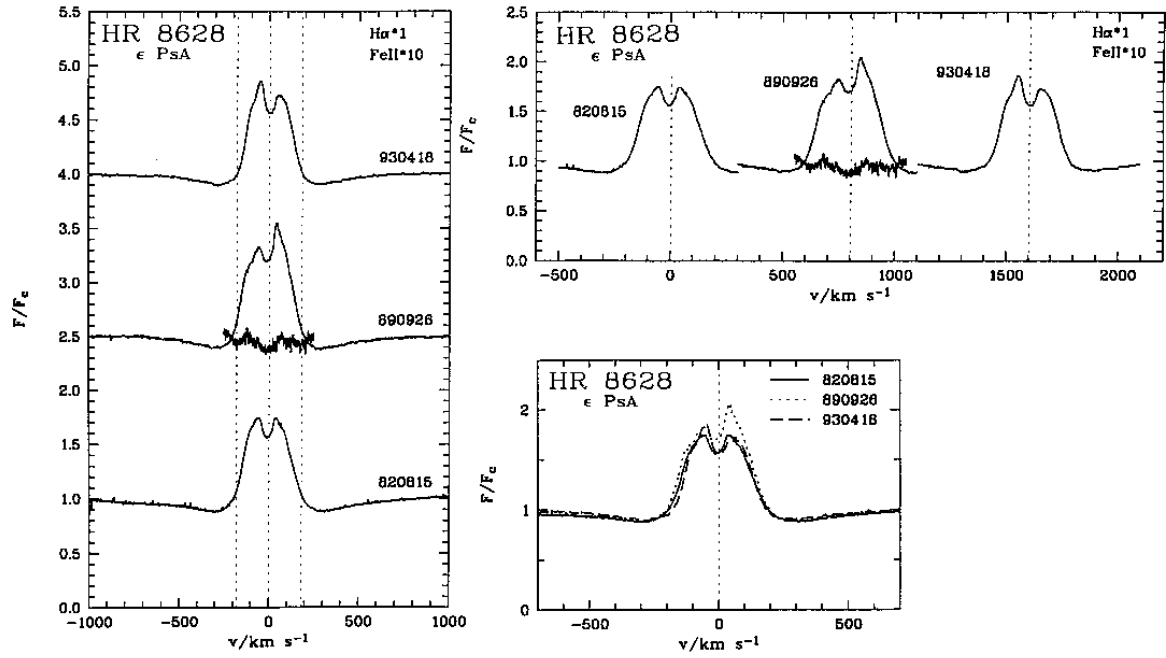**Fig. 76.** Hα and λ5317 profiles for HR 8438. No trace of Fe II emission is visible
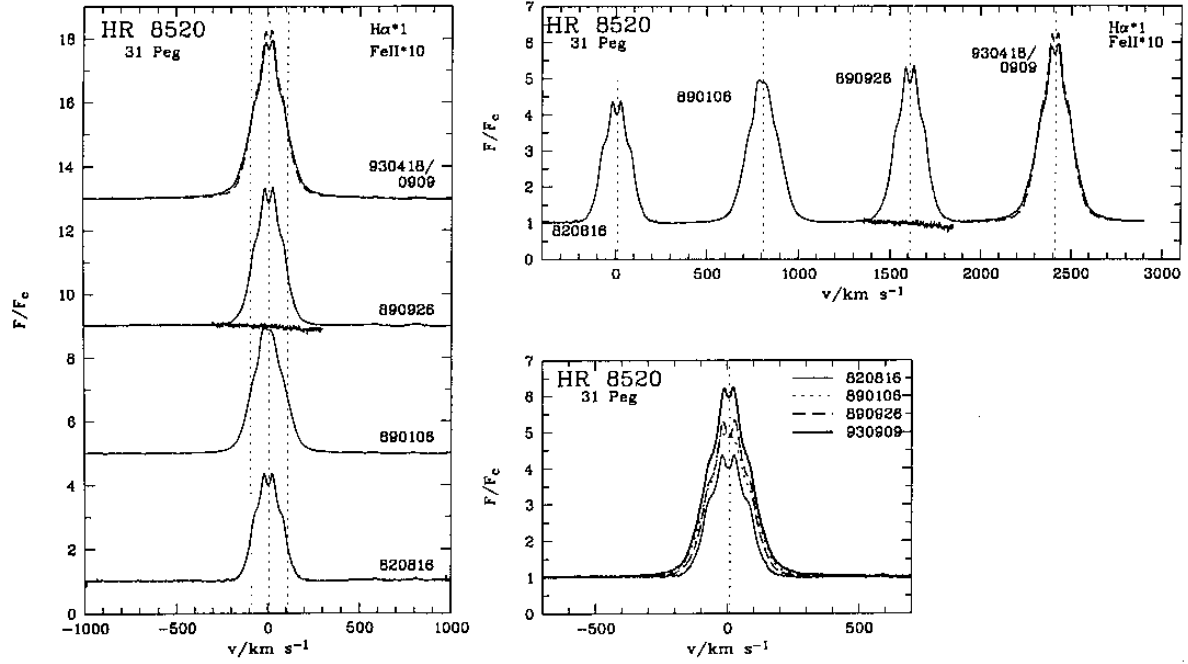
Fig. 77. Hα and λ5317 profiles for HR 8520. No trace of Fe II emission is visible. The 890106 profile from Sl92 is not fully resolved
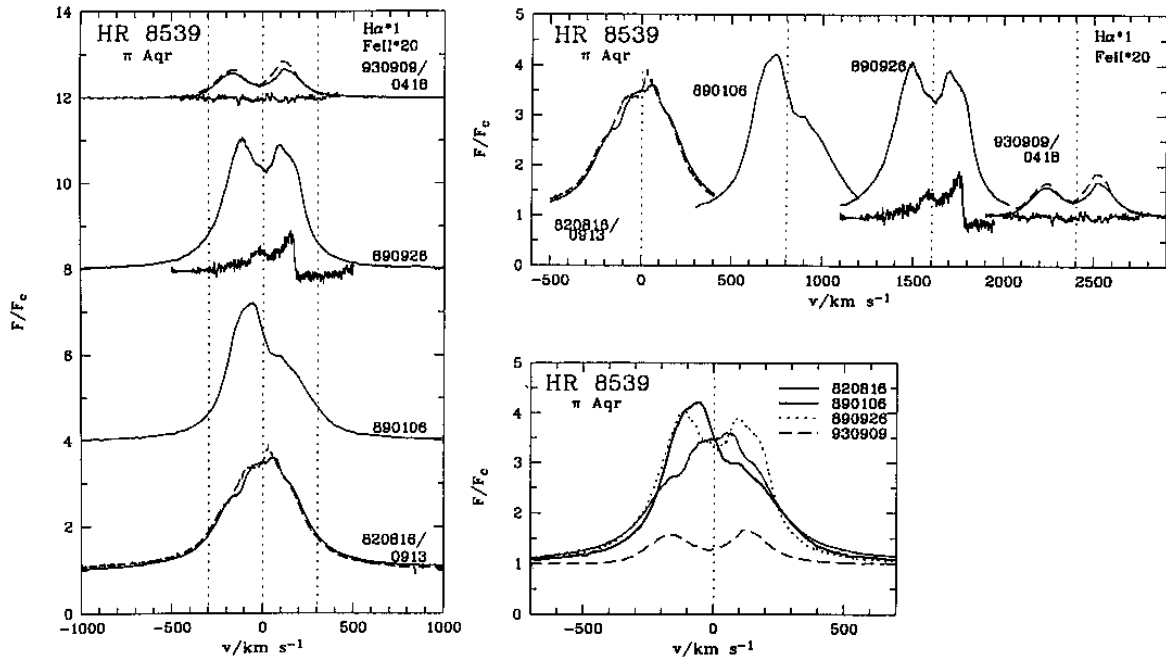
Fig. 78. Hα and Fe II profiles for HR 8539

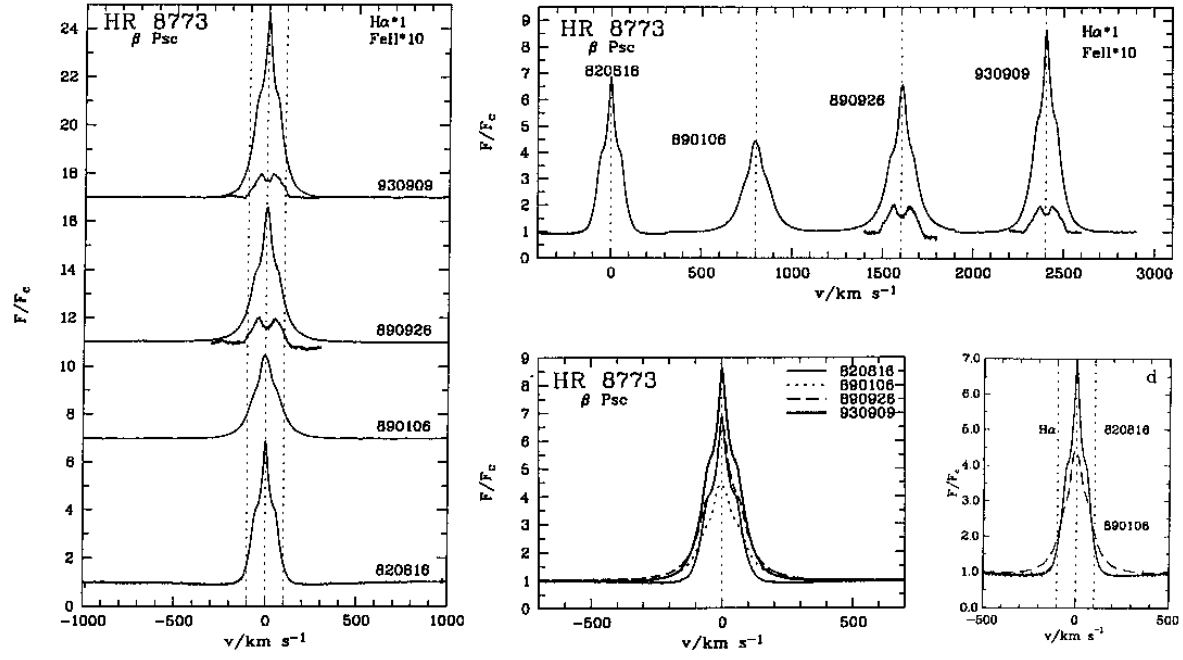**Fig. 79.** Hα and Fe II profiles for HR 8628. The Fe II emission is spurious

Fig. 80. Hα and Fe II profiles for HR 8773. Panel d shows the variations of Hα width and height between 1982 and 1989
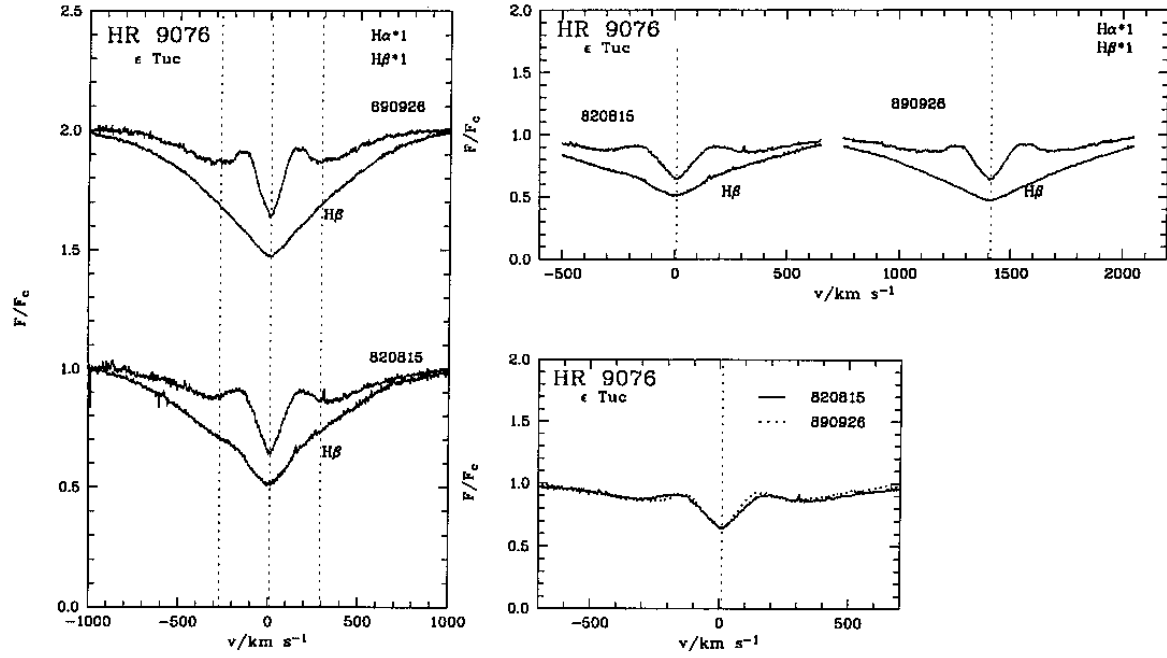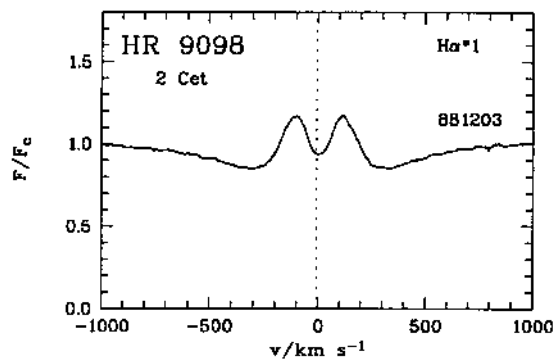
Fig. 81. Hα and Hβ profiles for HR 9076

Fig. 82. Hα profile for HR 9098